Two-electron processes and correlation effects in ion-atom collisions : a close-coupling approach at intermediate energies

Junwen Gao

To cite this version:

Junwen Gao. Two-electron processes and correlation effects in ion-atom collisions : a close-coupling approach at intermediate energies. Atomic Physics [physics.atom-ph]. Sorbonne Université; China Academy of Engineering Physics (Chine ; 1958-..), 2019. English. NNT : 2019SORUS117 . tel-02944710

HAL Id: tel-02944710
https://theses.hal.science/tel-02944710

Submitted on 21 Sep 2020

Sorbonne Université

École doctorale : Chimie physique et chimie analytique de Paris Centre
Laboratoire de Chimie Physique–Matière et Rayonnement (UMR 7614)

and

China Academy of Engineering Physics

Graduate school of CAEP
Institute of Applied Physics and Computational Mathmatics

Two-electron processes and correlation effects in ion-atom collisions: a close-coupling approach at intermediate energies

Junwen Gao
Dissertation for the degree of Philosophiae Doctor (Ph.D.)

Supervisors:
Prof. Alain Dubois
Prof. Jianguo Wang

May, 2019

To the Memory of my beloved Mother and Father.
As you look down from heaven,
I hope you're proud of your young boy.

Acknowledgements

The thesis have been conducted within the framework of a cotutelle agreement between the two institutions, Laboratoire de Chimie Physique–Matière et Rayonnement (LCPMR) at Sorbonne Université and Institute of Applied Physics and Computational Mathmatics (IAPCM) at China Academy of Engineering Physics. The thesis have been financed by a China Scholarship Council (CSC) scholarship, within a CSC-SU program.

I would first like to thank my supervisors Alain Dubois and Jianguo Wang for their advice and guidance throughout my studies, and for constantly pushing me to improve all aspects of my work. I am also grateful to Nicolas Sisourat for his guidance and assistance, who gave me unstinting support during the work carried out on developing the new computer programs. I would like to thank Yong Wu for all his help and encouragements during the writing of this thesis.

Besides my supervisors, I would like to thank the rest of my thesis committee: Prof. Henri Bachau, Prof. Jianmin Yuan, Prof. Yizhi Qu, and Prof. Xinwen Ma for generously offering their time, support, guidance and good will throughout the preparation and review of this manuscript.

I would like to thank Meiyi, Jiatai, Hang, Peng, Xuan and Aladine for all the good times we had together. My sincere thanks also go to Aicha, Solène, Selma, Tsveta, Bastien and Basile for creating a good atmosphere in the office room, it gave me great memories that I will never forget. I would also like to thank all the other members of LCPMR during my time. I am also grateful to all my group members in IAPCM during my time, Bin He, Ling Liu, Jiguang Li, Xiaoying Han, Chuanying Li, Congzhang Gao, Yigeng Peng, Fuyang Zhou, Tiecheng Li, Yulong Ma, Xiaoqing Hu, Kun Wang, Xuhai Hong, Xiaohe Lin and Xingyu Li for their helpful discussions and invaluable guidance.

My thanks to my friends away from work, in particular to Menglan He, Zhi Li,

Yuxun Wang, Tianyi Liu, Lin Li and Fang Lei. I will, especially, remember all the climbing, hiking, traveling, drinking that we did together. Thanks for giving me wonderful memories in Paris.

Finally, thanks to my whole family and my fiancee for their love, continuing support and encouragement.

Abstract

This thesis presents a non perturbative theory to describe multi-electronic processes occurring in the course of ion-atom collisions. The treatment is semiclassical in that the relative target-projectile motion is described by classical straight-line constant velocity trajectories, while the electronic dynamics is treated quantum mechanically, by solving non perturbatively the time-dependent Schödinger equation. The treatment has been implemented in a new version of two-active-electron computer code. Besides the long and complex development and tests of the code, the last three years have been especially devoted to understanding of the physics of specific heavy particle scattering events. We have undertaken the study of three collision systems with various features: (i) low charge ion-ion collisions with an extreme importance of electronic correlation ($H^+ + H^-$ collisions), (ii) multiply charged projectile-atom collisions (C^{4+} + He) and (iii) He^+ + He collisions with the dynamical treatment of the three electrons. Our guideline was always to target systems for which experimental and theoretical results were available (at least in some energy domain), with still open questions, related, for example, to strong disagreement between the various data. We have tried as much as our computing resources and allowed it to produce results with controlled convergence. These investigations were carried out in a very wide, up to three decades, energy domain with same collision description (i.e. same basis sets), which brought continuity and coherence on the predictions and the interpretations of the results and of the underlying mechanisms giving rise to the processes considered.

Firstly, we have investigated the double electron capture (DEC) process in the $H^+ + H^-$ collision system. Despite the apparent simplicity of this highly correlated system, all previous calculations fail to reproduce the measured experimental total cross sections. Our results reproduce well the experimental data in both magnitude and shape. Furthermore, we demonstrate that the oscillations stem from coherence effects between double electron capture and other two-electron inelastic channels, namely the transfer-excitation processes. An extended Rosenthal-like model based on a molecular treatment of the collision supports our interpretation. Our results shed new light on this old but challenging problem.

Secondly, the electron capture processes in C^{4+} + He collisions have been studied in a wide energy domain. The results of our calculations are compared with available theoretical predictions and experimental measurements: very good agreements are found for both total and state-selective single electron capture (SEC) and DEC cross sections. We extend the knowledge on that system to high energies for which only a single series of data exists. The mechanisms responsible of SEC and DEC processes as well as the role of electronic correlations in the collisions have been further studied by additional *restricted* two-active-electron and single-active-electron calculations. Furthermore, the observed oscillations in the small-angle angular-differential cross sections for both SEC and DEC have also been investigated by the simulated Fraunhofer-type diffraction pattern.

Lastly, an extended three active electrons approach has been adopted on the study of He^+ + He collisions. Total, state-selective and angular-differential cross sections are presented and compared with available experimental and theoretical results. A prominent oscillatory energy dependence structure in the transfer-target-excitation cross sections is observed and explained by a strong competition between these channels and the projectile-excitation processes. Moreover, the angular-differential cross sections considered in this study exhibit an oscillatory structure which is interpreted within a simple Fraunhofer-type diffraction model. For the two highest considered collision energies, the cross sections show a different pattern for which both Fraunhofer-type diffraction and Thomas mechanism have to be advocated.

Résumé (bref)

Cette thèse présente une théorie non perturbative pour décrire les processus multi-électroniques intervenant au cours des collisions ion-atome. Le traitement choisi est semiclassique en ce sens que le mouvement relatif cible-projectile est décrit par des trajectoires classiques (mouvement rectiligne uniforme), tandis que la dynamique électronique est traitée quantiquement, en résolvant de manière non perturbative l'équation de Schrödinger dépendante du temps. Cette approche théorique a été codée au cours de la thèse dans une nouvelle version du code informatique à deux électrons actifs et mise en œuvre à l'étude de plusieurs systèmes de collision. Outre le développement long et complexe et les tests du code, les trois dernières années ont été spécialement consacrées à la compréhension de la physique d'événements spécifiques de diffusion de particules lourdes. Nous avons entrepris l'étude de trois types de systèmes de collision : par ordre d'apparition dans cette thèse, (i) collisions ion-ion faiblement chargé avec une extrême importance de la corrélation électronique ($H^+ + H^-$), (ii) collisions entre projectiles multiplement chargés et atome (C^{4+} + He) et (iii) collisions He^+ + He avec un traitement très original prenant en compte des trois électrons dans la dynamique. Le choix de ces systèmes était guidé sur des systèmes *benchmark* pour lesquels des résultats expérimentaux et théoriques étaient disponibles (au moins dans certains domaines énergétiques), et présentant des questions ouvertes, liées par exemple à de forts désaccords entre les données existantes. Systématiquement, nous avons essayé de produire des résultats avec une convergence contrôlée permettant des interprétations physiques originales.

Nous avons étudié le processus de double capture (DEC) dans le système de collision $H^+ + H^-$. Malgré la simplicité apparente de ce système hautement corrélé, tous les calculs précédents ne reproduisent pas les sections efficaces totales expérimentales. Nos résultats reproduisent bien les données expérimentales à la fois en amplitude et en forme. Nous avons réussi à démontrer que les oscillations résultent d'effets d'interférences entre la double capture et d'autres canaux inélastiques à deux électrons, à savoir les processus de transfert-excitation. Un modèle (basé sur une image moléculaire de la collision) du type Rosenthal étendu aux spécificités du système a corroboré notre interprétation. Nos résultats ont apporté un nouvel éclairage sur ce problème ancien et complexe.

Dans une seconde étape, les processus de capture dans les collisions C^{4+} + He ont été étudiés dans un vaste domaine d'énergie couvrant presque trois décades. Les résultats de nos calculs sont comparés aux prévisions théoriques et mesures expérimentales disponibles : de très bons accords sont trouvés pour les sections efficaces totales et sélectives de simple (SEC) et double capture (DEC). Nous avons étendu les connaissances sur ce système aux hautes énergies pour lesquelles il n'existait qu'une

seule série de données. Les mécanismes responsables des processus SEC et DEC ainsi que le rôle des corrélations électroniques dans ces collisions ont été déterminés à l'aide de calculs modèles, à un et deux électrons actifs. En outre, les oscillations observées aux petits angles dans les sections efficaces différentielles angulaires pour SEC et DEC ont également été étudiées et interprétées en termes de phénomènes de diffraction du type Fraunhofer.

Finalement, une approche étendue à trois électrons actifs a été adoptée pour l'étude des collisions $He^+ + He$. Les sections efficaces totales, sélectives en état et différentielles (en angle) sont présentées et comparées aux résultats expérimentaux et théoriques disponibles. On observe des structures prononcées en fonction de l'énergie d'impact pour les sections efficaces de transfert-excitation.Â Elles sont expliquées par des effets d'interférences entre ces canaux et les processus d'excitation du projectile. De plus, les sections efficaces différentielles angulaires considérées dans cette étude présentent de nouveau des oscillations marquées, expliquées par un modèle de diffraction de type Fraunhofer simple, en compétition avec le mécanisme de Thomas.

List of Publications

1. **J. W. Gao**, Y. Wu, J. G. Wang, A. Dubois and N. Sisourat, "Double electron capture in $H^+ + H^-$ collisions", *Physical Review Letters* **122**, 093402 (2019).

2. **J. W. Gao**, Y. Wu, J. G. Wang, N. Sisourat, and A. Dubois, "State-selective electron transfer in He^++He collisions at intermediate energies", *Physical Review A* **97**, 052709 (2018).

3. **J. W. Gao**, Y. Wu, N. Sisourat, J. G. Wang, and A. Dubois, "Single- and double-electron transfer in low- and intermediate-energy C^{4+}+He collisions", *Physical Review A* **96**, 052703 (2017).

The following papers are not discussed in the thesis:

4. **J. W. Gao**, Y. Wu, Z. P. Zhong and J. G. Wang, "The influence of density in ultracold neutral plasma", *Physics of Plasma* **23**, 123507 (2016).

5. **J. W. Gao**, X. Y. Han, J. G. Wang and J. M. Li, "R-matrix calculations of the photoionization cross-sections of Ti^{2+}", *MNRAS* **454**, 315-321 (2015).

6. I. Rabadán, L. Méndez, **J. W. Gao**, Y. Wu, and J. G. Wang, "*Ab initio* calculation of electron-capture cross sections in H^+ + BeH collisions", *Physical Review A* **96**, 032714 (2017).

Contents

List of Figures

List of Tables

Résumé (long)

La compréhension des processus électroniques intervenant dans les collisions atomiques et moléculaires est nécessaire pour la modélisation de systèmes complexes tels que les plasmas de laboratoire ou astrophysiques et la radiobiologie. D'un point de vue fondamental, les collisions sont les “nano-laboratoires” optimaux pour l'étude des systèmes quantiques à plusieurs corps et de leur dynamique. Les aspects fondamentaux et appliqués concernant les collisions ont donc stimulé la montée en puissance de nombreux domaines de recherche qui ont conduit naturellement, dans les années 90, à l'extension des méthodologies théoriques et expérimentales développées vers l'étude des systèmes atomiques et moléculaires en champs laser forts et ultra-courts. Dès le début du développement de la mécanique quantique, d'importants efforts théoriques, allant de modèles classiques simples, tels que ceux de Thomas ou de Landau-Zener, à l'élaboration d'approches quantiques et semiclassiques élaborées ont été poursuivis pour comprendre et modéliser les systèmes de collision. En fait, on peut affirmer que les processus mono-électroniques, tels que le transfert d'électron, l'excitation et l'ionisation, sont maintenant bien compris pour les systèmes de collision ion-atome où la corrélation ne joue pas un rôle important. En général, cela n'est pas vrai pour les systèmes dans lesquels:

- un grand nombre de canaux sont ouverts et susceptibles de se produire de manière couplée, en particulier lorsque des processus multi-électroniques risquent de se produire et de concurrencer les processus mono-électroniques;

- le rôle des corrélations électroniques est important, de sorte qu'un traitement de corrélation cohérent est requis, au-delà des approximations habituelles

d'électrons ou d'événements indépendants;

— des partenaires moléculaires sont impliqués, où la géométrie et les caractéristiques multicentriques des systèmes de collision doivent être prises en compte.

Les théoriciens ont toujours du mal à comprendre et à modéliser des systèmes de collision à plusieurs, dès deux, électrons. En particulier, dans la région d'énergie d'impact intermédiaire, les approches perturbatives et l'utilisation du potentiel modèle pour décrire les corrélations de manière moyenne peuvent être inadéquates en raison des couplages forts entre les différents canaux de réaction et des effets de corrélation électronique. Par conséquent, des approches semi-classiques ou quantiques non perturbatives à deux ou plusieurs électrons actifs sont le plus souvent nécessaires mais restent encore très peu développées ou utilisées.

Cette thèse présente une théorie non perturbative pour décrire les processus multi-électroniques intervenant au cours des collisions ion-atome. Le traitement choisi est semiclassique en ce sens que le mouvement relatif cible-projectile est décrit par des trajectoires classiques (mouvement rectiligne uniforme), tandis que la dynamique électronique est traitée quantiquement, en résolvant de manière non perturbative l'équation de Schrödinger dépendante du temps. Cette dernière est résolue en développant la fonction d'onde électronique totale sur des états propres des partenaires isolés de la collision. Nous avons implémenté cette approche dans une nouvelle version du code informatique à deux électrons actifs, dans laquelle une stratégie optimisée d'évaluation des différents éléments de la matrice de couplage a été adoptée, de sorte qu'une réduction considérable des ressources informatiques, en mémoire et en temps CPU, puisse être atteinte. Le détail du cadre théorique de l'approche semi-classique non perturbative et de la mise en œuvre par ordinateur est présenté au Chapitre 2. À notre reconnaissance, c'est un code original et unique où deux électrons actifs dans un événement de diffusion peuvent être décrits avec l'approche SemiClassical Atomic Orbital Close-Coupling (SCAOCC) avec une telle efficacité de telle sorte l'on puisse atteindre une convergence très raisonnable des résultats. C'est très précieux pour l'interprétation des données au niveau le plus fondamental et également pour calculer des sections efficaces pour différentes applications, comme la physique des plasmas ou la radiobiologie. Cela nous a permis d'étudier divers systèmes de collision à plusieurs électrons pour lesquels des processus multi-électroniques sont probables et les corrélations électroniques jouent un rôle crucial.

Outre le développement long et complexe et les tests du code, les trois dernières années ont été spécialement consacrées à la compréhension de la physique d'événements spécifiques de diffusion. Nous avons entrepris l'étude de trois systèmes de collision aux caractéristiques différentes: par ordre d'apparition dans cette thèse,

(i) collisions ion-ion faiblement chargé avec une extrême importance de la corrélation électronique ($H^+ + H^-$),

(ii) collisions entre projectiles multiplement chargés et atome (C^{4+} + He) et

(iii) collisions He^+ + He avec un traitement original prenant en compte les trois électrons dans la dynamique.

Le choix de ces systèmes était guidé vers des systèmes benchmark pour lesquels des résultats expérimentaux et théoriques étaient disponibles (au moins dans certains domaines énergétiques), et présentaient des questions ouvertes, liées par exemple à de forts désaccords entre les données existantes. Nous avons essayé systématiquement de produire des résultats avec une convergence contrôlée permettant des interprétations physiques originales et fiables. Ces études ont été menées dans un très large domaine d'énergie, jusqu'à trois ordres de grandeur, avec la même description de collision (c'est-à-dire les mêmes ensembles de base), ce qui permet une continuité et une cohérence des prévisions. Les ingrédients importants pour décrire avec précision ces processus ont également été élucidés. De plus, nous avons fourni des interprétations convaincantes et argumentées des résultats et des mécanismes sous-jacents à l'origine des processus considérés.

Pour le système de collision $H^+ + H^-$ présenté au Chapitre 3, le processus de double capture électronique (DEC) est un défi pour les théoriciens depuis des décennies. Nous l'avons étudié avec une approche à deux électrons actifs entièrement corrélés. Nos calculs couvrent un vaste domaine d'énergie allant de 0.06 à 20 keV, couvrant ainsi les trois séries de données expérimentales disponibles. Contrairement à tous les calculs précédents, nos sections efficaces montrent une bonne concordance avec les résultats expérimentaux, à la fois en amplitude et en forme. Â Il convient de noter que nos sections efficaces calculées pour la capture simple et pour l'ionisation sont également en très bon accord avec les résultats expérimentaux disponibles. Décrire correctement ces processus dominants à un seul électron est en effet essentiel pour reproduire quantitativement la section efficace du DEC. De plus, nos résultats ab initio suggérent que les oscillations observées dans la section efficace de double capture ne proviennent pas d'interférences entre les voies covalente et ionique du système H_2, comme cela a été précédemment exposé, mais d'interférences entre la capture et des processus de transfert-excitation. Un mécanisme complexe impliquant un modèle moléculaire à trois états et deux croissements évités renforce notre interprétation. Les sections efficaces expérimentales pour les processus de transfert-excitation ne sont pas disponibles et nous espérons que nos résultats encourageront la poursuite des travaux expérimentaux pour confirmer notre interprétation.

Pour le système de collision C^{4+} + He présenté au Chapitre 4, les processus de capture à un et deux électrons (SEC et DEC) ont été étudiés en utilisant la méthode SCAOCC à deux électrons actifs. Tout d'abord, les sections efficaces SEC et DEC totales et sélectives en état final ont été calculées dans une vaste région d'énergie allant de 0.06 à 300 keV/u en utilisant une base unique et très large pour atteindre une convergence raisonnable et contrôlée. Nos calculs actuels concordent bien avec les mesures et calculs disponibles pour ces deux types de sections efficaces, à la fois en ce qui concerne la SEC et la DEC dans les régions parfois restreintes où ces précédentes études avaient été conduites. Nos prédictions étendent les résultats aux hautes énergies, en particulier au-delà de 3 keV/u, où nos calculs concordent bien mieux avec les données expérimentales que les calculs à bases moléculaires. De plus, grâce â des calculs modèles (mais non perturbatifs) que nous avons effectués, il a été observé que les corrélations électroniques jouent un rôle essentiel dans ce système de collision pour lequel les approximations du type “électrons indépendants” et “événements indépendants” sont bien trop simplistes et en mauvais accord avec nos calculs complets et les données expérimentales. Nous avons également démontré que, contrairement à ce qui avait été conclu lors d’études précédentes, le processus de la SEC est indépendant du processus de DEC dans la région des faibles énergies d’impact, où le processus de capture d’électrons vers $C^{3+}(2p)$ est dominé par un mécanisme direct. Aux hautes énergies où les résultats étaient rares, nous avons montré qu’un mécanisme en une étape domine la dynamique du DEC, en désaccord avec une étude précédente dans laquelle un mécanisme de transfert séquentiel avait été invoqué. Pour ce domaine énergétique, des travaux expérimentaux seraient utiles pour tirer des conclusions définitives et confirmer nos données. Dans une seconde étape, nous présentons également l’étude des sections efficaces différentielles angulaires pour les énergies d’impact de 0.8, 10, 40 et 100 keV/u. Nos calculs actuels concordent bien avec les résultats expérimentaux et théoriques disponibles á la plus basse énergie et étendent nos connaissances pour des énergies d’impact supérieures pour lesquelles il n’existe pas de résultat expérimental ou théorique. Nous avons montré que les oscillations observées dans les sections efficaces différentielles angulaires aux petits angles pour les SEC et DEC découlent du phénomène de diffraction du type Fraunhofer pour les processus électroniques directs, en une étape.

Pour le système de collision $He^{+} + He$ présenté au Chapitre 5, nous avons étudié les processus de transfert d’électrons en utilisant une approche SCAOCC à trois électrons, dans laquelle les calculs ont été effectués à l’aide d’un ancien code, non optimisé, développé dans le groupe et écrit pour gérer jusqu’à quatre électrons actifs. Premièrement, les sections efficaces totales et sélectives en état ont été calculées dans une région d’énergie allant de 1 à 225 keV/u et comparées aux résultats expérimentaux et théoriques disponibles : un très bon accord avec les expériences les plus récentes et les plus détaillées est observé. Des comparaisons de nos résultats avec d’autres calculs théoriques démontrent davantage l’importance d’une approche non perturbative et de la prise en compte la plus exacte possible de la corrélation électronique dans ce système. De plus, nous avons montré que les sections efficaces de transfert et d’excitation de la cible présentent une évolution non monotone en fonction de d'énergie: elle est attribuée à une forte compétition entre les processus de transfert-excitation de la cible et d'excitation du projectile. Deuxièmement, nous avons calculé les sections efficaces différentielles angulaires pour les trois processus de transfert vers l'état fondamental, l'excitation de la cible et le processus à deux électrons de transfert-excitation de la cible. Pour le premier processus, nos résultats sont en excellent accord avec les données expérimentales pour toutes les énergies d'impact considérées. De plus, les oscillations observées dans les sections efficaces différentielles pour les trois processus ont été interprétées de nouveau en termes d'un modèle simple basé sur la diffraction de type Fraunhofer et qui semble être valable pour les trois processus et toutes les énergies considérées dans ce travail. Le pic de Thomas a également été observé dans les sections efficaces différentielles pour le processus de transfert-excitation de la cible pour des énergies d'impact supérieures de 60 keVu. Dans ces dernier cas, le pic de Thomas se recouvre avec le premier maximum de type Fraunhofer et masque la structure oscillante liée à la diffraction.

En résumé, on peut affirmer que, grâce aux développements antérieurs du groupe et à ces trois années de travail, nous avons atteint une qualité jamais atteinte de la description des processus multi-électrons intervenant dans les collisions ion-atome. Nous avons en effet montré que nous avions obtenu des résultats en accord avec les données expérimentales. Cela ne signifie pas que des améliorations ne seront pas nécessaires à l'avenir, mais que le champ de recherche théorique est maintenant prêt à s'attaquer à l'étude de systèmes complexes pertinents pour les applications.

Ce travail et les développements qui ont été réalisés au cours de ces dernière années permettent d'envisager de nombreuses perspectives intéressantes. A court terme, le code de calcul orbital atomique semi-classique close-coupling à deux et trois électrons actifs peut être utilisé pour étudier un certain nombre de systèmes de collision importants en physique des plasmas, chauds et froids, impliquant des projectiles mono- et multi-chargés (par exemple, le tungstène à divers stades d'ionisation) entrant en collision avec des atomes d'hélium ou de lithium mais également aussi avec des cibles moléculaires simples (par exemple H_2.). De plus, nous pouvons également étudier les systèmes de collision impliquant des molécules diatomiques plus complexes, telles que O_2, N_2 et CO, en utilisant des potentiels de modèle pour décrire l'interaction électronique avec les noyaux (approximation du cœur gelé). Ces systèmes de collision ont suscité un vif intérêt car ils conviennent parfaitement aux travaux expérimentaux, mais n'ont pu faire l'objet, à quelques exceptions près, qu'à des travaux théoriques approchés.

D'autre part, à plus long terme, nous aimerions étendre notre code de collision à plusieurs électrons actifs et cibles multicentriques, c'est-à-dire permettant de traiter des molécules plus complexes, au-delà des molécules diatomiques. En fait, le code actuel est prêt pour ce développement, car le codage pour les évaluations de tous les éléments de la matrice de couplage est déjà fait. Cependant, le temps d'ordinateur prohibitif de ce type de calculs nécessitera une optimisation supplémentaire et une nouvelle stratégie, notamment pour la construction des ensembles de base. Ce code trouverait de nombreuses applications: un candidat idéal est bien sûr l'étude des collisions entre ions et molécules H_2O. Comme ce dernier représente 70% (en masse) du corps humain et qu'il est l'une des espèces les plus abondantes de l'univers, la compréhension des mécanismes fondamentaux intervenant lors des collisions avec un ion revêt donc une importance considérable, notamment en radiobiologie et en astrophysique.

Un autre objectif pour de futurs développements (également liés à la construction des bases de calcul) est la description du processus d'ionisation par la génération et l'utilisation plus contrôlées de pseudo-états d'énergie positive ou se situant au-dessus de seuils d'ionisation. Par exemple, la récente approche de discrétisation du continuum en paquets d'onde développée par un groupe australien permet de générer des pseudo-états avec des énergies et des distributions définies. La mise en œuvre de ce type de méthode, qui couvre de manière rigoureuse le continuum, dans notre approche à électrons actifs multiples, améliorera la précision des calculs et étendra la plage de prévisibilité de notre code aux énergies d'impact plus élevées et aux processus d'ionisation. Elle permettrait de produire des résultats de référence pour des systèmes étudiés jusqu'à maintenant à l'aide de modèles extrêmement approchés.

Chapter 1

Introduction

Within the vast field of atomic physics, the study of the collisions between ion with atom/molecule has been for one of the most active areas of research. The electronic processes occurring in the course of collisions between projectile (P) and target (T) particles[1] are classified according to the final state of the collision partners; they are defined as follows,

— the elastic process: the internal energies of T and P do not change, but the incident particles are deflected through a certain angle,

$$P + T \to P + T. \tag{1.1}$$

— the excitation: it is characterized by a modification of the internal energy of at least one of the collision partners with the promotion of one electron to an orbital of higher energy,

$$\begin{aligned} P + T &\to P + T^{*} \\ &\to P^{*} + T. \end{aligned} \tag{1.2}$$

— the electron ionization: in this category, one or both collision partners are ionized with the ejection of one electron, leaving a positive ion, or ions,

$$\begin{aligned} P + T &\to P + T^{+} + e^{-} \\ &\to P^{+} + T + e^{-}. \end{aligned} \tag{1.3}$$

— the electron capture (also named as electron transfer, charge transfer, or charge exchange): one or more electrons is transferred from one collision

---

[1] P and T can be atoms or molecules, neutral or in an ionic state.

partner to the other, in ground or excited state,

$$P + T \rightarrow P^- + T^+. \tag{1.4}$$

It should be noted that more complex electronic processes combined by several of these elementary processes also exist, as for example, the transfer-excitation and double transfer processes,

$$P + T \rightarrow P^- + T^{+*}, \tag{1.5}$$

$$P + T \rightarrow P^{2-} + T^{2+}. \tag{1.6}$$

These electronic processes occurring in the course of atomic and molecular collisions take place at the ångstrom and femtosecond [2] scales but play an important role in the temporal evolution and in the physical and chemical properties of macroscopic complex systems. The understanding of these electronic processes and the detailed knowledge of the corresponding cross sections present therefore a great interest in various domains.

In astrophysics, X-rays should be generated throughout the heliosphere as a consequence of electron transfer collisions between highly charged solar wind ions, such as O^{7+}, N^{6+}, C^{5+}, Fe^{12+}, *etc.* and interstellar neutrals. The high charge state solar wind ions resulting from these collisions are left in highly excited states and emit extreme ultraviolet or soft X-ray photons. This solar wind charge exchange mechanism applied to cometary neutrals has been used to explain the soft X-ray emission observed from comets [1]. As shown in Figure 1.1, the scheme of the solar wind and comet interaction is presented, the electronic processes are likely to occur in the collision between a heavy solar wind ion O^{7+} and a cometary neutral water molecule,

$$O^{7+} + H_2O \rightarrow O^{6+*} + H_2O^+. \tag{1.7}$$

This process is followed by the decay of the excited O^{6+*}, with emission of one or more photons. For example, the emission lines appear in the Chandra X-ray Observatory spectrum of comet C/LINEAR 1999 S4 measured near 560 eV [1, 2] is certainly a combination of the two O^{6+} lines: O^{6+} $(1s2p \rightarrow 1s^2)$ at 568.4 eV, and O^{6+} $(1s2s \rightarrow 1s^2)$ at 560.9 eV. The charge exchange mechanism mentioned above successfully explains the observations in astrophysics.

---

[2] for collisions in the keV energy range which will be considered in the foillowing.

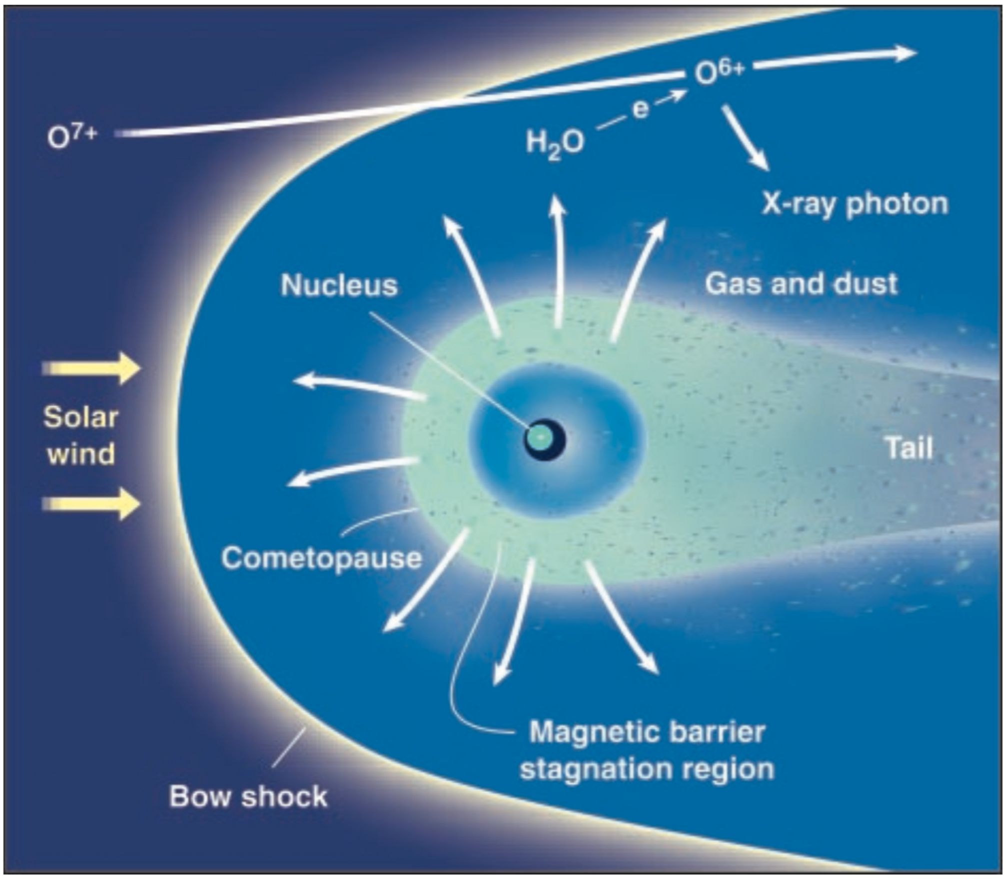

Figure 1.1 – Scheme of the solar wind and comet interaction [1]. An electron capture process occurring in the collision between a heavy solar wind ion and a cometary neutral water molecule, followed by the emission of an x-ray photon. The Sun is toward the left.

In the fusion plasmas, charge exchange spectroscopy provides an excellent diagnostic to investigate the concentration of impurities or the temperature distribution of the edge plasma region via the use of optical transitions that follow electron capture from a neutral atom into excited states of an impurity ion. (see [3] and references therein). As an example, at the poloidal divertor tokamak Axially Symmetric Divertor Experiment (ASDEX) Upgrade (shown in Figure 1.2) [4], a neutral lithium beam [5] is used for edge plasma analysis, where the measurements of the ion temperatures of carbon and helium are based on the following electronic reactions,

$$\begin{aligned}
&Li + He^{2+} \rightarrow Li^{+} + He^{+*} \\
&He^{+*} \rightarrow He^{+'} + hv \quad (n = 4 \rightarrow n = 3, \lambda = 468.5\,nm) \\
&Li + C^{6+} \rightarrow Li^{+} + C^{5+*} \\
&C^{5+*} \rightarrow C^{5+'} + hv \quad (n = 8 \rightarrow n = 7, \lambda = 529.0\,nm),
\end{aligned} \tag{1.8}$$

where λ is the observed wavelength of the emission lines.

Another example is the hadron therapy in medical sciences [6, 7]. This is an

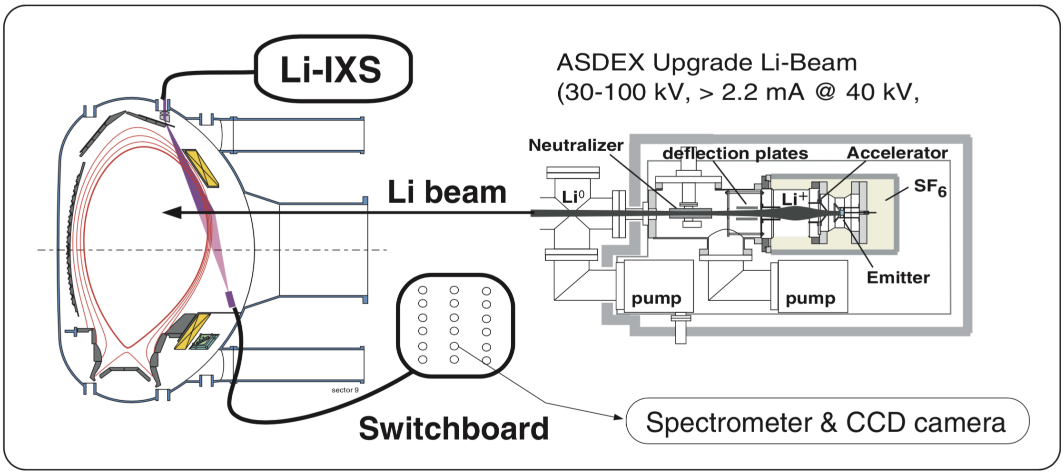

Figure 1.2 – Lithium beam at Axially Symmetric Divertor Experiment (ASDEX) Upgrade, injector set-up, injection geometry and observation diagnostics (schematic) [4].

innovative technique to cure cancer, killing radioresistant and inoperable cancer cells by irradiating them with a beam of particles, mainly protons but also fully stripped carbon ions. The energy transfer between the ions and the biological molecules is essential to this cancer therapy.

On the other hand, from the fundamental point of view, these collisions are the optimal "laboratories" for the study of many-body quantum systems and of their dynamics. The fundamental and applied aspects which concern the collisions have therefore stimulated the rise of a rich domain of research which led naturally in the nineties to the continuous development of experimental and theoretical methodologies, extending to new fields such as astrophysics, i.e., the study of the interactions of matter with strong and ultra-short lasers. On the theoretical point of view, important theoretical efforts have been pursued from the start of the quantum mechanics to understand and model collision systems: from simple treatments such as Thomas [8] or Landau-Zener [9, 10] models to elaborate quantum approaches (quantum mechanical close-coupling appraoches [11, 12]). In fact, the cross sections of the electronic processes depend strongly on the impact energy (velocity) and three characteristic regions can be defined according to the value of the ratio between the velocity of the projectile v_p and the velocity of the electrons of target v_e. Note that these domains correspond also to different theoretical approaches. Therefore, it is useful to make distinctions between low-, intermediate-, and high-energy region according to whether $v_p/v_e \ll 1$, $v_p/v_e \approx 1$, or $v_p/v_e \gg 1$, respectively. As shown in Figure 1.3, the theoretical descriptions of electronic transitions in the collisions can also be classified into three categories:

- $v_p/v_e \ll 1$. In the low-energy region, electron capture processes are dominant. The collision can be described by the electronic states of the transient molecule formed by the two collision partners [13, 14]. Electronic transitions then take place through the degenerate (or quasi-degenerate) region between

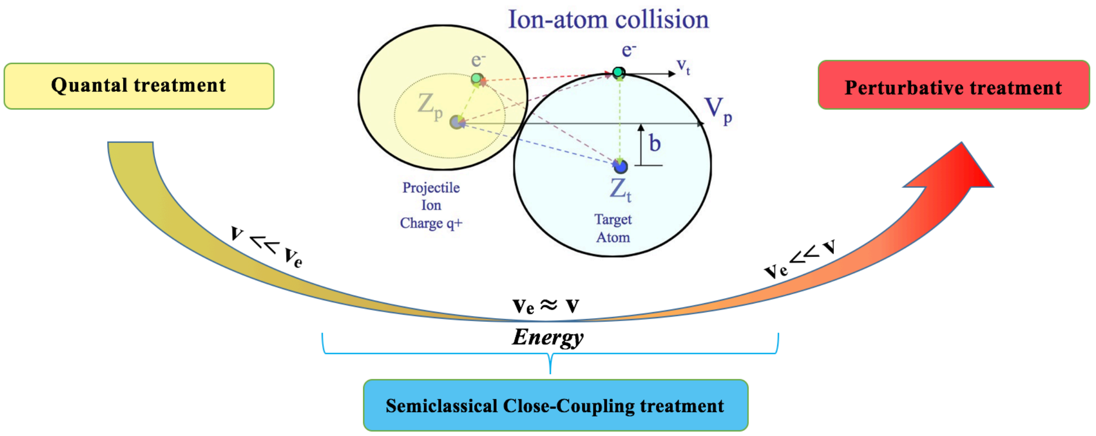

Figure 1.3 – Schematic diagram of different theoretical treatments that can be applied in the corresponding impact energy region.

the initial and final molecular states during the collision, i.e. at avoided crossings between the molecular curves corresponding to these states. Quantal calculations, non-perturbative molecular descriptions in which both the projectile and electronic motions are described quantum mechanically, are necessary.

— $v_p/v_e \gg 1$. In the high-energy region, excitation and ionization dominate. The interaction time between two collision partners is extremely short (attosecond) and the projectile is seen to act as a small perturbation on the target wavefunction. The approaches, which are based on simple forms of perturbation theory such as first-order Born approximation [15] or elaborate Continuum Distorted Wave-Eikonal Initial State (CDW-EIS) method [16], are adequate to lead to accurate scattering cross sections.

— $v_p/v_e \approx 1$. At intermediate energies, a number of channels such as electron transfer, excitation and ionization are populated with comparable strength and likely to happen in a coupled way. Classical and semi-classical nonperturbative treatments are then necessary. The latter one, which is unavoidable in this energy domain but often difficult to implement particularly when interest is in detailed results like the population of projectile or target subshells, is presented in more detail in the Chapter 2 of this thesis. The classical trajectory Monte Carlo (CTMC) methods, which describe the dynamics of all the particles in a classical way developed initially by R. Abrines and I. C. Percival [17], have the advantage to be simply implemented and extended by some approximations to the study of multi-electronic systems [18].

To date, one can state that mono-electronic processes, such as single electron capture, excitation and ionization, are now well understood for ion-atom collision systems where the electronic correlations do not play an important role. However, this is not true for systems in which:

— a large number of channels are open and likely to happen in a coupled way, particularly when multi-electronic processes are likely to occur and compete with mono-electronic ones.

— the role of electronic correlations is important so that a coherent correlation treatment is required, beyond the usual independent electrons or events approximations.

— molecular partners are involved, where the geometry and multi-center features of the collision systems must be considered.

It still remains a challenge for theoreticians to understand and model multiple and even two electrons collision systems. In particular, in the intermediate impact energy region, perturbative approaches and the use of model potential to describe correlations in an average way may be inadequate due to the strong couplings between various channels and electronic correlation effects. The challenge is not just confined in the atomic and molecular collisions, but also presented in the study of many-body quantum systems and of their dynamics, with or without strong and ultra-short laser interactions. Consequently, non perturbative two- and multi-active-electron semi-classical or quantum approaches are still required.

In this context, we have studied the electronic processes occurring in the course of atomic and molecular collisions in the intermediate energy range (0.06-300 keV/u). We have used a semi-classical non perturbative approach developed and implemented in the group for many years [19–21]. During this thesis, a new version of two-active-electron computer code based on this approach has been developed by using an optimized strategy for the evaluations of different coupling matrix elements [22–24]. A considerable reduction of computer resources demanding in memory and CPU time was achieved. We have applied the computer code on the study of electronic processes in various collision systems. The objective is to bring in new cross sections and provide further physical insight into the understanding of these collision systems. The present thesis is organized as follows.

In Chapter 2, we present the theoretical framework of the semi-classical non perturbative approach. The impact parameter approximation is applied to establish the electronic time-dependent Shrödinger equation (TDSE) (also named eikonal equation (equation (2.23)) describing collision systems composed of two nuclei (or nuclei with frozen core electrons) and two active electrons. A semi-analytical method is adopted to solve the TDSE, which is based on the expansion of the electronic wavefunction on a set of analytically well-defined functions in the Hilbert's space. The end of this Chapter will be dedicated to the computer implementation of our theoretical approach.

In Chapter 3, we have applied our fully correlated two-active-electron semi-classical non perturbative approach to the study of $H^+ + H^-$ collision system, where the main attention is focus on the double electron capture (DEC) process. Our calculated cross section reproduces in an unprecedented way the experimental ones in both magnitude and overall oscillatory structure. The ingredients needed to describe accurately the DEC process in such a complex system have also been elucidated. Furthermore, our investigation suggests that the observed oscillations in the DEC cross sections come from a more complex mechanism than the one discussed so far.

Chapter 4 is devoted to the study of single electron capture (SEC) and double electron capture (DEC) processes in C^{4+} + He collision system. The system still remains challenging due to the electronic correlations and strong couplings of many channels. We use a large basis set within our semi-classical non perturbative approach, ensuring a controlled convergence of the cross sections, which are in very good agreements with experiments for both total and state-selective SEC and DEC processes. In order to provide further physical insight on this collision system, the mechanisms giving rise to SEC and DEC have been further studied and discussed. Furthermore, the angular-differential cross sections for SEC and DEC are presented to give a sharper probe of process mechanisms. The observed oscillatory structures in these cross sections have also been investigated by simulated Frauhofer-type diffraction patterns.

In Chapter 5, an extended three-active-electron approach has been applied on the investigation of He^{+} + He collisions. Although there are only three electrons involved, the system are sufficiently complex to give rise to the main types of inelastic reactions observed in ion-atom collisions. In this Chapter, total, state-selective cross sections from a converged calculations for various electronic processes, i.e., ground-state transfer, transfer to excited state, target-excitation, projectile-excitation as well as electron-transfer-target-excitation, have been presented and directly compared with available experimental and theoretical results. The structures observed in these cross sections have been further discussed and interpreted. In addition, we have also presented the angular-differential cross sections to provide the analysis of the spatial selectivity. More importantly, the oscillatory structure observed in the angular-differential cross sections has been interpreted from a simple model.

The conclusions and perspectives will be given in the end. Atomic units will be used throughout, unless explicitly indicated otherwise.

Chapter 2

The semiclassical non perturbative approach

2.1 Introduction

In atomic and molecular physics, the study of ion-atom/molecule collisions has a long tradition. From the start of quantum mechanics, the theoretical treatments relating to the collisions have been the subject of numerous books and publications, see for example [25–28]. The atomic and molecular collision systems are genuinely described by the time-independent Schrödinger equation, with specific asymptotic (dissociative) conditions. On the contrary to the stationary cases, it is generally impossible to treat exactly the dynamics of them, even for the simplest one, the H^+ - H collision system. It is therefore clear that the description of electronic processes occurring during a collision can only be made by using approximations, which are generally relevant within a specific impact energy domain. In the present thesis, we have studied the electronic processes occurring in the course of ion-atom/molecule collisions in a wide energy domain ranging from about 100 eV/u to several hundreds of keV/u. In this context, semiclassical methods are the most used approaches by making use of the fact that, the *de Broglie* wavelength associated with the relative motion of the heavy particle is very small compared with the distance over which the interaction takes place. Then the heavy-particle motion follows a classical trajectory; only the electronic motion needs to be treated quantum mechanically.

In this Chapter, we shall describe the semiclassical non perturbative approach used in the thesis. The approach is well established as the standard method in the description of inelastic processes in ion-atom/molecule collisions at intermediate energies (see the pioneering work of [29]), where, an atomic orbital (AO) expansion of the electronic wavefunction is frequently regarded as appropriate for collisions [30]. Since the interplay between many open channels are taken into account through a non perturbative treatment, our approach is also named semiclassical atomic orbital close-coupling (SCAOCC) method. We have adopted the impact parameter approximation in the method. This approximation allows to transform the time-independent Schrödinger equation of the complete system to the time-dependent Schrödinger equation for the electrons in the field of moving nuclei, which is also called eikonal equation, by analogy with the optics. The outline of this development will be presented in the next section of this Chapter. It should be noted that we will describe our approach in a general way for both ion-atom and ion-molecule collisions, where the multi-center feature has also been implemented in the new version of two-active-electron computer code, though only the investigations of ion-atom collisions are considered in this thesis. In the third section of this Chapter, we present the method used to solve the eikonal equation for two-active-electron system. It is followed by the computer implementation of our theoretical approach in section 2.4. Finally, the computational methods for total and differential cross sections will be presented.

2.2 The eikonal equation

In general, the ion-atom/molecule collision system can be described by the time-independent Schrödinger equation, which, in the inertial reference frame, is written as,

$$\hat{H}^{tot}\Psi_{sys} = E^{tot}\Psi_{sys}, \tag{2.1}$$

where $\hat{H}^{tot}$ is the total Hamiltonian of the system, and E^{tot} is the corresponding energy. The Hamiltonian is commonly expressed as the sum of the kinetic and potential energies operators of the system in the form (expressed in a.u.),

$$\hat{H}^{tot} = \hat{T} + \hat{V} \tag{2.2}$$

with

$$\hat{T} = \sum_{I=1}^{n_N} -\frac{1}{2M_I}\, \bigtriangledown^2_{R_I} + \sum_{i=1}^{n_e} -\frac{1}{2}\bigtriangledown^2_{r_i}, \tag{2.3}$$

$$\hat{V} = \sum_{I=1}^{n_N}\sum_{i=1}^{n_e} V_{Ii} + \sum_{I=1}^{n_N}\sum_{J=I}^{n_N} V_{IJ} + \sum_{i=1}^{n_e}\sum_{j=i}^{n_e} V_{ij}, \tag{2.4}$$

where $\vec{R}_I$ and $\vec{r}_i$ are the positions of nuclei (of mass M_I) and electrons (of mass m_e=1 a.u.), respectively. The potential energy operator including the interactions of all the particles together, consists of three parts: the "core-electron" interactions V_{Ii}, the internuclear interactions V_{IJ} and interelectronic interactions V_{ij}. For simplicity, we will present, in the following, the treatment for ion-atom and ion-molecule (diatomic molecules will be used as an example) collisions in the formalism with two active electrons. The atomic physicists are known to count one, two, and then many and we think indeed that the development of the formalism for two-electron systems is sufficient to give a general insight of the multi-electron problem. Moreover, we will place ourselves in the infinite nuclear mass approximation, i.e., the mass of electrons will be neglected with respect to that of the nuclei. The Hamiltonian is then expressed for ion-atom collisions by,

$$\hat{H}^{tot} = -\frac{1}{2}\bigtriangledown^2_{r_1} - \frac{1}{2}\bigtriangledown^2_{r_2} - \frac{1}{2\mu_{TP}}\bigtriangledown^2_{R} - \frac{1}{2M_{tot}}\bigtriangledown^2_{R_G} + \hat{V} \tag{2.5}$$

and for ion-molecule collisions,

$$\hat{H}^{tot} = -\frac{1}{2}\bigtriangledown^2_{r_1} - \frac{1}{2}\bigtriangledown^2_{r_2} - \frac{1}{2\mu_{TP}}\bigtriangledown^2_{R} - \frac{1}{2\mu_{AB}}\bigtriangledown^2_{R_{AB}} - \frac{1}{2M_{tot}}\bigtriangledown^2_{R_G} + \hat{V}, \tag{2.6}$$

where $\vec{R}_G$ is the position of the center of mass for the total system. The masses μ_{TP}, μ_{AB}, and M_{tot} are defined as

$$\begin{aligned} \mu_{TP} &= \frac{M_T M_P}{M_T + M_P}, \qquad \mu_{AB} = \frac{M_A M_B}{M_A + M_B}, \\ M_{tot} &= M_T + M_P \end{aligned} \tag{2.7}$$

and, for ion-molecule collisions, $M_T = M_A + M_B$, the subscripts T, P, A and B denoting the target, projectile, and the two nuclei of the molecular target, respectively.

The internal kinetic energy $\hat{T}^{int}$ relies only on the internal coordinates, so that $\hat{T}$ in equation (2.2) can be rewritten as

$$\hat{T} = \hat{T}^{int} - \frac{1}{2M_{tot}} \nabla^2_{R_G} . \tag{2.8}$$

As a consequence of that, the system Hamiltonian can be separated by

$$\hat{H}^{tot} = \hat{H}^{int}(\vec{r}_1, \vec{r}_2, \vec{R}) - \frac{1}{2M_{tot}} \nabla^2_{R_G} . \tag{2.9}$$

The Schrödinger equation then separates and can be written in the form of,

$$\hat{H}^{int}\Psi_{int} = E^{int}\Psi_{int} \tag{2.10}$$

$$-\frac{1}{2M_{tot}} \nabla^2_{R_G} \Psi_G = E^G \Psi_G \tag{2.11}$$

with

$$\Psi_{sys} = \Psi_{int}\Psi_G, \qquad E^{sys} = E^{int} + E^G, \tag{2.12}$$

where $\Psi_G = e^{i\vec{k}_G \cdot \vec{R}_G}$ describes the motion of a free particle, and $E^G = k_G^2/2M_{tot}$ is the corresponding kinetic energy.

After separating the variables from the center of mass, the internal Hamiltonian for ion-atom is expressed as,

$$\hat{H}^{int} = -\frac{1}{2} \nabla^2_{r_1} - \frac{1}{2} \nabla^2_{r_2} + \hat{V} - \frac{1}{2\mu_{TP}} \nabla^2_R \tag{2.13}$$

and for ion-molecule,

$$\hat{H}^{int} = -\frac{1}{2} \nabla^2_{r_1} - \frac{1}{2} \nabla^2_{r_2} + \hat{V} - \frac{1}{2\mu_{TP}} \nabla^2_R - \frac{1}{2\mu_{AB}} \nabla^2_{R_{AB}} . \tag{2.14}$$

In the keV/u energy range, the electronic processes take place in a time range much shorter (subfemtosecond) than the vibrational and rotational motions of any molecule ($> 10fs$). Making use of this fact, the rovibrational sudden approximation, in which the nuclei of the molecular target are frozen during the collisions stage (i.e., fixed internuclear distance R_{AB}), is used in our approach for the ion-molecule collisions. Consequently, the vibrational kinetic energy operator $-\frac{1}{2\mu_{AB}}\nabla^2_{R_{AB}}$ associated with the motion of molecular nuclei can be neglected. Thus, equations (2.13) and (2.14) can be rewritten in a general form,

$$\hat{H}^{int} = \hat{H}^{el} - \frac{1}{2\mu_{TP}} \bigtriangledown_R^2 \tag{2.15}$$

with the electronic Hamiltonian,

$$\hat{H}^{el} = -\frac{1}{2} \bigtriangledown_{r_1}^2 - \frac{1}{2} \bigtriangledown_{r_2}^2 + \hat{V}. \tag{2.16}$$

In addition, the nuclear masses are much larger than that of electrons so that the kinetic energy $(-\frac{1}{2\mu_{TP}} \bigtriangledown_R^2)$ associated with target and projectile relative motion is significantly larger than the internal (electronic) energy of the system for the keV/u impact energy range. This allows us to consider that the relative motion of nuclei is independent with that of electrons. Therefore, the Ψ_{int} can be approximately written as,

$$\Psi_{int} = \Xi(\vec{R})\Psi(\vec{R}, \vec{r}_1, \vec{r}_2). \tag{2.17}$$

Under the framework of this approximation, the dependence on $\vec{R}$ is mainly contained in $\Xi(\vec{R})$ so that the term $\bigtriangledown_R^2 \Psi(\vec{R}, \vec{r}_1, \vec{r}_2)$ is negligibly small [25]. Moreover, In the impact energy domain under consideration, scattering is predominantly in the forward direction with respect to the initial direction of the projectile. This suggests to express the function $\Xi(\vec{R})$ in the approximate form of a plane wave [28],

$$\Xi(\vec{R}) = e^{i\vec{k}\cdot\vec{R}} \tag{2.18}$$

with the wave vertor

$$\left|\vec{k}\right| = \sqrt{2\mu_{TP} E^{int}}. \tag{2.19}$$

Using equations (2.15-2.19), the Schrödinger equation (2.10) becomes,

$$\left[\hat{H}^{el} - \frac{i}{\mu_{TP}} \vec{k} \cdot \vec{\bigtriangledown}_R\right] \Psi = 0. \tag{2.20}$$

Let us now apply to our approach the impact parameter approximation, which is validate since the *de Broglie* wavelength associated with the relative motion of the heavy particle is very small compared with the distance over which interaction takes place. As a consequence of the previous approximations, it is then coherent to describe the relative heavy particle motion as classical trajectories, in the straight-line, constant velocity approximation,

$$\vec{R}(t) = \vec{b} + \vec{v}_P t, \tag{2.21}$$

where $\vec{b}$ is the impact parameter and $\vec{v}_P$ is the relative velocity between target and projectile, with

$$\vec{v}_P = \frac{1}{\mu_{TP}} \vec{k}. \tag{2.22}$$

It should be noted that, as the collision geometries shown in Figure 2.1, for clarity we locate the origin of the reference on the center of mass of the target, this does

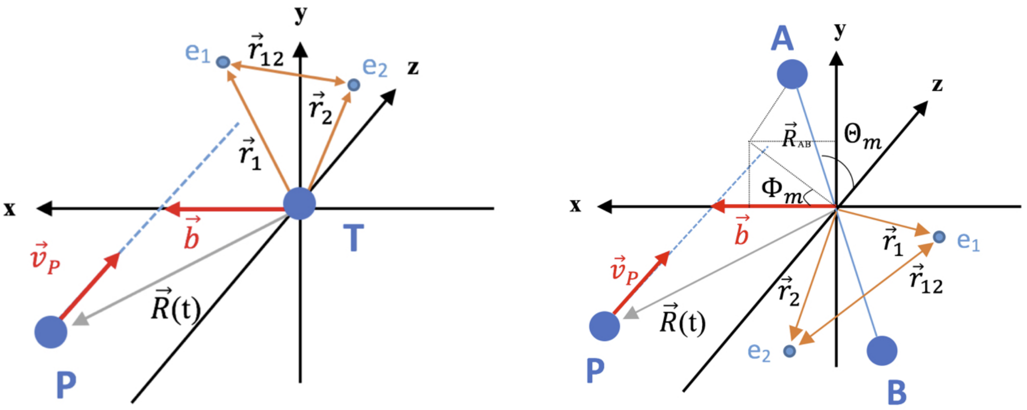

(a) ion-atom collisions (b) ion-molecule collisions

Figure 2.1 – Collision geometry. (a) The impact parameter $\vec{b}$ and velocity $\vec{v}_P$ define the collision plane (xz) and $\vec{R}(t)$ the projectile (P) trajectory with respect to the target (T). The positions of two electrons with respect to the target center of mass are denoted $\vec{r}_1$, $\vec{r}_2$, and $\vec{r}_{12}$ is the relative vector between the two electrons. (b) Same as (a), but for molecular target, where $\vec{R}_{AB}$ is the internuclear vector of the molecular target; the angles (Θ_m, Φ_m) define the molecular orientation with respect to $\vec{v}_P$ and $\vec{b}$. Note that for clarity we locate the origin of the reference on the center of mass of target; this does not restrict the generality of our results which are Galilean invariant.

not restrict the generality of our approach, which is Galilean invariant. The impact parameter $\vec{b}$ and velocity $\vec{v}_P$ define the collision plane (xz) and $\vec{R}(t)$ is the projectile trajectory with respect to the target. The positions of two electrons with respect to the target center are denoted $\vec{r}_1$, $\vec{r}_2$, and $\vec{r}_{12}$ is the relative vector between the two electrons. For the molecular target in Figure 2.1(b), $\vec{R}_{AB}$ is the internuclear vector of the molecular target. The angles (Θ_m, Φ_m) define the molecular orientation with respect to $\vec{v}_P$ and $\vec{b}$.

The insertion of equation (2.21) into equation (2.20) results in a time-dependent Schrödinger equation describing the dynamics of electrons in the collision system, and is finally written as,

$$i\hbar \frac{\partial}{\partial t} \Psi = \hat{H}^{el} \Psi, \tag{2.23}$$

which is the so-called eikonal equation. It should be noted that the b-dependent phase (i.e., common phase due to the "core-core" interaction (V$_{TP}$ or V$_{AP}$ and V$_{BP}$) in the Hamiltonian [31]) plays an important role in computing the angular differential cross sections which will be presented in section 2.5.2. In the following, the method used to solve the eikonal equation will be presented, as well as the definition of the total and angular differential cross sections of the electronic processes occurring in the course of ion-atom/molecule collisions.

2.3 Solving the eikonal equation

The time-dependent Schrödinger equations is not generally solvable in closed forms. From the beginning of modern quantum mechanics, significant theoretical efforts have been devoted to finding efficient and accurate numerical procedures to solve this equation. Most of them involve the use of grid methods, which were initially developed for nuclear collisions [32–35], and gradually adapted to the description of ion-atom collisions [36, 37], and then widely used in the study of the interactions between atoms/molecules and intense laser fields [38–41]. Recently, as the increase of the computer performance, the methods have been applied again in the collision field [42–44]. The grid methods are based on the discretization of time and space using the finite-difference methods, which are totally numerical without providing the analytical solution of the wavefunction but its value on a spatial grid, for a given time. However, the grid methods are not efficient enough so that the implementation is generally limited to the systems for which the spatial dimensions are reduced to one or two dimensions. Therefore, the description for a collision system with two or multiple active electrons in the three-dimensional space are absolutely not possible for now. In this context, a semi-analytical method is adopted to solve the eikonal equation in this thesis. The method is based on the expansion of the electronic wavefunction on a set of analytically well-defined functions in the Hilbert's space. These functions should span a large enough - however finite - space in order to obtain the convergence of the results. The expansion coefficients are then solutions of a system of first-order coupled differential equations derived from the matrix expression of the eikonal equation. The time evolution of the system is treated numerically in order to obtain the final transition probabilities and cross sections of the electronic processes. This semi-analytical method that we shall call it Hilbert basis method in this thesis, has already been successfully applied to the study of the single- [24, 25, 28, 45–47] and two-active-electron [23, 48, 49] collision systems where the inter-electronic interactions are considered exactly in the latter cases.

In the following, we will present the formalism of the Hilbert basis method for a two-active-electron collision system, which we have used and implemented in the new version of the computer code.

2.3.1 The asymptotic states

We shall treat a collision system which consists of a projectile ion P and a two-active-electron target T [1]. At large separations, the interactions between T and P are negligible small so that the target and projectile can be considered isolated. Thus, three asymptotic conditions are possible for the collision system:

— Before the collision, the two electrons are attached to the target T, where the electronic state Φ_i^{TT} satisfies the Schrödinger equation,

$$\hat{H}_{el}^{TT}\Phi_i^{TT}(\vec{r}_1,\vec{r}_2) = E_i^{TT}\Phi_i^{TT}(\vec{r}_1,\vec{r}_2), \tag{2.24}$$

---

[1] We have chosen to illustrate the method through this kind of systems, though totally general and dealing with systems where one electron is located on each center initially.

where $\hat{H}_{el}^{TT}$ is the Hamiltonian that describes the $T + 2e^-$ system, and E_i^{TT} is the corresponding energy;

— After the collision, if only one electron is captured by the projectile, and the other remains on the target. The electronic state can be expressed as a product of wavefunction of two asymptotic subsystem $(T+e^-)$ and $(P+e^-)$, both of which satisfy the Schrödinger equation,

$$\hat{h}_{1(2)}^{T(P)}\Phi_{i(j)}^{T(P)} = \varepsilon_{i(j)}^{T(P)}\Phi_{i(j)}^{T(P)}, \tag{2.25}$$

where $\hat{h}_{1(2)}^{T(P)}$ is the Hamiltonian that describes the $T+e^-$ (or $P+e^-$) system, and $\varepsilon_{i(j)}^{T(P)}$ is the corresponding energy;

— If the two electrons are captured to the projectile $(P + 2e^-)$, where the electronic state Φ_i^{PP} satisfies the Schrödinger equation,

$$\hat{H}_{el}^{PP}\Phi_i^{PP}(\vec{r}_1, \vec{r}_2) = E_i^{PP}\Phi_i^{PP}(\vec{r}_1, \vec{r}_2), \tag{2.26}$$

where $\hat{H}_{el}^{PP}$ is the Hamiltonian that describes the $P + 2e^-$ system, and E_i^{PP} is the corresponding energy.

To solve the eikonal equation (2.23), the wavefuction can be expanded on a basis set of states of isolated collision partners, which are composed of these asymptotic states.

2.3.2 The description of electronic wave function

In our approach, the states of the isolated collision partners of target and projectile (the asymptotic states mentioned above) are described by linear combinations of spin-adapted (singlet or triplet) products of Gaussian-type orbitals (GTOs) centered on the target or projectile. In the spherical coordinates, the GTOs are defined as:

$$G_{\alpha,l,m}(\vec{r}) = Y_{l,m}(\vec{r})r^l e^{-\alpha r^2}, \tag{2.27}$$

where $Y_{l,m}(\vec{r})$ is the spherical harmonics functions. The one-electron states of the target and projectile are then written as the weighted sum of the GTOs,

$$\phi(\vec{r}) = \sum_i^N c_i G_{\alpha_i,l_i,m_i}(\vec{r}), \tag{2.28}$$

and the two-electron states of the target and projectile are defined as,

$$\Phi(\vec{r}_i, \vec{r}_2) = \sum_i^N \sum_{j=i}^N C_{ij}[G_{\alpha_i,l_i,m_i}(\vec{r}_1)G_{\alpha_j,l_j,m_j}(\vec{r}_2) \pm G_{\alpha_j,l_j,m_j}(\vec{r}_1)G_{\alpha_i,l_i,m_i}(\vec{r}_2)], \tag{2.29}$$

where the symmetry of the states depends on the spin state of the collision system, the sign + and − are given for the singlet (symmetry) and triplet (anti-symmetry), respectively. The coefficients c_i and C_{ij} are obtained respectively by the diagonalization on a set of GTOs of the Hamiltonian for one- and two-electron states of the isolated target (or projectile) considered.

Thus, the total electronic wave function $\Psi(\vec{r}_i, \vec{r}_2, t)$ for the collision system can be expressed as a sum of N_T (N_P) one-electron states and N_{TT} (N_{PP}) two-electron states of the target (projectile),

$$\begin{aligned}
\Psi(\vec{r_1}, \vec{r_2}, t) = &\sum_{i=1}^{N_{TT}} c_i^{TT}(t)\Phi_i^{TT}(\vec{r_1}, \vec{r_2})e^{-iE_i^{TT}t}F^T(\vec{r_1})F^T(\vec{r_2}) \\
&+ \sum_{j=1}^{N_{PP}} c_j^{PP}(t)\Phi_j^{PP}(\vec{r_1}^P, \vec{r_2}^P)e^{-iE_j^{PP}t}F^P(\vec{r_1})F^P(\vec{r_2}) \\
&+ \sum_{k=1}^{N_T}\sum_{l=1}^{N_P} c_{kl}^{TP}(t)\Big[\phi_k^T(\vec{r_1})\phi_l^P(\vec{r_2}^P)F^T(\vec{r_1})F^P(\vec{r_2}) \\
&\pm \phi_k^T(\vec{r_2})\phi_l^P(\vec{r_1}^P)F^P(\vec{r_1})F^T(\vec{r_2})\Big]e^{-i(\varepsilon_k^T+\varepsilon_l^P)t},
\end{aligned} \tag{2.30}$$

where T (P) and TT (PP) superscripts denote states and corresponding energies for which one and two electrons are on the target (projectile), respectively. The time evolution of the wave function is carried by the coefficients $c_i^A(t)$ ($A = TT, TP$, and PP). When $t \to infinity$ (the target and projectile are separated infinitely), these coefficients correspond to the amplitudes of the transition probabilities. As shown in Figure 2.1, the center of mass of the target locates at the origin of the reference, and the projectile is moving as a classical straight-line trajectory with a velocity v_P. Obviously, at infinite separations after the collision, if an electron in a bound state is attached to the projectile, then the corresponding wavefunction carries an additional linear momentum as well as associated kinetic energy. It is the reason why, the electronic translation factors (ETF) $F^{T(P)}(\vec{r}_{1(2)})$ are introduced in equation (2.30), ensuring Galilean invariance of the results and to remove spurious dipolar coupling terms in the final equations to be solved [25]. In the frame of reference shown in Figure 2.1, the ETF can be defined as,

$$\begin{aligned}
&F^T(\vec{r}_{1(2)}) = 1, \\
&F^P(\vec{r}_{1(2)}) = e^{-\frac{i}{2}v^2t}e^{i\vec{v}\cdot\vec{r}_i}.
\end{aligned} \tag{2.31}$$

It should be noted that the form of $F^{T(P)}(\vec{r}_{1(2)})$ depends on the choice of coordinate system but the effect of ETF relies only on the relative velocity between projectile and target, the choice of coordinate system does not restrict the generality of our approach. Moreover, the ETF is used specifically for the description of the dynamics of the collision, which makes it more complex in the computations of the integrals for coupling matrix elements since the standard strategies used in the quantum chemistry computation are no longer adapted.

2.3.3 The coupled differential equations

The insertion of the equation (2.30) into the equation (2.23) results in a system of first-order coupled differential equations (CDEs), which are written in matrix form as

$$i\frac{d}{dt}\mathbf{c}(t) = \mathbf{S}^{-1}(\vec{b},\vec{v},t)\mathbf{M}(\vec{b},\vec{v},t)\mathbf{c}(t), \tag{2.32}$$

where $\mathbf{c}(t)$ is the column vector of the time-dependent expansion coefficients, i.e. c^{TT}, c^{PP} and c^{TP} in equation (2.30) and $\mathbf{S}$, $\mathbf{M}$ are the overlap and coupling matrices, respectively. The coupling matrix $\mathbf{M}$ is defined as,

$$\mathbf{M} = \begin{pmatrix}
M_{(TT)_1,(TT)_1} & \cdots & M_{(TT)_1,(TP)_1} & \cdots & M_{(TT)_1,(PP)_1} & \cdots & M_{(TT)_1,(PP)_{N_P}} \\
M_{(TT)_2,(TT)_1} & \cdots & M_{(TT)_2,(TP)_1} & \cdots & M_{(TT)_2,(PP)_1} & \cdots & M_{(TT)_2,(PP)_{N_P}} \\
M_{(TT)_3,(TT)_1} & \cdots & M_{(TT)_3,(TP)_1} & \cdots & M_{(TT)_3,(PP)_1} & \cdots & M_{(TT)_3,(PP)_{N_P}} \\
\cdots & \cdots & \cdots & \cdots & \cdots & \cdots & \cdots \\
M_{(TT)_{N_T},(TT)_1} & \cdots & M_{(TT)_{N_T},(TP)_1} & \cdots & M_{(TT)_{N_T},(PP)_1} & \cdots & M_{(TT)_{N_T},(PP)_{N_P}} \\
M_{(TP)_1,(TT)_1} & \cdots & M_{(TP)_1,(TP)_1} & \cdots & M_{(TP)_1,(PP)_1} & \cdots & M_{(TP)_1,(PP)_{N_P}} \\
M_{(TP)_2,(TT)_1} & \cdots & M_{(TP)_2,(TP)_1} & \cdots & M_{(TP)_2,(PP)_1} & \cdots & M_{(TP)_2,(PP)_{N_P}} \\
\cdots & \cdots & \cdots & \cdots & \cdots & \cdots & \cdots \\
M_{(PP)_1,(TT)_1} & \cdots & M_{(PP)_1,(TP)_1} & \cdots & M_{(PP)_1,(PP)_1} & \cdots & M_{(PP)_1,(PP)_{N_P}} \\
\cdots & \cdots & \cdots & \cdots & \cdots & \cdots & \cdots \\
M_{(PP)_{N_P},(TT)_1} & \cdots & M_{(PP)_{N_P},(TP)_1} & \cdots & M_{(PP)_{N_P},(PP)_1} & \cdots & M_{(PP)_{N_P},(PP)_{N_P}}
\end{pmatrix}. \tag{2.33}$$

The corresponding matrix elements $M_{A,B}$ are difined as,

$$\begin{aligned}
M_{A_i,B_j} &= \left\langle \Phi_i^A(\vec{r_1},\vec{r_2})F^A(\vec{r_1},\vec{r_2})\right| H^{el} \left|\Phi_j^B(\vec{r_1},\vec{r_2})F^B(\vec{r_1},\vec{r_2})\right\rangle \\
&= \left\langle \Phi_i^A(\vec{r_1},\vec{r_2})F^A(\vec{r_1},\vec{r_2})\right| T_1 + T_2 \left|\Phi_j^B(\vec{r_1},\vec{r_2})F^B(\vec{r_1},\vec{r_2})\right\rangle \\
&+ \left\langle \Phi_i^A(\vec{r_1},\vec{r_2})F^A(\vec{r_1},\vec{r_2})\right| V_{T_1} + V_{T_2} \left|\Phi_j^B(\vec{r_1},\vec{r_2})F^B(\vec{r_1},\vec{r_2})\right\rangle \\
&+ \left\langle \Phi_i^A(\vec{r_1},\vec{r_2})F^A(\vec{r_1},\vec{r_2})\right| V_{P_1} + V_{P_2} \left|\Phi_j^B(\vec{r_1},\vec{r_2})F^B(\vec{r_1},\vec{r_2})\right\rangle \\
&+ \left\langle \Phi_i^A(\vec{r_1},\vec{r_2})F^A(\vec{r_1},\vec{r_2})\right| \frac{1}{r_{12}} \left|\Phi_j^B(\vec{r_1},\vec{r_2})F^B(\vec{r_1},\vec{r_2})\right\rangle,
\end{aligned} \tag{2.34}$$

where the superscripts $A(B)$ could equal to TT (PP) or TP, which denote states of two electrons on the target (projectile) or one electron on the target and the other one on the projectile, respectively. Note that the state $\Phi_i^{(TP)}(\vec{r_1},\vec{r_2})$ is the product of one-electron states of the corresponding isolated collision partners, i.e., $\Phi_{i1}^{(T)}(\vec{r_1})\Phi_{i2}^{(P)}(\vec{r_2})$. The function $F^{A(B)}(\vec{r_1},\vec{r_2})$ is the product of the the corresponding ETF (equation 2.31) for each of the electrons. $T_{1(2)}$ is the kinetic energy of the first (second) electron, and $V_{T_i(P_i)}$ is the interaction potential between the electron and the target (projectile) nucleus (and inner electrons, in the frozen-core approximation). The last term in equation (2.34) stands for the interelectronic repulsions.

The overlap matrix $\mathbf{S}$ in equation (2.32) is given by,

$$\mathbf{S} = \begin{pmatrix} S_{(TT)_1,(TT)_1} & \cdots & S_{(TT)_1,(TP)_1} & \cdots & S_{(TT)_1,(PP)_1} & \cdots & S_{(TT)_1,(PP)_{N_P}} \\ S_{(TT)_2,(TT)_1} & \cdots & S_{(TT)_2,(TP)_1} & \cdots & S_{(TT)_2,(PP)_1} & \cdots & S_{(TT)_2,(PP)_{N_P}} \\ S_{(TT)_3,(TT)_1} & \cdots & S_{(TT)_3,(TP)_1} & \cdots & S_{(TT)_3,(PP)_1} & \cdots & S_{(TT)_3,(PP)_{N_P}} \\ \cdots & \cdots & \cdots & \cdots & \cdots & \cdots & \cdots \\ S_{(TT)_{N_T},(TT)_1} & \cdots & S_{(TT)_{N_T},(TP)_1} & \cdots & S_{(TT)_{N_T},(PP)_1} & \cdots & S_{(TT)_{N_T},(PP)_{N_P}} \\ S_{(TP)_1,(TT)_1} & \cdots & S_{(TP)_1,(TP)_1} & \cdots & S_{(TP)_1,(PP)_1} & \cdots & S_{(TP)_1,(PP)_{N_P}} \\ S_{(TP)_2,(TT)_1} & \cdots & S_{(TP)_2,(TP)_1} & \cdots & S_{(TP)_2,(PP)_1} & \cdots & S_{(TP)_2,(PP)_{N_P}} \\ \cdots & \cdots & \cdots & \cdots & \cdots & \cdots & \cdots \\ S_{(PP)_1,(TT)_1} & \cdots & S_{(PP)_1,(TP)_1} & \cdots & S_{(PP)_1,(PP)_1} & \cdots & S_{(PP)_1,(PP)_{N_P}} \\ \cdots & \cdots & \cdots & \cdots & \cdots & \cdots & \cdots \\ S_{(PP)_{N_P},(TT)_1} & \cdots & S_{(PP)_{N_P},(TP)_1} & \cdots & S_{(PP)_{N_P},(PP)_1} & \cdots & S_{(PP)_{N_P},(PP)_{N_P}} \end{pmatrix}, \tag{2.35}$$

where the same notation as for the coupling matrix (equation (2.33)) is used. Note that the $\mathrm{S}_{(TT)_i,(TT)_j}$, $\mathrm{S}_{(PP)_i,(PP)_j}$ are one center integrals, which are therefore reflecting the orthonormalization of the basis sets on each center. The matrix elements $S_{A,B}$ are defined as,

$$S_{A_i,B_j} = \left\langle \Phi_i^A(\vec{r_1},\vec{r_2})F^A(\vec{r_1},\vec{r_2}) \middle| \Phi_j^B(\vec{r_1},\vec{r_2})F^B(\vec{r_1},\vec{r_2}) \right\rangle . \tag{2.36}$$

The column vectors of the expansion coefficients $\mathbf{c}(\mathrm{t})$ in equation (2.32) can be expressed as,

$$\mathbf{c}(t) = \begin{pmatrix} c^{(TT)_1}(t) \\ c^{(TT)_2}(t) \\ c^{(TT)_3}(t) \\ \cdots \\ c^{(TT)_{N_T}}(t) \\ c^{(TP)_1}(t) \\ c^{(TP)_2}(t) \\ \cdots \\ c^{(PP)_1}(t) \\ \cdots \\ c^{(PP)_{N_P}}(t) \end{pmatrix}. \tag{2.37}$$

To solve the system of the first-order coupled differential equations (equation (2.32)) resulting from the expansion of the wave function on the states of the target and the projectile, different matrix elements, expressed as multiple integrals, must be evaluated, where several different types are sorted out:

- The computations of one-electron multi-center (one, two, or three centers) integrals with or without potential interactions, and with or without ETF.

- The computations of two-electron multi-center (one, two, or three centers) integrals with or without ETF.

The method and strategy for computations of these integrals are presented in the section 2.4.2 (for more details, see [23] and the references therein).

The system of first-order coupled differential equations (equation (2.32)) are then solved for a set of initial conditions (initial state i, and given values of the impact parameter b and the projectile velocity v_P) using a robust predictor-corrector time-step method developed by Shampine and Gordon [50]. The probability of a transition $i \to f$ is given by the coefficients c_f ($\equiv c^{TT}$, c^{PP} or c^{TP}) as,

$$P_{fi}(b, v_P) = \lim_{t \to \infty} |c_f(t)|^2. \tag{2.38}$$

2.4 Implementation

2.4.1 The selection of GTOs

In the early days of quantum chemistry so-called Slater-type orbitals (STOs) were used as basis functions due to their similarity with the eigenfunctions of the hydrogen atom. These functions have the advantage that they have direct physical interpretation and thus are naturally good basis for molecular orbitals. However, from a computational point of view the STOs have the severe shortcoming that most of the required integrals needed in the course of the implementation must be calculated numerically which drastically decreases the speed of the computations. In this context, the Gaussian-type orbitals (GTOs) were proposed by Boys [51] in 1950 due to the fact that STOs can be approximated as linear combinations of GTOs which greatly simplified the evaluation of the integrals. They have been widely used in the quantum chemistry calculations since then. GTOs make *ab initio* calculations feasible by allowing analytical evaluations of certain integrals necessary for the calculations, which leads to a considerable speedup of the calculations over STOs expansions.

In our implementation, we use a linear combination of Cartesian Gassian-type orbitals (GTOs) to describe the states of isolated collision partners, written as

$$\chi_k(\vec{r}) = N_k x^{u^k} y^{v^k} z^{w^k} e^{-\alpha_k r^2}; k = 1, 2, ..., N, \tag{2.39}$$

where N_k is a normalization factor, u_k, v_k and w_k are positive integers or zero[2]. In order to obtain a good description of the important states of isolated collision partners, the optimization of the exponents α_k in equation (2.39) is necessary. However, an optimization procedure in which all the exponents of GTOs are optimized is extremely time consuming and can be done in practice only to a limited number

---

[2] The Cartesian coordinates allow the description of any spherical harmonics for a given ℓ, since all combinations of u_k, v_k and w_k, such $u_k + v_k + w_k = \ell$ are included.

of Gaussian functions at a time. For this reason, Reeves and Harrison [52] suggested firstly in 1963 to use the even-tempered GTOs based on intuitive reasoning. Later this basis was proposed again by Ruedenberg *et al.* [53]. This time it was based on the empirical observation that when full optimization is performed the optimized exponents obtained follow an almost straight line on the logarithmic scale. The exponents in the even-tempered set also form such a straight line, reducing the number of parameters to optimize to two. In practice, the exponents in the Gaussian even-tempered basis are chosen such as they follow a geometric series,

$$\alpha_k = \alpha_1 \epsilon^{k-1}; k = 1, 2, ..., N, \tag{2.40}$$

where only two parameters α_1 and ϵ are needed to be optimized. Note that the Gaussian even-tempered basis was thought to be chosen based mainly on empirical results. However, recently, Cherkess *et al.* [54] have shown how and why the well-known Gaussian even-tempered basis spans the Hilbert space evenly based on rigorous numerical ground using a Gram-Schmidt orthogonalization procedure. In our implementation, the GTOs has been optimized using equation (2.40) and selected based on two criteria: (i) large enough to describe accurately the important target and projectile states and (ii) still computationally tractable. In addition, convergence tests of the cross sections have been performed by comparing the results from various basis sets with increasing size. The basis sets used to study different collision systems in this thesis are presented in Appendix B.

2.4.2 The evaluation of one- and two-electron integrals

To solve the system of the first-order coupled differential equations (equation (2.32)), the computations of the overlap and coupling matrix elements (equation (2.35) and equation (2.33)) are required, which is the heaviest part, i.e., very demanding in computer resources, memory, and CPU time. Procedures for the evaluation of one-electron and two-electron two-center integrals have been presented respectively in Caillat *et al.* [47] and Wang *et al.* [22], and extended to the evaluations of one-electron and two-electron multi-center integrals by Sisourat *et al.* [23] (and references therein). Despite that, the cumbersome calculations require us to develop a new strategy for the evaluation of these integrals, less demanding in computer resources, memory, and CPU time. The new strategy based on evaluating these integrals using recursive relationships has been developed in our group and implemented in the study for one-active-electron collision systems [24]. In this thesis, we have extended this strategy for the evaluation of two-electron integrals and implemented in the new version of the two-active-electron computer code, where a significantly reduction of the memory requirement is found, especially when considering high angular momentum GTOs ($l > 4$, GTOs up to $l = 7$ have been tested). This new strategy used for the evaluation of the one- and two-electron integrals is presented in the following.

One-electron integrals

The computations of the overlap matrix elements (equation (2.35)), as well as parts of coupling matrix elements (first three terms in equation (2.34), i.e., the kinetic energy of the first (second) electron and the interaction potential between the electron and the target or projectile nucleus) require the evaluations of the following one-electron integrals,

$$S_{lmn} = \int d\vec{r} x^l y^m z^n e^{-\alpha r^2 + i\vec{v}\cdot\vec{r}} \tag{2.41}$$

and

$$V_{lmn} = \int d\vec{r} x^l y^m z^n e^{-\alpha r^2 + i\vec{v}\cdot\vec{r}} \frac{e^{-\beta(r-R_i)^2}}{\left|\vec{r} - \vec{R}_i\right|}, \tag{2.42}$$

where R_i and β are chosen to describe the Coulombic potential or a model one. In the former case, β is set to zero and R_i is the position of a nuclei. The overlap integral S_{lmn} can be rewritten as derivatives of the genuine integral J_0 as

$$S_{lmn} = \lim_{\vec{a}\to\vec{v}} \left(- i\frac{\partial}{\partial_{a_x}} \right)^l \left(- i\frac{\partial}{\partial_{a_y}} \right)^m \left(- i\frac{\partial}{\partial_{a_z}} \right)^n J_0 \tag{2.43}$$

with

$$J_0 = \left(\frac{\pi}{\alpha}\right)^{3/2} e^{-(v_x^2+v_y^2+v_z^2)/4\alpha}. \tag{2.44}$$

From equations (2.43) and (2.44), one can obtain the following recursion relation,

$$S_{lmn} = -\frac{(l-1)}{2\alpha} S_{(l-2)mn} - \frac{v_x}{2\alpha} S_{(l-1)mn} \tag{2.45}$$

In the same manner as for the overlap integral, the potential integral can be rewritten as derivatives of the genuine integral $J_1^{(0)}$ as

$$V_{lmn} = \lim_{\vec{a}\to\vec{v}} \left(- i\frac{\partial}{\partial_{a_x}} \right)^l \left(- i\frac{\partial}{\partial_{a_y}} \right)^m \left(- i\frac{\partial}{\partial_{a_z}} \right)^n J_1^{(0)} \tag{2.46}$$

where $J_1^{(0)}$ is given by

$$J_1^{(0)} = \frac{2\pi}{\alpha} e^{-\alpha R_i + \frac{A^2}{4\gamma}} F^{(0)}\left(\frac{1}{2}, \frac{3}{2}, \frac{-B^2}{4\gamma}\right) \tag{2.47}$$

and $A^2 = -a^2 + r\beta R_i^2 + 4i\beta\vec{a}\cdot\vec{R}_i$, $B^2 = -a^2 + 4\alpha R_i^2 + 4i\alpha\vec{a}\cdot\vec{R}_i$, $\gamma = \alpha + \beta$ and $F^{(0)}$ is the confluent hypergeometric function of the first kind [55]. Using equation (2.46) and the notation $F^{(k)}(a,b,z) = \frac{d^k}{dz^k}F(a,b,z)$, the following recursion relation is then obtained,

$$\begin{aligned} V_{lmn}^{(k)} = {} & \frac{(l-1)}{2\gamma} V_{(l-2)mn}^{(k)} + \left(\frac{i}{2\gamma}\right)(v_x + 2i\beta R_x) V_{(l-1)mn}^{(k)} \\ & - \frac{(l-1)}{2\gamma} V_{(l-2)mn}^{(k+1)} + \left(\frac{i}{2\gamma}\right)(-v_x + 2i\alpha R_x) V_{(l-1)mn}^{(k+1)} \end{aligned} \tag{2.48}$$

The relations are initiated by the direct evaluation of S_{lmn} and $V_{lmn}^{(k=0)}$ for $l, m, n = 0$ and 1 from equations (2.43) and (2.46), respectively. Equivalent relations for all terms are obtained by circular permutation of l, m and n in equations (2.45) and (2.48).

Two-electron integrals

The computations of the interelectron repulsion part of coupling matrix elements (the last terms in equation (2.34)) require the evaluations of the following two-electron integral,

$$U = \iint d\vec{r_1} d\vec{r_2} e^{-\alpha_a r_1^2} x_1^{u_a} y_1^{v_a} z_1^{w_a} e^{-\alpha_b r_2'^2} x_2'^{u_b} y_2'^{v_b} z_2'^{w_b} \frac{e^{i\vec{v}\cdot(\vec{r_1}-\vec{r_2})}}{|\vec{r_1}-\vec{r_2}|} \tag{2.49}$$

which can be expressed in terms of the genuine integral,

$$\begin{aligned} U = & \lim_{\vec{a},\vec{b}\to 0} (-i\frac{\partial}{\partial a_x})^{u_a} (-i\frac{\partial}{\partial a_y})^{v_a} (-i\frac{\partial}{\partial a_z})^{w_a} (-i\frac{\partial}{\partial b_x})^{u_b} \\ & (-i\frac{\partial}{\partial b_y})^{w_b} (-i\frac{\partial}{\partial b_z})^{w_b} I(\alpha_a, \alpha_b) \\ with & \\ I = & \iint d\vec{r_1} d\vec{r_2} e^{-\alpha_a r_1^2 - \alpha_b r_2'^2} \frac{e^{i\vec{v}\cdot(\vec{r_1}-\vec{r_2})}}{|\vec{r_1}-\vec{r_2}|} e^{i\vec{a}\cdot\vec{r_1}+i\vec{b}\cdot\vec{r_2}} \end{aligned} \tag{2.50}$$

The integral I can be evaluated analytically,

$$\begin{aligned} I = & \frac{\pi^{\frac{5}{2}}}{\alpha^{\frac{1}{2}} \alpha_a^{\frac{3}{2}} \alpha_b^{\frac{3}{2}}} e^{-\alpha_b R^2} e^{\frac{B^2}{4\alpha_a}} e^{\frac{D^2}{4\alpha_b}} F(\frac{1}{2}, \frac{3}{2}, -\frac{\beta^2}{\alpha}) \\ with & \\ \alpha = & \frac{1}{4\alpha_a} + \frac{1}{4\alpha_b}, \beta = \frac{B}{4\alpha_a} - \frac{D}{4\alpha_b} \\ B = & i(\vec{a}+\vec{v}), D = 2\alpha_b \vec{R} + i(\vec{b}-\vec{v}) \end{aligned} \tag{2.51}$$

Using equation (2.50) and the notation $F^{(k)}(a,b,z) = \frac{d^k}{dz^k} F(a,b,z)$, the recursion relation with respect to the first three parameters u_a, v_a and w_a can be obtained

$$\begin{aligned} U^{(r)}(u_a, v_a, w_a) = & \frac{u_a - 1}{2\alpha_a} [U^{(k)}(u_a - 2, v_a, w_a) - \frac{\alpha_b}{\alpha_a + \alpha_b} U^{(k+1)}(u_a - 2, v_a, w_a)] \\ & + \frac{i}{2\alpha_a} [(a_x + v_x) W^{(k)}(u_a - 1, v_a, w_a) \\ & - \frac{1}{\alpha_a + \alpha_b} (\alpha_b a_x - \alpha_a b_x + v_x(\alpha_a + \alpha_b) + 2i\alpha_a \alpha_b R_x) U^{(k+1)}(u_a - 1, v_a, w_a)] \\ & + \frac{u_b}{2(\alpha_a + \alpha_b)} U^{(k)}(u_a - 1, v_a, w_a, u_b - 1, v_b, w_b) \end{aligned} \tag{2.52}$$

where

$$U^{(k)}(u_a, v_a, w_a) = (-i)^{u_a} (-i)^{v_a} (-i)^{w_a} W^{(k)}(u_a, v_a, w_a)$$

$$W^{(k)}(u_a - 2, v_a, w_a) = \frac{\pi^{\frac{5}{2}}}{\alpha^{\frac{1}{2}} \alpha_a^{\frac{3}{2}} \alpha_b^{\frac{3}{2}}} e^{-\alpha_b R^2} e^{-i\vec{b}\cdot\vec{R}} e^{\frac{D^2}{4\alpha_b}} \frac{\partial^{u_a - 2}}{\partial a_x^{u_a - 2}} [e^{\frac{B^2}{4\alpha_a}} F^{(k)}(\tfrac{1}{2}, \tfrac{3}{2}, -\tfrac{\beta^2}{\alpha})]$$

and the recursion relation with respect to the last three parameters u_b ,v_b and w_b is

$$\begin{aligned} U^{(k)}(u_b, v_b, w_b) &= \frac{u_b - 1}{2\alpha_b}[U^{(k)}(u_b - 2, v_b, w_b) - \frac{\alpha_a}{\alpha_a + \alpha_b}U^{(k+1)}(u_b - 2, v_b, w_b)] \\ &+ \frac{i}{2\alpha_b}[(b_x - v_x)W^{(k)}(u_b - 1, v_b, w_b) \\ &+ \frac{1}{\alpha_a + \alpha_b}(\alpha_b a_x - \alpha_a b_x + v_x(\alpha_a + \alpha_b) + 2i\alpha_a\alpha_b R_x)U^{(k+1)}(u_b - 1, v_b, w_b)] \\ &+ \frac{u_a}{2(\alpha_a + \alpha_b)}U^{(k)}(u_a - 1, v_a, w_a, u_b - 1, v_b, w_b) \end{aligned} \tag{2.53}$$

where

$$\begin{aligned} U^{(k)}(u_b, v_b, w_b) &= (-i)^{u_b}(-i)^{v_b}(-i)^{w_b}W^{(k)}(u_b, v_b, w_b) \\ W^{(k)}(u_b - 2, v_b, w_b) &= \frac{\pi^{\frac{5}{2}}}{\alpha^{\frac{1}{2}}\alpha_a^{\frac{3}{2}}\alpha_b^{\frac{3}{2}}}e^{-\alpha_b R^2}e^{\frac{B^2}{4\alpha_a}}\frac{\partial^{u_b-2}}{\partial b_x^{u_b-2}}[e^{\frac{D^2}{4\alpha_b}-i\vec{b}\cdot\vec{R}}F^{(k)}(\tfrac{1}{2}, \tfrac{3}{2}, -\tfrac{\beta^2}{\alpha})]. \end{aligned}$$

Note that there is also a cross term $\frac{u_a}{2(\alpha_a+\alpha_b)}U^r(u_a - 1, v_a, w_a, u_b - 1, v_b, w_b)$ in equations (2.52) and (2.53), and equivalent relations for all terms are obtained by circular permutation of u, v and w. The relations are initiated by the direct evaluation of $U^{(k=0,1)}$ for $u_{a,b}$,$v_{a,b}$ and $w_{a,b} = 0$ and 1, respectively (in total 128 initial values).

2.4.3 The evolution of the system of coupled differential equations

The time evolution of the system of coupled differential equations (equation (2.32)) is treated numerically, where a predictor-corrector method is considered. In numerical analysis, predictor-corrector methods belong to a class of algorithms designed to integrate ordinary differential equations to find an unknown function that satisfies a given differential equation. All such algorithms proceed in two steps:

— The initial, "prediction" step, starts from a function fitted to the function-values and derivative-values at a preceding set of points to extrapolate this function's value at a subsequent, new point.

— The next, "corrector" step refines the initial approximation by using the predicted value of the function and another method to interpolate that unknown value of the function at the same subsequent point.

The two steps above make sure that the predictor-corrector method is reliable and numerically stable. In our implementation, we use a robust predictor-corrector time-step variable method developed by Shampine and Gordon [50]. The method adapts the time step automatically according to the evolution of the expansion coefficients during the integration procedure, to guarantee a given accuracy. Since the time step is varied, and we do not know which time grid point will be used during the dynamics, the overlap and coupling matrix elements are evaluated on a set of fixed time grid along the projectile trajectory and systematically interpolated using Lagrange interpolation scheme during the dynamics. Note that the time grid should be large enough to ensure the quality of the interpolation and the convergence of the predictor-corrector strategy. In our implementation, the following parameters were used: the overlap and coupling matrix elements are evaluated on a set of grid of 100 points ranging from -100 a.u. to $+100$ a.u. at intermediate and high impact energies. For the very low impact energy (less than 1 keV/u), the number of points was increased to about 300.

2.4.4 The structure of the computer code

We have developed a new version of two-active-electron computer code written in *FORTRAN 90*, which is an implementation of the semiclassical non perturbative approach. The structure of the computer code can be classified into various stages:

— Initialization:
(i) the selection and optimization of the GTO exponents to describe the one- and two-electron states for each of the isolated collision partners;
(ii) input the selected GTO exponents, the projectile velocity, impact parameters and a set of fix time grid, as well as the information of target and projectile.

— Getting states: the diagonalization of the one- and two-electron Hamiltonians for each of the isolated partners using the set of GTOs input in the first stage.

— Matrices evaluation: the evaluation of the overlap and coupling matrix elements on the set of grid points along the projectile trajectory.

— Dynamics: the integration in time of the system of first-order coupled differential equations for the initial conditions input in the first stage.

— Cross sections: the evaluation of total or angular differential cross sections.

Among these stages, the *Matrices evaluation* and *Dynamics* parts are the most expensive parts in computer resources (memory, and CPU time). For this reason, these two parts of the code have been parallelized using the Message Passing Interface (MPI) protocol. The latter makes it possible to perform calculations on different processors, taking advantage of architectures of multicore processors and clusters. The efficiency of the parallelization has been tested on the collision system He^{2+} + He, where a set of 28 GTOs (10 for $l = 0$, 6×3 for $l = 1$) are used on both projectile and target centers. In Figure 2.2, the wall time (wall-clock time) and speedup of calculations as functions of the number of used CPU processors are presented, where a dramatic decreasing of the computation time can be seen. One can also observed from Figure 2.2 that the speedup is nearly a linear growth as the increase of the number of CPU cores. We thus conclude that the computational efficiency of our new version of two-active-electron computer code has been considerably improved

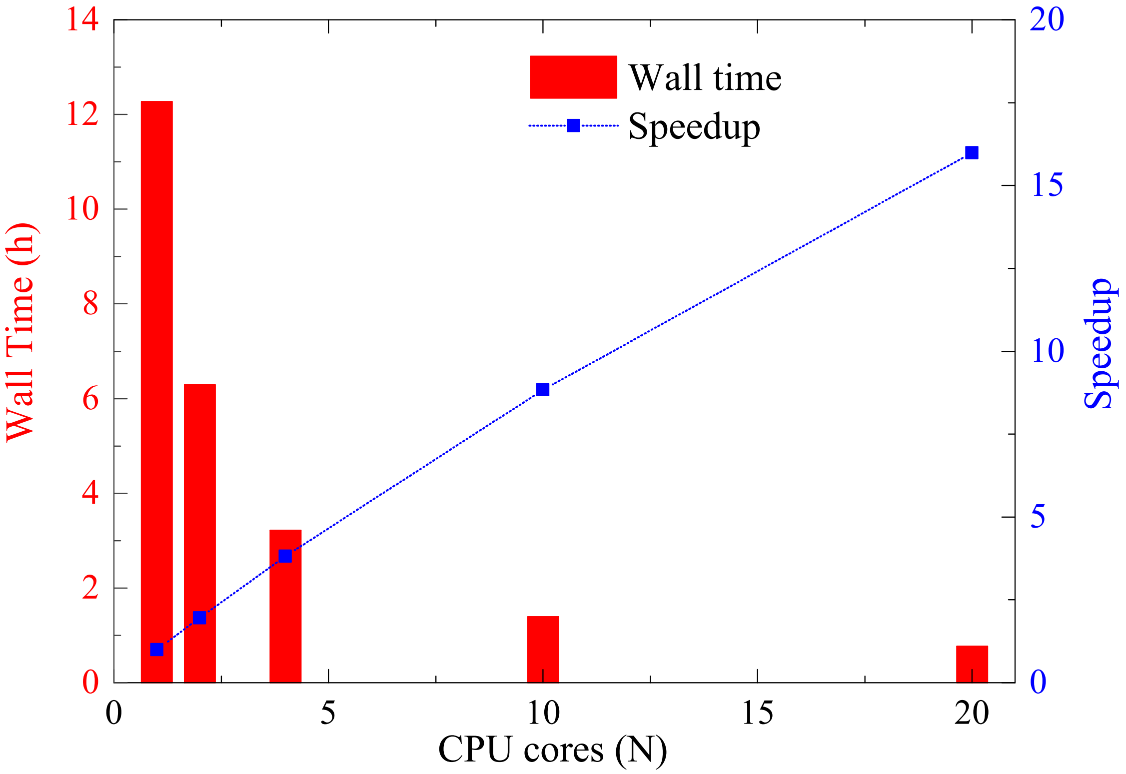

Figure 2.2 – The test of the parallelization effeciency on the collision system He^{2+} + He. The wall (wall-clock) time (red) and speedup (blue) of calculations as functions of the number of used CPU processors.

by the implementation of MPI protocol. Note, finally, that several calculations can be run at the same time for different impact parameters if necessary, which can further improve the computational efficiency.

For the *Cross sections* part, the calculations of total and angular differential cross sections are performed using other independent self-written codes. The details of the method to compute total and angular differential cross sections are presented in section 2.5.

2.5 Cross sections

2.5.1 Total cross sections

In the course of ion-atom/molecule collision, different electronic processes can be activated on each center by the interaction due to the other collision partner. To describe the selectivity of these processes in a quantitative way, we need to be able to calculate the total cross sections. In the context of semiclassical approximation, the calculation of the total sections is based on the transition probabilities (equation 2.38). For the atomic target, the cross sections of an electronic process with respect to the transition $i \rightarrow f$ for a given projectile volecity v_P are calculated as,

$$\sigma_{fi}(v_P) = 2\pi \int_0^{+\infty} bP_f(b, v_P)db, \tag{2.54}$$

where the total cross sections only depend in the impact velocity v_P.

When the target is a molecule, the degrees of the freedom must be taken into account in the calculation of cross sections, within the sudden approximation previously described. It means decoupling of the dynamics of the target nuclei with respect to the electronic one: the vibration and rotational degrees of freedom are treated incoherently with respect to the electronic wavefunction and the cross sections are then averaged over the possible orientations of the molecule with respect to the velocity direction. That is to say, the internuclear distance R_{AB} and the molecular orientation (Θ_m, Φ_m) with respect to the velocity of the projectile must be considered (see Figure 2.1). The total cross section for a given molecular orientation can be calculated as follows:

$$\sigma_{fi}(v_P, R_{AB}, \Theta_m, \Phi_m) = \int\int d^2\vec{b} P_f(v_P, \vec{b}, R_{AB}, \Theta_m, \Phi_m), \tag{2.55}$$

in polar coordinates,

$$\sigma_{fi}(v_P, R_{AB}, \Theta_m) = \int_0^{2\pi} d\Phi_b \int_0^{\infty} bP_f(v_P, \vec{b}, R_{AB}, \Theta_m, \Phi_m)db \tag{2.56}$$

where the dependence upon Φ_m disappears after integration over Φ_b, the total cross sections (averages over the degrees of freedom of the molecule) are then given by,

$$\sigma_{fi}^{tot}(v_P) = \int_0^{\pi} \int_0^{\infty} \rho(\Theta_m)\rho(R_{AB})\sigma_{fi}(v_P, R_{AB}, \Theta_m)dR_{AB}d\Theta_m, \tag{2.57}$$

where $\rho(\Theta_m)$, $\rho(R_{AB})$ are respectively the distribution of molecules over Θ_m and R_{AB}. The distribution of the molecules according to Θ_m is given isotropically by

$$\rho(\Theta_m) = \frac{1}{2} sin(\Theta_m). \tag{2.58}$$

The distribution of the internuclear distance $\rho(R_{AB})$ of the target molecule is generally that corresponding to a given vibrational state (for example, the ground state for H_2) but can also be that of a superposition of vibrational states of the molecule under consideration. In the latter case, the cross sections should then be evaluated for different values of R_{AB} and generally averaged over the initial vibrational state distribution. However, it has been shown that considering only the equilibrium distance value R_{eq} is sufficient to obtain accurate cross sections [23, 56–58]. In the following we therefore consider only a molecular target fixed at the equilibrium geometry (the so-called Franck-Condon approximation; cf. [59]). Thus, the $\rho(R_{AB})$ can be expressed as,

$$\begin{aligned} \rho(R_{AB}) = 1 \quad if \quad R_{AB} = R_{eq} \\ \rho(R_{AB}) = 0 \quad if \quad R_{AB} \neq R_{eq}. \end{aligned} \tag{2.59}$$

The total cross sections (equation (2.57)) can be rewritten as,

$$\sigma_{fi}^{tot}(v_P) = \frac{1}{2}\int_0^\pi d\Theta_m sin(\Theta_m)\sigma_{fi}(v_P, R_{eq}, \Theta_m). \tag{2.60}$$

Since the computations of the probabilities are rather demanding, especially when involving numerous target orientation (Θ_m, Φ_m), it is often chosen to evaluate cross sections directly comparable with experimental data through an approximated averaging procedure using only three characteristic molecular orientations; namely (Θ_m, Φ_m) =(0,0), (0,$\frac{\pi}{2}$), ($\frac{\pi}{2}$,$\frac{\pi}{2}$):

$$\begin{aligned} &\sigma_{fi}^{tot} = \frac{1}{3}[\varrho_{fi}(v_P, R_{eq}, 0, 0) + \varrho_{fi}(v_P, R_{eq}, 0, \frac{\pi}{2}) + \varrho_{fi}(v_P, R_{eq}, \frac{\pi}{2}, \frac{\pi}{2})] \\ &with \\ &\varrho_{fi}(v_P, R_{eq}, \Theta_m, \Phi_m) = 2\pi \int bP_f(v_P, b, R_{eq}, \Theta_m, \Phi_m)db. \end{aligned} \tag{2.61}$$

This approximation has been widely used and proven to give good estimates of the total cross sections [23, 56, 58, 59].

2.5.2 The angular differential cross sections

As we mentioned in the section 2.5.1, the selectivity of the electronic processes during ion-atom/molecule collisions with respect to impact energies is well described by total cross sections. However, these quantities do not allow the analysis of the spatial selectivity. This is described by probabilities which are however not experimental observables. To be able to compare with experiments, one should evaluate differential cross sections with respect to scattering angle, which provides a much sharper probe of process mechanisms and reveals collision dynamics. Various derivations of the methods to calculate differential cross sections (quantal quantities) from semiclassical probability amplitudes have been given in the literature [60–63]. Here we briefly outline only the main features of the method. The relationship between the angular differential cross sections and the standard integral expression of scattering amplitude f_{fi} from the state i to the state f can be expressed as,

$$\frac{d\sigma_{fi}}{d\Omega} = \frac{k_f}{k_i}|f_{fi}(\Omega)|^2, \tag{2.62}$$

where the angles Ω are the spherical angles of the final momentum vector $\vec{k}_f$, the scattering amplitude $f_{fi}(\Omega)$ is given by,

$$f_{fi}(\Omega) = -\frac{\mu}{2\pi}\sum_q \int d\vec{r}_i \int d\vec{R}\Phi_f^{k_f *}(\{\vec{r}_q\}, \vec{R})V_f(\{\vec{r}_q\}, \vec{R})\Psi_i^{k_i}(\{\vec{r}_q\}, \vec{R}), \tag{2.63}$$

where $V_f(\{\vec{r}_q\}, \vec{R})$ is the final channel electrostatic interaction that the detected particle feels (core + electronic processes), μ is the final channel reduced mass. The wavefunction $\Phi_f^{k_f}(\{\vec{r}_q\}, \vec{R})$ describes the final stationary scattering state of the separated collision partners, which satisfies the Schrödinger equation

$$(\hat{H}^{int} - V_f)\Phi_f^{k_f} = E_f\Phi_f^{k_f} \tag{2.64}$$

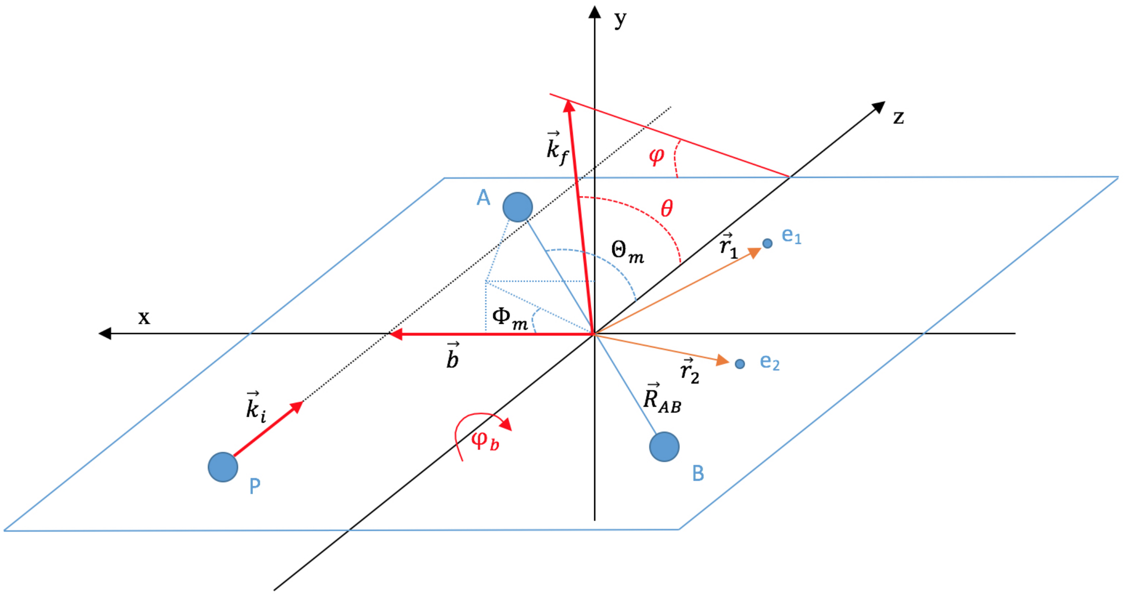

Figure 2.3 – Collision geometry. $\vec{R}_{AB}$ is the internuclear vector of the molecular target, and the positions of two electrons with respect to the target center of mass are denoted $\vec{r}_1$, $\vec{r}_2$. The angles (Θ_m,Φ_m) define the molecular orientation with respect to the initial momentum vector $\vec{k}_i$ (the projectile $\vec{v}_P$) of the projectile and the impact parameter $\vec{b}$, and $\vec{k}_f$ is the momentum vector of the projectile after scattering, defined by the angles (θ,ϕ). φ_b is the azimuthal angle used to define the direction of $\vec{b}$ with respect to x axis, $\varphi_b = 0$ in the present case.

with

$$\Phi_f^{k_f}(\{\vec{r}_q\},\vec{R}) = e^{-i\vec{k}_f\cdot\vec{R}}\phi_f(\{\vec{r}_q\},t), \tag{2.65}$$

where ϕ_f is the asymptotic states for the corresponding electronic processes presented in section 2.3. Ψ^{k_i} is the solution of the complete Schrödinger equation of the system, which can be written in the semiclassical impact parameter approximation as,

$$\Psi^{k_i}(\{\vec{r}_q\},\vec{R}) = e^{-i\vec{k}_i\cdot\vec{R}}\Psi(\{\vec{r}_q\},t), \tag{2.66}$$

in which the $\Psi(\{\vec{r}_q\},t)$ is the solution of the eikonal equation (2.23).

In the context of the semiclassical impact parameter approximation, the trajectory is defined as $\vec{R}(t) = \vec{b} + \vec{v}_P t$, leads to $d\vec{R} = v_P\,dt\,d^2\vec{b}$. Using equations (2.65) and (2.66) in (2.63), we find that

$$f_{fi}(\theta,\varphi) = \lim_{t\to+\infty} -i\frac{\mu v_P}{2\pi}\int\int d^2\vec{b}\, e^{-i(\vec{k}_i-\vec{k}_f)\cdot\vec{R}}\left\langle\phi_f\right| V_f \left|\Psi\right\rangle . \tag{2.67}$$

The initial momentum vector $\vec{k}_i$ (the projectile $\vec{v}_P$) and the impact parameter $\vec{b}$ are defined as shown in Figure 2.3. And $\vec{k}_f$ is the momentum vector of the projectile after scattering, defined by the angles (θ,ϕ). In the small-angle approximation, the vector $(\vec{k}_i - \vec{k}_f)$ is perpendicular to $\vec{k}_i$, and forms an angle $(\varphi - \varphi_b)$ with the impact parameter $\vec{b}$, where φ_b is the azimuthal angle used to define the direction of $\vec{b}$ with respect to x axis, $\varphi_b = 0$ in the case of Figure 2.3. Then, we can obtain that

$$(\vec{k}_i - \vec{k}_f) \cdot \vec{R} \approx 2\mu v_P\, b\, sin(\frac{\theta}{2})\, cos(\varphi - \varphi_b), \tag{2.68}$$

and the final expression of the scattering amplitude,

$$f_{fi}(\theta, \varphi) = -i\frac{\mu v_P}{2\pi} \int d^2\vec{b}\, e^{-2i\mu v_P\, b\, sin(\frac{\theta}{2})\, cos(\varphi - \varphi_b)} a_{fi}(v_P, \vec{b}, R_{AB}, \Theta_m, \Phi_m), \tag{2.69}$$

with

$$a_{fi}(v_P, \vec{b}, R_{AB}, \Theta_m, \Phi_m) = \langle \phi_f | \, V_f \, | \Psi \rangle \,, \tag{2.70}$$

where R_{AB} is the internuclear distance of the molecular target, and the angles (Θ_m, Φ_m) define the molecular orientation (see Figure 2.3).

Ion-atom collisions

The parameters R_{AB}, Θ_m and Φ_m disappear if we consider an atomic target, the coefficients a_{fi} are then expressed as,

$$a_{fi}(v_P, \vec{b}) = \bar{c}_{fi}(v_P, \vec{b}) e^{i(m_i - m_f)\varphi_b} \tag{2.71}$$

due to the cylindrical collision symmetry of the atomic states in the xyz frame, c_{fi} is independent with the azimuthal angle φ_b. m_i and m_f are the initial and final magnetic quantum numbers with respect to the z axis. It should be noted that all b-dependent phases (i.e., common phases due to the core-core interaction in the Hamiltonian [31]) contributing to the collision amplitudes $\bar{c}_{fi}$ in the complete solution of the close-coupled impact parameter equations should be included in equation (2.71). It is precisely the complete phase information that allows the extraction of the angular predictions from straight-line trajectory collision amplitudes. Explicitly, the amplitudes are,

$$\bar{c}_{fi}(v_P, b) = c_{fi}(v_P, b) e^{\left(\frac{i}{v} 2Z^T Z^P ln(b)\right)}, \tag{2.72}$$

where the nuclear charges of the target and projectile are denoted as Z_T and Z_P, the amplitude $c_{fi}(v_P, b)$ is the solution of the coupled differential equation (2.32). In polar coordinates, the equation (2.69) then rewritten as

$$\begin{aligned} f_{fi}(\theta, \varphi) = -i\frac{\mu v_P}{2\pi} \int_0^\infty bdb \int_0^{2\pi} d\varphi_b\, c_{fi}(v_P, b) \\ \times\, e^{-i\{2\mu v_P\, b\, sin(\frac{\theta}{2})\, cos(\varphi - \varphi_b) + (m_f - m_i)\varphi_b - \frac{2Z^T Z^P ln(b)}{v}\}}, \end{aligned} \tag{2.73}$$

Using the definition of the Bessel function of the first kind,

$$J_n(x) = \frac{i^n}{2\pi} \int_0^{2\pi} d\varphi_b e^{i(x cos(\varphi - \varphi_b) + n(\varphi - \varphi_b)}, \;\; n \; positive\, integer. \tag{2.74}$$

We find that,

$$\begin{aligned} f_{fi}(\theta, \varphi) = \mu v_P (-i)^{1 + |m_f - m_i|} \int_0^\infty bdb e^{-i[(m_f - m_i)\varphi - 2Z_T Z_P / v_P]} \\ \times J_{|m_f - m_i|}\left(2\mu v_P\, b\, sin(\frac{\theta}{2})\right) c_{fi}(v_P, b). \end{aligned} \tag{2.75}$$

Finally, the angular differential cross sections for scattering from the state i to the state j is given in the term of the scattering amplitude $f_{fi}(\theta, \varphi)$ by,

$$\frac{d\sigma_{fi}}{d\Omega} = |f_{fi}(\theta, \varphi)|^2, \tag{2.76}$$

Ion-molecule collisions

For a molecule target, it is more complex since it is not a cylindrical collision symmetry system any more, and the V_{TP} between the target and projectile is a two-center potential. The coulombic phase and the scattering amplitudes have to be redefined. Using x_A and x_B to denote the nuclear centers of the molecule target along the x axis perpendicular to $\vec{k}_i$. The phase is then given by

$$\Phi_{TP} = \frac{Z_P}{v_P}\left(Z_A ln([bcos\varphi_b - x_A]^2 + [bsin\varphi_b]^2) + Z_B ln([bcos\varphi_b - x_B]^2 + [bsin\varphi_b]^2)\right), \tag{2.77}$$

where Z_A and Z_B are chargers of the corresponding nuclear centers A and B of the molecule target. In contrast to the ion-atom collision, the integration over φ_b is nontrivial the scattering amplitudes can only be obtained by a double integration,

$$\begin{aligned} f_{fi}(\theta, \varphi) = -i\frac{\mu v_P}{2\pi}\int_0^\infty bdb \int_0^{2\pi} d\varphi_b\, c_{fi}(v_P, b, \varphi_b, R_{AB}, \Theta_m, \Phi_m) \\ \times\, e^{-i\{2\mu v_P\, b\, sin(\frac{\theta}{2})\, cos(\varphi-\varphi_b)+(m_f-m_i)\varphi_b-\Phi_{TP}\}}. \end{aligned} \tag{2.78}$$

These integrals are evaluated carefully due the important oscillatory behavior of the integrand. The results can be checked by the integration of the differential cross sections over the scattering angle, to be equal to the total cross sections calculated from semiclassical probabilities. The codes used to evaluated these differential quantities are home-made and do not required important computer resource.

The laboratory and center of mass systems

Experimentally the cross sections are measured in the laboratory reference system while the calculations are performed in the center of mass system. In order to obtain comparable results with the experimental data, a transformation of coordinates is necessary. From the definition of differential cross sections, we know that the same number of particles A are emitted into the solid angle $d\Omega$ about the direction (θ, φ) in the center of mass reference as are emitted into the solid angle $d\Omega_L$ about the direction (θ_L, φ_L) in the laboratory reference. Thus the laboratory and center of mass differential cross sections are related by [64]

$$\frac{d\sigma}{d\Omega_L}(\theta_L, \varphi_L) sin\theta_L d\theta_L d\varphi_L = \frac{d\sigma}{d\Omega}(\theta, \varphi) sin\theta d\theta d\varphi. \tag{2.79}$$

Using the relationship,

$$\begin{aligned} \varphi_L &= \varphi, \\ tan\theta_L &= \frac{sin\theta}{cos\theta + \tau} \end{aligned} \tag{2.80}$$

with

$$\tau = \frac{m_P}{m_T}, \tag{2.81}$$

where m_P and m_T are the mass of the projectile and target. The relationship bwteen θ_L and θ in equation (2.65) can also be written as

$$cos(\theta_L) = \frac{cos\theta + \tau}{(1 + 2\tau cos\theta + \tau^2)^{1/2}} \tag{2.82}$$

so that the transformation of angular differential cross sections from the center of mass to the labratory reference can be performed by

$$\frac{d\sigma}{d\Omega_L}(\theta_L, \varphi_L) = \frac{1 + 2\tau cos\theta + \tau^2)^{3/2}}{|1 + \tau cos\theta|} \frac{d\sigma}{d\Omega}(\theta, \varphi). \tag{2.83}$$

Chapter 3

Double-electron capture in low-energy $H^+ + H^-$ collisions

3.1 Introduction

In atomic and molecular collisions, inelastic electron processes involving only a single electron, such as $H^+ + H$ [65], or $He^{2+} + H_2^+$ [66], are fairly well understood [46], while our knowledge on multi-electron ones is still far from complete. A striking example is the $H^+ + H^-$ collision system. As a benchmark, it has been extensively investigated for more than five decades. Despite its apparent simplicity, a complete description of the electronic dynamics of this system remains a challenge owing to the predominant role of the electronic correlation. Most of the previous works focused on single electron capture (SEC) processes, i.e., the mutual neutralization of H^+ and H^- [22,67–75]. Studies of double electron capture (DEC) are however more scarce. The cross section of DEC were firstly measured by Brouillard *et al.* [76] in 1979, for impact energies ranging from 60 to 400 eV. In the same year, Peart and Forrest [77] extended these measurements for energies up to about 1 keV. More recently, Braüning *et al.* [78] resumed this study for higher energies up to 25 keV. The three series of experiments show that the DEC cross section oscillates. These oscillations have been attributed to quantum interferences between the gerade and ungerade ionic states of the transient molecule formed during the collision. However, all previous theoretical investigations of the DEC process failed to reproduce the experimental oscillations and/or the magnitude of the cross section, illustrating the complexity of this collision system.

Together with their experimental investigation in [76], the authors modeled the DEC process using a semiclassical method based on molecular states of H_2. They obtained cross section that exhibits an oscillatory pattern but were one order of magnitude larger than the experimental ones. Later, semiclassical calculations extended the study to energies up to several keV [22, 72]. The cross section was again too large and the oscillations observed in the theoretical cross section was not consistent with the measured ones. More recently, Braüning *et al.* [78] and Mezei *et al.* [79] evaluated the DEC cross section using molecular treatments, with a rather simple two-state model in the first case and using a fully quantum treatment in the latter. They both overestimate the cross section by at least one order of magnitude.

Furthermore, the latter calculations focused on low impact energies collisions, E≤ 90 eV, which only overlap in a narrow energy domain with experiments.

In the present work, we focus on the study of double electron capture (DEC) processes occuring in the collision,

$$H^+ + H^- \to H^- + H^+ (DEC), \tag{3.1}$$

which covers a wide energy region ranging from 0.06 to 20 keV. We use a fully correlated two-active-electron semiclassical atomic-orbital close-coupling (SCAOCC) method presented in Chapter 2 (see also [23,80–82]) with a large basis set, ensuring a controlled convergence of the cross sections. For single electron processes, i.e., single electron capture (SEC) and single ionization (SI),

$$H^+ + H^- \to H + H \qquad (SEC) \tag{3.2}$$

$$H^+ + H^- \to H^+ + H + e^- \qquad (SI), \tag{3.3}$$

the cross sections dominate the DEC process ones. Describing properly these single electron processes, i.e., SEC and SI, is therefore essential to reproduce quantitatively the DEC cross section. Thus, the SEC and SI cross sections are first discussed and compared with available theoretical and experimental results. The main objective is then focused on the DEC cross sections, which are presented and compared with available theoretical and experimental results: our calculated cross sections agree well with the experimental ones. Possible reasons for remaining disagreements are also discussed. Furthermore, the DEC cross section shows clear oscillations as a function of the collision energy, which has been attributed to quantum interferences between the gerade and ungerade ionic states of the transient molecule formed during the collision. However, our investigation suggests that the observed oscillations come from a more complex mechanism than the one discussed so far.

3.2 Calculation details

We use a fully correlated two-active-electron semiclassical atomic-orbital close-coupling (SCAOCC) method, which has previously been described in Chapter 2. The treatment is semiclassical in that the relative target-projectile motion is described by classical straight-line constant velocity trajectories, while the electronic dynamics is treated quantum mechanically, by solving non perturbatively the time-dependent Schödinger equation. The latter is solved by expanding the total electronic wavefunction into the eigenstates of the isolated collision partners. In the present calculations, these eigenstates are obtained by diagonalizing the corresponding Hamiltonian matrices in the basis set $B1_H$ of properly antisymmetrized products of Gaussian-type orbitals (GTOs). The basis set $B1_H$ (a set of 45 GTOs: 11 for $l = 0$, 8×3 for $l = 1$, and 2×5 for $l = 2$) are presented in Appendix B.1. This allows

Table 3.1 – Energies (in a.u.) of H and H^- computed with our GTO basis set $B1_H$ compared exact results for H and experimental data for H^- [83].

	State	E_{B1_H}	E_{exact}		State	E_{B1_H}	$E_{expt.}$
H	1s	-0.4999	-0.5000	H^-	$1s^2$	-0.5267	-0.5277
	2s	-0.1250	-0.1250				
	3s	-0.0555	-0.0556				
	4s	-0.0312	-0.0313				
	2p	-0.1250	-0.1250				
	3p	-0.0555	-0.0556				
	4p	-0.0311	-0.0313				
	3d	-0.0517	-0.0556				

the inclusion of 1977 states, describing elastic, SEC and DEC channels, as well as ionisation, through the pseudostates of energy lying above ionization thresholds. In Table 3.1, we give the energies of the important H and H^- states, together with exact results for H and experimental data for H^- [83] for comparison. The overall agreement between our calculated energies and experimental results is generally very good, which indicates that these eigenstates of the isolated collision partners, H and H^-, are both described properly with our GTO basis set $B1_H$.

In fact, the basis set $B1_H$ has been selected using two criteria: (i) large enough to describe accurately the important target and projectile states and (ii) still computationally tractable. Convergence tests have been performed by comparing the present results with those from two different basis sets: (i) $B2_H$ includes 32 GTOs, 9 for $l = 0$, 6×3 for $l = 1$, and 1×5 for $l = 2$, which allows the inclusion of 1425 states and (ii) $B3_H$ includes 55 GTOs, 11 for $l = 0$, 8×3 for $l = 1$, and 4×5 for $l = 2$, which allows the inclusion of 3725 states. The detail of $B2_H$ and $B3_H$ are presented in Appendix B.1. We have checked the convergence of DEC cross sections at three distinctive impact energies, 0.08, 0.5, and 9 keV/u. As can be seen in Figure 3.1, the convergence for DEC cross section can be evaluated to be better than 10% for impact energies above 0.2 keV and smaller than 30% for lower energies.

3.3 Results and discussion

3.3.1 The cross sections for single electron processes

Single electron capture

In Figure 3.2, the single electron capture (SEC) cross sections are shown, together with previous experimental [67, 71, 84] and theoretical [22, 68, 72] results for comparison. The SEC cross sections are very large (10^{-14} cm^2) around 1 keV and decrease rapidly (two orders of magnitude differences for the impact energies

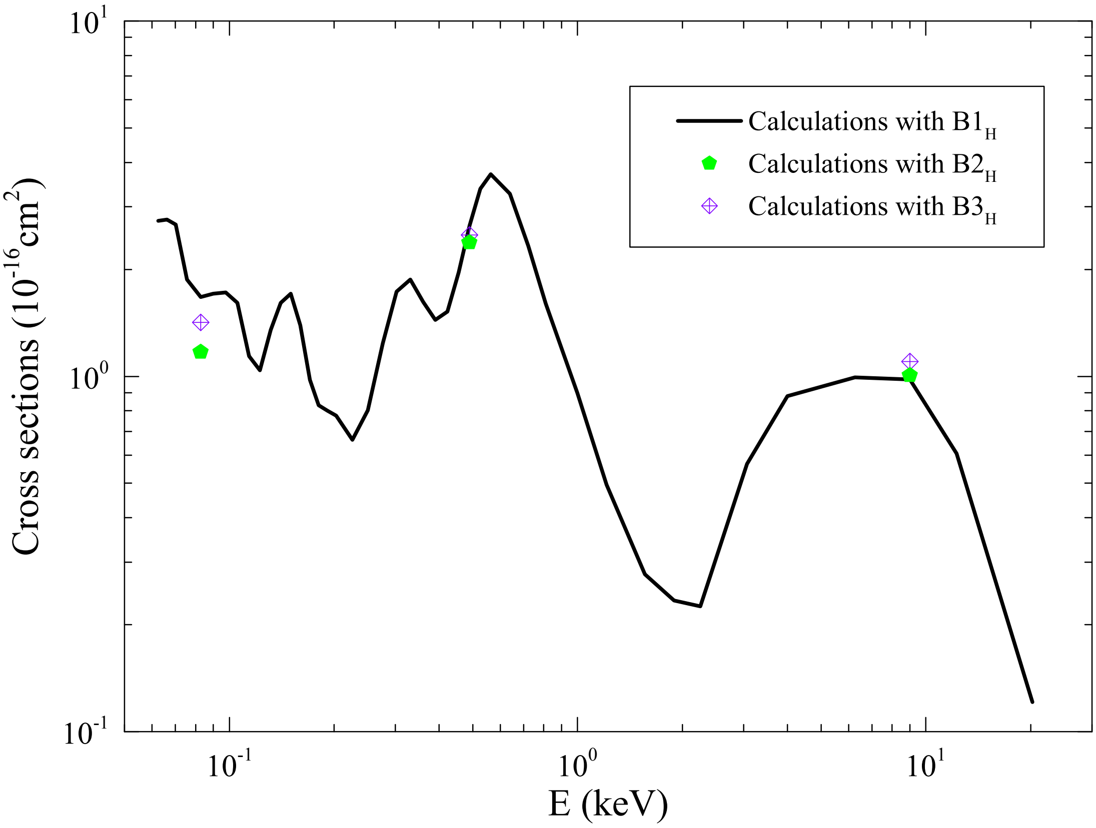

Figure 3.1 – Convergence tests with three different basis sets: black solid line, the calculations with B1$_H$; green solid pentagon, the calculations with B2$_H$; purple crossed diamond, the calculations with B3$_H$.

between 1 and 20 keV). As one can observe from Figure 3.2, our calculations agree quite well with available experimental measurements of [67,71,84] in the respective overlapping energy regions. Comparing with available theoretical calculations, a very good agreement can be found between the present results and these of two-electron coupled-channel calculations [72] in the whole overlapping energy region and, for impact energies below 5 keV, the SCAOCC calculations of Wang *et al.* [22]. For impact energies above 5 keV, the SCAOCC calculations of Wang *et al.* [22] overestimate the experimental measurements of [71], and show oscillatory structures. This may be due to the fact that only the ground state of H$^-$ and H(n = 1, 2, 3)−H(1s) two-centre states are included in their calculations so that the results may be not converged. The one-electron close-coupled calculations of Ermolaev [68] underestimate the experimental data of [67, 71, 84] in the whole overlapping energy region, while their results with independent particle model (IPM) corrections overestimate the experimental data [71] for impact energies higher than 5 keV. This tends to prove that electronic correlations play a crucial role in H$^+$ + H$^-$ collisions systems, for which one-electron calculations or the IPM approximations seem inadequate.

Furthermore, in order to provide more insights into the mechanisms responsible of the SEC channels, the transition probabilities of the pure SEC and transfer-

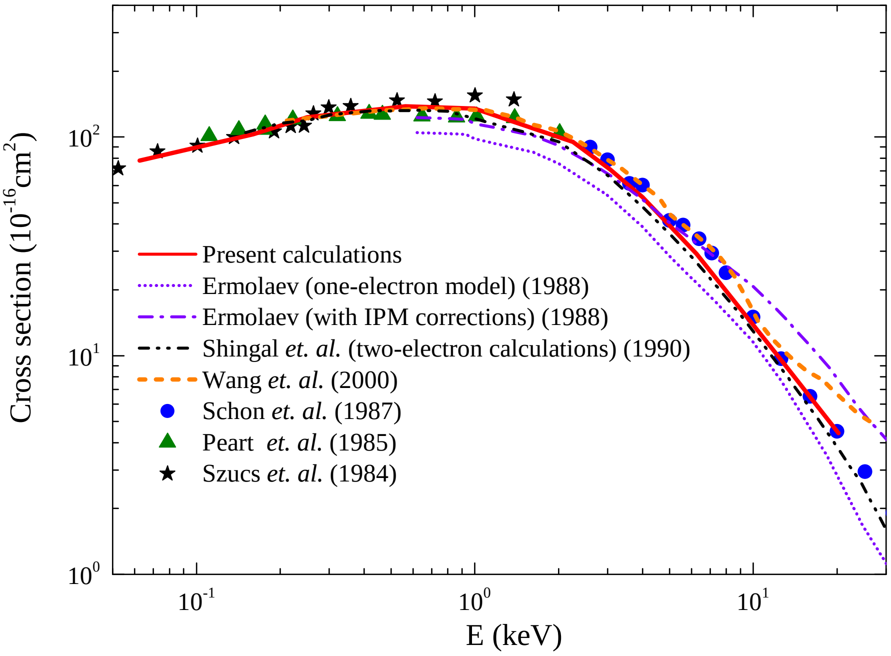

Figure 3.2 – Single electron capture cross section as a function of the impact energy. Red solid line denotes the present calculations; purple solid line is for the one-electron coupled-channel calculations of Ermolaev [68]; purple dash-dot line is for the one-electron coupled-channel calculations with IPM corrections from [68]; black solid line stands for two-electron coupled-channel calculations of Shingal *et al.* [72]; yellow dash-line is for the SCAOCC calculations of Wang *et al.* [22]. Blue solid circle denotes the experiment from Schon *et al.* [71]; green triangle is for the experiment from Peart *et al.* [67]; black star stands for the experiment from Szucs *et al.* [84].

excitation channels H(1s) + H(2ℓ) are present in Figure. 3.3 for impact energies 0.25, 1, 9, and 20.25 keV, respectively. At lower impact energies, the pure SEC transition probabilities are much larger than that of TE process and extend over a wide range of impact parameters up to b $\approx$ 15 a.u. This illustrates the action of the previous radial couplings observed in molecular calculations [73, 85] between 4_g and 2_g states and between 3_u and 1_u states (see Figure 3.8). In contrast, the TE processes are only likely at small b. It should be noted that, for high impact energies, the TE process, though involving two electrons: one electron transfer and the other remaining in the ground state of the target, becomes more important than the pure SEC (see Figure 3.3(d)).

Single ionization

The single ionization cross sections were measured by Melchert *et al.* [86] and Peart *et al.* [87] in the keV energy range. In Figure 3.4, our calculated single ionization cross sections are presented together with the experimental results of Melchert

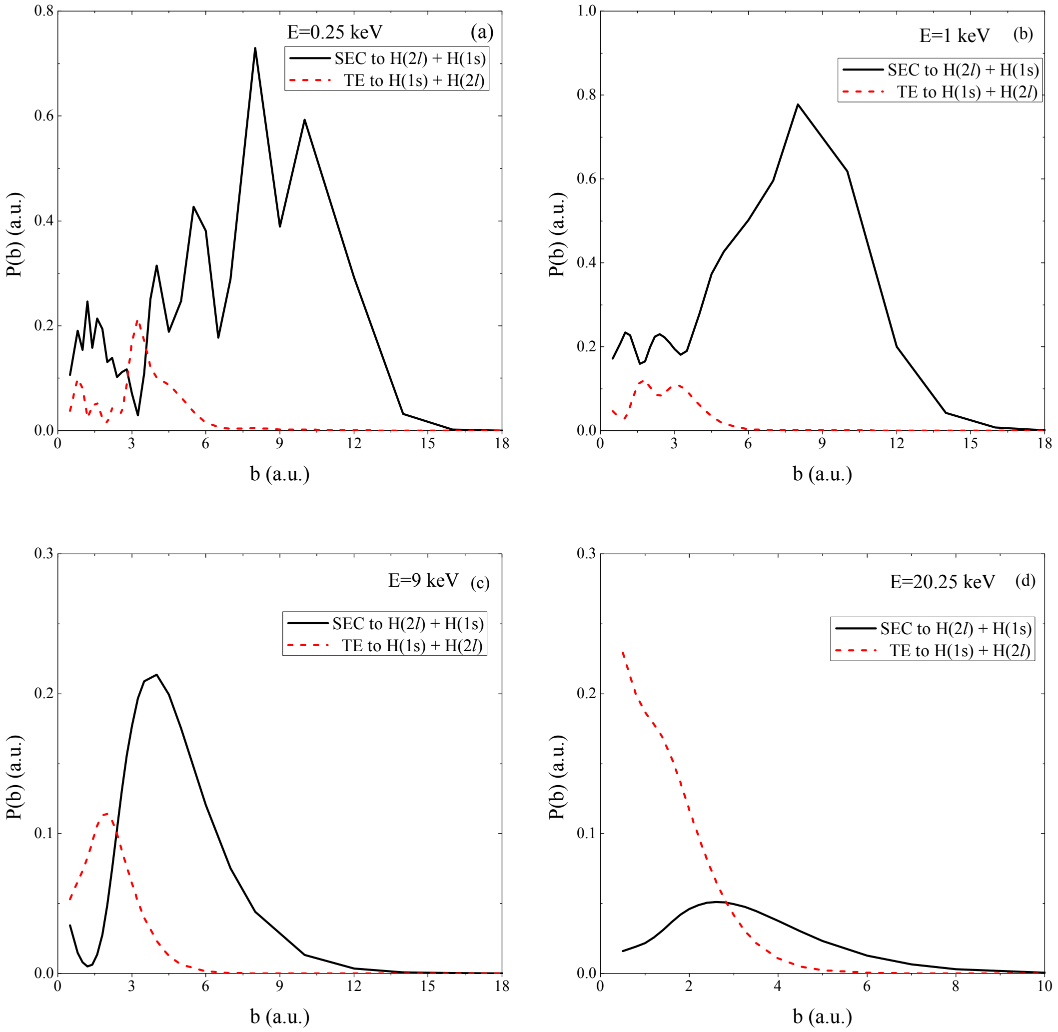

Figure 3.3 – Transition probabilities for pure SEC and TE processes as functions of impact parameter b for impact energies 0.25, 1, 9, and 20.25 keV, respectively. Black solid line denotes pure SEC process; red dash line stands for TE process.

et al. [86] and Peart *et al.* [87], and semiclassical molecular orbital close-coupling (SCMOCC) calculations of Errea *et al.* [88] for comparison. It should be noted that the electron is loosely bound, with a ionization threshold of H^- about 0.028 a.u. (see Table 3.1), which explains the very large value of the ionization cross sections (larger than 10^{-16} cm^2 nearly in the all energy range considered. As it is shown in Figure 3.4, our calculations agree well with the experimental data and the SCMOCC calculations for E > 1 keV, showing that the single ionization process is described quite reasonably in our calculations. For lower impact energies, no experimental cross sections have been reported. The comparison with the SCMOCC calculations of [88] shows that the cross sections of the latter decrease faster than ours. We may attribute the disagreement to the use of a one-electron model and of a small number of pseudo states in the close-coupling expansion in the SCMOCC calculations [88].

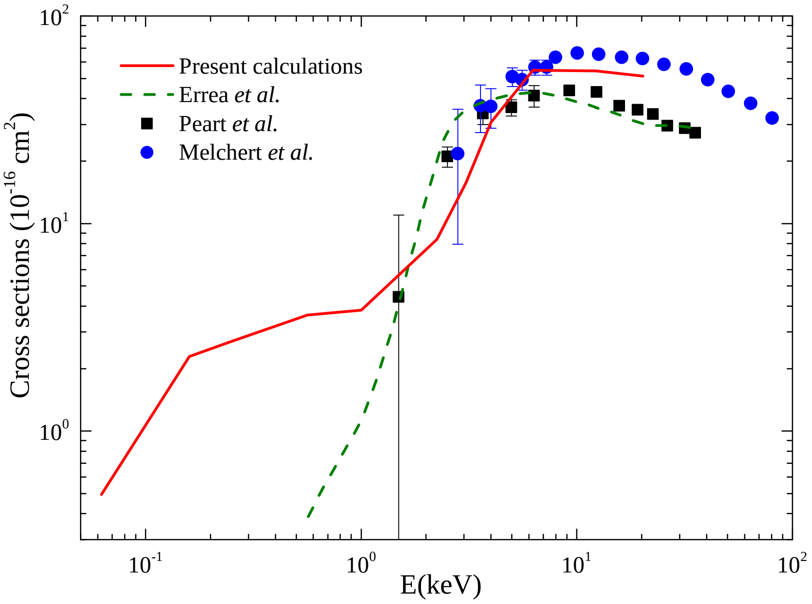

Figure 3.4 – Single ionization cross section as a function of the impact energy. Red solid line: the present calculations; green dash-line: the SCMOCC calculations of Errea *et al.* [88]. blue circle: experiments of Melchert *et al.* [86]; black square: experiments of Peart *et al.* [87].

Further experimental investigations will be useful to draw definite conclusions.

Note that to compute the single ionization cross sections at low collisions, we have removed the contribution of some target pseudo states the energy of which showing resonance or quasi-resonance with highly excited states centered on the projectile. A similar procedure was applied in the SCMOCC calculations (see [88] for more details).

Despite the uncertainty in the single ionization cross sections at low collision energies, it is clear that ionization exceeds DEC for energies ranging from 0.1 to 20 keV. We therefore think that describing properly the ionization process is essential to reproduce quantitatively the DEC cross sections.

The general discussion above shows that the single electron processes, i.e., SEC and SI, are described quite reasonably in our calculations. We turn now to the study of the DEC processes, where all previous calculations fail to reproduce the measured experimental total cross sections.

3.3.2 Double electron capture cross sections

The present DEC cross sections are displayed in Figure 3.5 and compared with available experimental [76–78] as well as theoretical [22, 72, 76, 78, 79] results. Although slightly higher than the experimental ones at the lowest collision energy, our cross sections are in good agreements with experiments over the whole collision en-

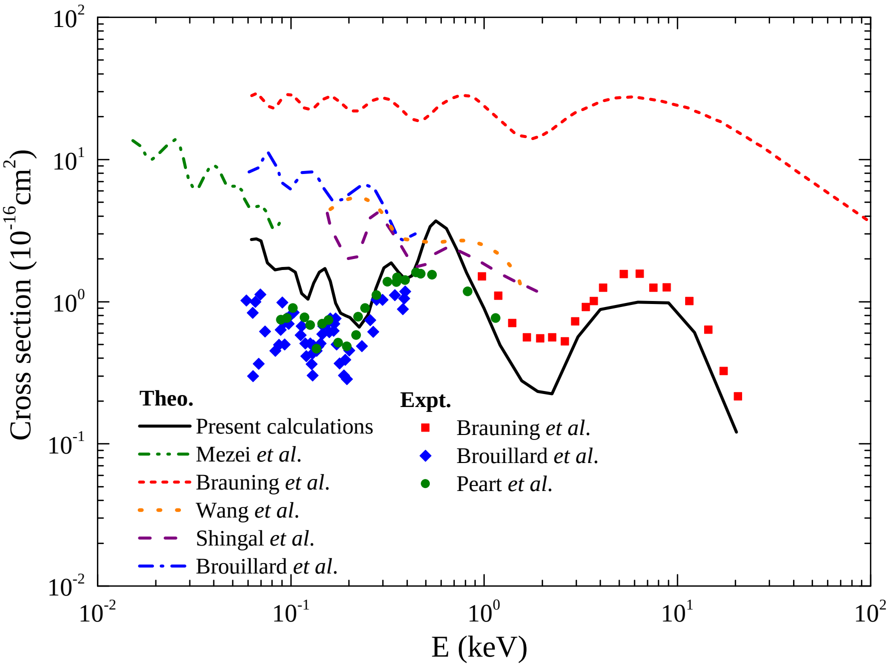

Figure 3.5 – Double electronic capture cross section as a function of the impact energy. Theory: black solid line, the present calcualtons; green dash-dot-dot line, molecular close-coupling calculations of Mezei *et al.* [79]; blue dash-dot line, semi-classical calculation of Brouillard *et al.* [76]; red dashed line, model based on the ion-pair splitting from Bräuning *et al.* [78]; red dotted line, the SCAOCC calculations of Wang *et al.* [22]; purple dash-dash-dotted line, the calculations of Shingal *et al.* [72]. Experiment: red square, measured by Bräuning *et al.* [78]; green circle, by Peart *et al.* [77]; blue diamond, by Brouillard *et al.* [76].

ergy range. Furthermore, the cross section shows a clear oscillatory structure whose period increases with increasing impact energies.

Our results are the first ones to reproduce well the experimental data in both magnitude and shape. We have compared our approach to the previous theoretical methods in order to elucidate what ingredients are needed to describe accurately the DEC process in such a complex system. The main differences between our calculations and the previous *ab initio* ones [22,72,76,79] are (i) the use of much larger basis set, (ii) the full treatment of electronic correlation and (iii) the inclusion of pseudo states which describe the electron continuum and thus the ionization process. Ionization is particularly important since it dominates the DEC process: our calculations show that the ionization cross section is in the order of 10^{-16}–10^{-15} cm^2 between 100 eV and 20 keV, thus exceeding the DEC cross section (see Figure 3.4). We thus think that describing properly the ionization process is essential to reproduce quantitatively the DEC cross section. It should be noted that our calculated SEC cross sections are also in very good agreements with available experimental

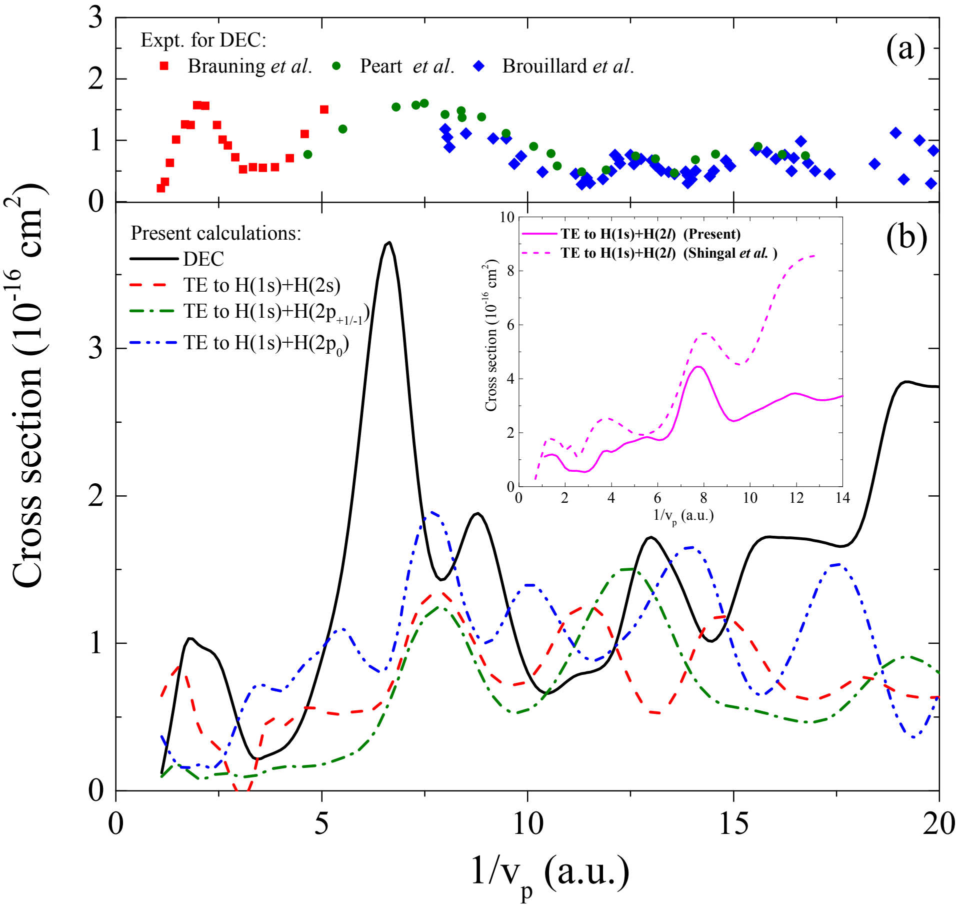

Figure 3.6 – (a) Experimental results [76–78] for DEC cross sections as functions of $1/\mathrm{v}_p$. (b) Present double electron capture and transfer-excitation (TE) cross sections as functions of $1/\mathrm{v}_p$. Black solid line denotes the DEC process; red dash line is for TE into the H(2s) channel; green dash-dot line is for TE into the H($2\mathrm{p}_{+1/-1}$) channel; blue dash-dot-dot line denotes TE into the H($2\mathrm{p}_0$) channel. In the inset, the present cross sections for TE to H(1s) + H(2ℓ) are presented and compared with the coupled-channel calculations reported in [72].

results [67, 71, 84] (see Figure 3.2).

We have further investigated the oscillatory structure in the DEC cross section based on our *ab initio* calculations. In Figure 3.6(b) we present as function of the inverse of the relative velocity, $1/\mathrm{v}_p$, the cross section of the DEC process together with the ones corresponding to the two-electron transfer-excitation (TE) processes, i.e. transfer of one electron to the ground state of the projectile while the second target electron is excited to the L shell (H(1s) + H(2ℓ)) processes. The experimental results [76–78] for DEC are presented in Figure 3.6(a) for comparison. To our knowledge, state-to-state cross section for the TE processes have never been reported experimentally. In the inset in Figure 3.6(b), the cross sections for TE to H(1s) + H (2ℓ) are presented and compared with coupled-channel calculations of [72].

Similarities in the oscillatory structures can be observed. However, the coupled-channel calculations of [72] show larger cross sections compared to the ones from the present calculations in the entire overlapping energy domain, the most likely reason of this discrepancy being the use of only 23-state basis and a lack of continuum states for describing ionization in their calculations.

In Figure 3.6(b) both the DEC and TE cross sections show clear periodic oscillations but with opposite phases, which suggests that the oscillatory patterns come from coherence effects between DEC and TE processes. Such interpretation is different from previous explanations [78] that attributed the oscillations to the interferences between the gerade and ungerade molecular curves describing the ion-pair (elastic and double capture) channels. As discussed in [78], the period of the oscillations should depend on the energy difference between the gerade and ungerade states of the pseudomolecule formed. However, using the potential energy curves of H_2 the authors could not reproduce the measured oscillation period. The authors had to introduce in their model ad hoc (i) cut-off and (ii) increase of the magnitude of the energy splitting in order to achieve a good agreement with the experimental oscillations. As shown below, a simple model based on our interpretation reproduces well the period observed experimentally and in our *ab initio* results without the need of adjustable parameters.

To support our interpretation of the oscillations as interferences between DEC and TE processes, we have extended a model proposed by Rosenthal and collaborators to explain the oscillations observed in the total cross section (i) for excitation of helium by helium ion impact (see also [89, 90] for more details on the model) and (ii) recently, for ionization and negative ion formation in H + H collisions [91]. Similar interferences between two inelastic channels leading to oscillations in total cross sections have been observed, see e.g., for two-electron exchange [92] and references therein. We introduce the details of the model below before being applied to the $H^+ + H^-$ collision system.

In the model proposed by Rosenthal and collaborators [89, 90], the system is described by a linear combination of three states of the transient molecule formed by the projectile and the target, where the total wave function is written as

$$\begin{aligned}\Phi(t,\vec{r}_1,\vec{r}_2) =& f_0(t)e^{-i\int_{-\infty}^{t} E_0 dt'}\phi_0(R,\vec{r}_1,\vec{r}_2) + f_1(t)e^{-i\int_{-\infty}^{t} E_1 dt'}\phi_1(R,\vec{r}_1,\vec{r}_2)\\ &+ f_2(t)e^{-i\int_{-\infty}^{t} E_2 dt'}\phi_2(R,\vec{r}_1,\vec{r}_2)\end{aligned} \tag{3.4}$$

with

$$H\phi_n(R,\vec{r}_1,\vec{r}_2) = E_n\phi_n(R,\vec{r}_1,\vec{r}_2), \tag{3.5}$$

where H is the Hamiltonian of the system and the states ϕ_0, ϕ_1, and ϕ_2 are defined such that:

— ϕ_0 describes asymptotically ($R \to \infty$) the elastic path.

— ϕ_1 and ϕ_2 represent any two inelastic processes.

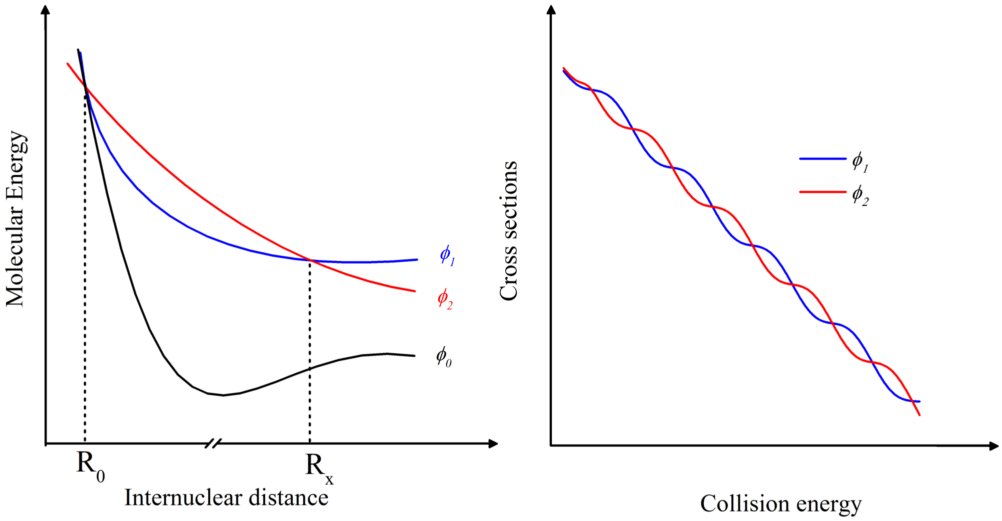

Figure 3.7 – The model proposed by Rosenthal and collaborators [89, 90]. Figure on the left: Molecular energy curves with an inner crossing and an outer crossing; Figure on the right: Cross sections of two inelastic processes.

The corresponding diabatic molecular energy curves are displayed schematically in Figure 3.7: the curve ϕ_0 crosses the curves ϕ_1 and ϕ_2 around R_0 (at time t_0), and the curves corresponding to the two inelastic processes cross again at large distances R_x ($\geq R_0$). The dynamics of the collision can be analyzed on these molecular energy curves: at the beginning of the collision, the system follows the curve ϕ_0 up to R_0 from which the system can be populated to different paths described by ϕ_0, ϕ_1 and ϕ_2. The wave function, after this first crossing around R_0, can then be written as [1],

$$\Phi(t) = f_0(t_0)e^{-i\int_{t_0}^{t} E_0 dt'}\phi_0(R) + f_1(t_0)e^{-i\int_{t_0}^{t} E_1 dt'}\phi_1(R) + f_2(t_0)e^{-i\int_{t_0}^{t} E_2 dt'}\phi_2(R). \tag{3.6}$$

We assume that the transition is done precisely at the crossing R_0 and the system evolves freely thereafter. The time t_0 is related to the position of the crossing R_0 and the velocity of the projectile v_P: $t_0 = \frac{R_0}{v_P}$. Then the system evolves from $R = R_0$ to $R = b$ ($< R_0$) and b to R_0 after the crossing. Each term of the right-hand side of equation (3.6) represents an accumulated phase from the corresponding traveled path, which depends on the corresponding electronic energy. Note that Rosenthal and collaborators [89, 90] assumed that the phase differences, which accumulated from R_0 to b and b to R_0, between the different paths are negligible, since the differences between the corresponding electronic energies are quite small. As the system separates and the internuclear separation passes through R_0 at t_0^{out}, the wave function can be written as,

---

[1] For simplicity, we have omitted in equation (3.5) the dependence on the position of electrons for ϕ_n.

$$\begin{aligned}\Phi(t) =& f_0(t_0^{out})e^{-i\int_{t_0^{out}}^{t} E_0 dt'}\phi_0(R) + f_1(t_0^{out})e^{-i\int_{t_0^{out}}^{t} E_1 dt'}\phi_1(R) \\ &+ f_2(t_0^{out})e^{-i\int_{t_0^{out}}^{t} E_2 dt'}\phi_2(R).\end{aligned} \tag{3.7}$$

On the way out, the phase of each passage will accumulate from R_0 to R_x. At t_x^-, just before the crossing R_x, the amplitudes of ϕ_1 and ϕ_2 are

$$\begin{aligned}f_1(t_x^-) &= f_1(t_0^{out})e^{-i\int_{t_0^{out}}^{t_x^-} E_1 dt} \\ f_2(t_x^-) &= f_2(t_0^{out})e^{-i\int_{t_0^{out}}^{t_x^-} E_2 dt}.\end{aligned} \tag{3.8}$$

The passage through the interaction region at R_x can be represented by a 2 × 2 unitary transformation so that the final amplitudes are given by

$$\begin{pmatrix} f_1(t_x^+) \\ f_2(t_x^+) \end{pmatrix} = \begin{pmatrix} c & d \\ -d^* & c^* \end{pmatrix} \begin{pmatrix} f_1(t_x^-) \\ f_2(t_x^-) \end{pmatrix}. \tag{3.9}$$

The unitarity of the transformation implies

$$\begin{aligned}|c|^2 + |d|^2 &= 1 \\ \left|f_1(t_x^+)\right|^2 + \left|f_2(t_x^+)\right|^2 &= \left|f_1(t_x^-)\right|^2 + \left|f_2(t_x^-)\right|^2.\end{aligned} \tag{3.10}$$

In the adiabatic limit we have $|c|^2 \sim 1$ while in the diabatic limit we have $|d|^2 \sim 1$. The final probabilities of states ϕ_1 and ϕ_2 are, respectively,

$$\begin{aligned}P_1(b) &= \left|f_1(t_x^+)\right|^2 = |c|^2\left|f_1(t_x^-)\right|^2 + |d|^2\left|f_2(t_x^-)\right|^2 + 2\left|cdf_1(t_x^-)f_2(t_x^-)\right|cos(\delta+\gamma) \\ P_2(b) &= \left|f_2(t_x^+)\right|^2 = |c|^2\left|f_2(t_x^-)\right|^2 + |d|^2\left|f_1(t_x^-)\right|^2 - 2\left|cdf_1(t_x^-)f_2(t_x^-)\right|cos(\delta+\gamma).\end{aligned} \tag{3.11}$$

where $\gamma = arg(d/c)$ is usually rather independent of velocity. The phase dependence of the mechanism thus manifests itself in the final term of equation (3.11), in terms of the velocity-dependent phase δ, which is given by

$$\delta = \frac{1}{v_P}\int_{R_0}^{R_x}(E_2 - E_1)dR. \tag{3.12}$$

The b dependence in the right terms of equation (3.11) is only related to the amplitudes f_n, while the coupling terms c and d, as well as the phase difference δ are independent of b. The cross sections for the transitions to ϕ_1 and ϕ_2 can be calculated by the integration of the probabilities $P_1(b)$ and $P_2(b)$ over the impact parameter b,

$$\begin{aligned} \sigma_1 &= A + Bcos(\delta) \\ \sigma_2 &= A^{'} - Bcos(\delta), \end{aligned} \tag{3.13}$$

where A, $A^{'}$ and B are constants from the integrals of equation (3.11). The term $Bcos(\delta)$ accounts for the oscillations observed experimentally. Because of the sign difference in front of this term in equation (3.13), σ_1 and σ_2 oscillate with opposite phases (shown schematically in Figure 3.7). According to the definition of δ (equation (3.12)) and equation (3.13), the cross sections show periodic behavior when presented as a function of $\frac{1}{v_P}$, where the period T is defined by

$$T = \frac{2\pi}{\int_{R_x}^{R_0} \Delta E dR}. \tag{3.14}$$

We have extended this model to our collisional system. A selection of the important H_2 adiabatic potential energy curves of the ${}^1\Sigma_g$ and ${}^1\Sigma_u$ states (noted below g and u states, respectively) converging asymptotically to $H^+ + H^-$ and H(1s) + H(2ℓ) are shown in Figure 3.8. At the internuclear distance R ≈ 15 a.u. [73, 85] the states 4_g and 3_u, corresponding asymptotically to $H^+ + H^-$ (elastic and DEC channels), exhibit strong radial couplings with, respectively, the states 2_g and 1_u (correlated asymptotically to the TE and pure SEC channels H(1s) + H(2ℓ)).

As the target and projectile approach each other on the *way in* the 4_g and 2_g (3_u and 1_u) states couple at R ≈ 15 a.u. Each pathway acquires a different phase according to the energy of the molecular state. There is another strong radial coupling for each symmetry at shorter R (about 1 a.u.) [73, 85] which mix again these states. Finally, the amplitudes of the inelastic channels acquire a different phase and are coherently mixed at R ≈ 15 a.u. on the *way out*. Following the model in [89, 90], the accumulated phases in the DEC and TE cross sections are twice than that given in equation (3.14),

$$T = \frac{2\pi}{2 \times \int_{R_x}^{R_0} \Delta E dR} = \frac{\pi}{\int_{R_x}^{R_0} \Delta E dR} \tag{3.15}$$

The difference between this period and the one expressed in [89, 90] is only a factor of 2 which comes from the accumulated phase of the inelastic amplitudes on the *way in* and on the *way out* in our case while in [89, 90] the phase difference takes place only on the *way out*.

It should be noted that our *ab initio* calculations show that only SEC probabilities are high up to b ≈ 15 a.u. (see Figure 3.3), which illustrates the action of the previous radial couplings observed in molecular calculations [73, 85]. In contrast, the TE processes are only likely at shorter b (see Figure 3.3) which is a necessary condition to observe the oscillations in the total cross sections [92]. These two facts show the clear effect of the inner crossing advocated in the model.

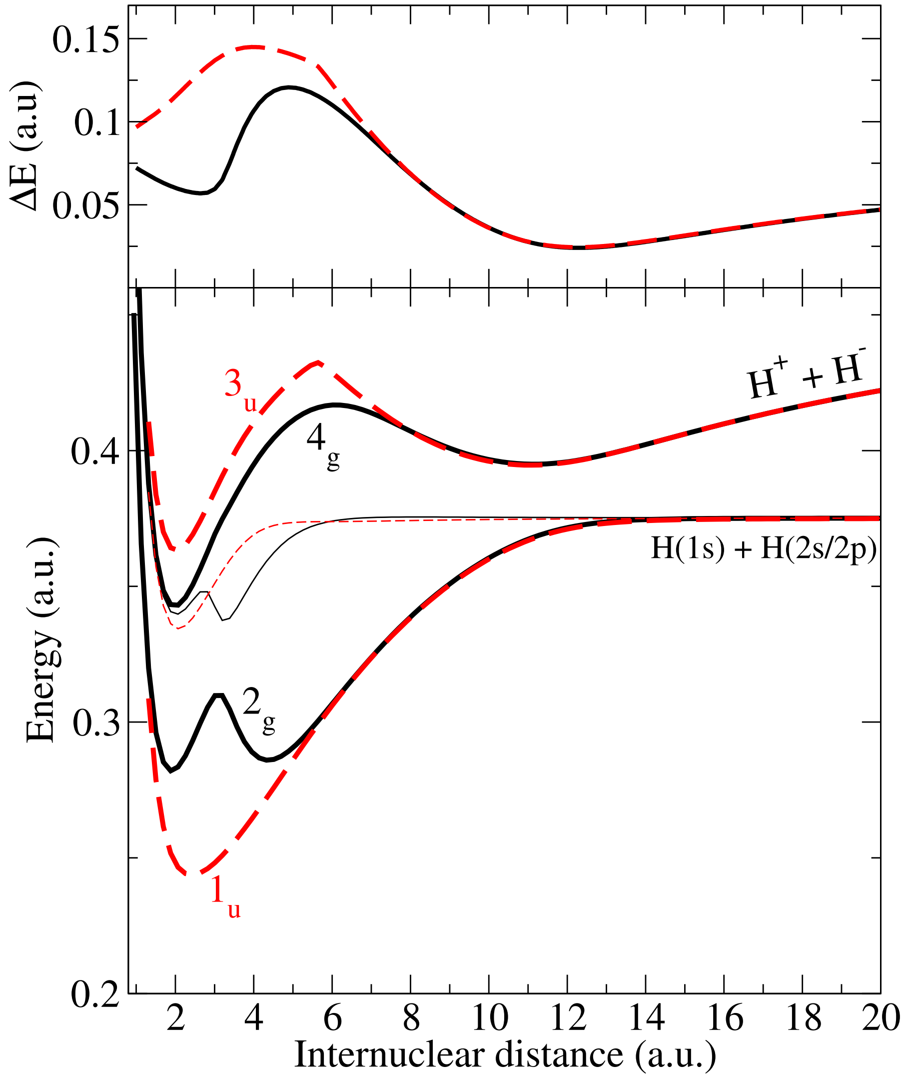

Figure 3.8 – Lower panel: Adiabatic potential energy curves of H_2. The ${}^1\Sigma_g$ and ${}^1\Sigma_u$ states (noted g and u, respectively) are shown in black lines and red dashed lines, respectively. Upper panel: Energy difference between 4_g and 2_g states (black line) and between 3_u and 1_u states (red dashed line).

Using the potential energy curves shown in Figure 3.8, we have calculated the energy difference between 4_g and 2_g states on the one hand and between 3_u and 1_u states on the other hand. The results are shown in the upper panel of Figure 3.8. We have integrated these energy differences between R = 1 a.u. and 15 a.u., according to the position of the strong radial couplings. The expected periods, according to our extended model, are about 3.7 and 3.1 a.u. for g and u symmetry, respectively. These periods agree well with the *ab initio* calculations which predict a period of about 3 a.u. for DEC and TE into H(2p$_0$) and H(2s) processes, supporting our interpretation.

Our *ab initio* calculations show that the oscillations in the cross section for TE into H(2p$_{\pm1}$) have a longer period (5-6 a.u., see Figure 3.6). To describe this process with our model, one has to include the Π_g and Π_u states of H_2 which can be populated by rotational couplings. To our knowledge, the rotational couplings between states of H_2 are not published. However, our *ab initio* calculations show that probabilities for SEC into $H(2p_{\pm1})$ extends up to $b = 15$ a.u., as for $H(2p_0)$ and H(2s). It is therefore reasonable to use the same integration range (i.e. $R =$ 1 a.u. and 15 a.u.) to develop our model for the Π states [93]: the period of the oscillations is then predicted to be about 6.0 and 6.6 a.u. for g and u symmetries, respectively, showing again an overall good agreement with the *ab initio* results.

3.4 Conclusion

The double electron capture process occurring in the course of $H^+ + H^-$ collisions has been a challenge for theoreticians for decades. We have investigated it with a fully correlated and converged two-active-electron approach [23, 80–82]. The present extensive calculations cover a wide energy domain from 0.06 to 20 keV overlapping with the three sets of available experimental data. In contrast to all previous calculations, our calculated cross section shows an overall good agreement with the experimental results in both magnitude and shape. It should be noted that our calculated single electron capture and single ionization cross sections are also in very good agreements with available experimental results. Describing properly these single electron processes is essential to reproduce quantitatively the DEC cross section. Furthermore, our *ab initio* results suggest that the oscillatory structures observed in the double electron capture cross section do not come from interferences between the g and u pathways of the ion-pair configuration as previously put forward but from interferences between double electron capture and transfer-excitation channels. A simple model supports this interpretation. Experimental cross section for transfer-excitation processes are not available and we hope that our results will encourage further experimental works to confirm our interpretation.

Chapter 4

Single- and double-electron transfer in C^{4+}+He collisions

4.1 Introduction

Over the past decades, electron capture processes for various carbon ions colliding with atoms or molecules have received a great deal of attention because of their importance in astrophysics and in the treatment of thermonuclear fusion plasmas. From a fundamental perspective, these systems are also of challenging importance due to the fact that their dynamics illustrates the effects of static and dynamical electronic correlations, strong Coulombic interactions and many likely open channels, especially in the intermediate impact energy domain. In particular, electron capture processes occurring in collisions between C^{4+} and He have been extensively studied for several decades up to very recently, see [94] and references therein, where the studies were concentrating on various impact energy (E) domains above eV/u. It has been shown in both experimental [95–102] and theoretical [94, 100, 102–105] investigations that the single electron capture (SEC) process

$$C^{4+} + He(1s^2) \rightarrow C^{3+} + He^{+} \tag{4.1}$$

dominates up to nearly two orders of magnitude the double electron capture (DEC) process

$$C^{4+} + He(1s^2) \rightarrow C^{2+} + He^{2+} \tag{4.2}$$

for $E \leq 2$ keV/u. Very recently, these investigations were extended by Yan *et al.* [94] to very low energies, from 6 to 10^{-6} keV/u, using a quantum-mechanical molecular-orbital close-coupling (QMOCC) method : good agreements with other available measurements and calculations for both total SEC and DEC cross sections have been obtained in the impact energy region where those studies overlapped. However, for energies higher than 3 keV/u, there are still large discrepancies between the available experimental and calculated results as well as a lack of data beyond 10 keV/u. In this energy region the semiclassical atomic orbital close-coupling (SCAOCC) method is expected to be more appropriate than MO-type approaches and has been applied by Hansen [103] to evaluate total SEC and DEC cross sections for energies up to 11 MeV/u. However the DEC cross sections obtained by Hansen were found to be smaller than the available experimental measurements, the most likely reason of this discrepancy being the use of restricted-size basis sets, which is an unavoidable limitation at that time due to the power of the computers.

In the present work, we study theoretically these two electronic processes in a wide energy region ranging from 0.06 to 300 keV/u. We use a two-active-electron semi-classical atomic orbital close-coupling (SCAOCC) method, which is presented in Chapter 2 of this thesis, with large basis sets ensuring a controlled convergence of the cross sections and providing new physical insight on this collision system. Total and state-selective SEC and DEC cross sections are first discussed and compared with available theoretical and experimental results. Moreover, we present additional coupled channel calculations using (i) one-active-electron basis set, i.e. with no dynamical correlation included, and (ii) two-active-electron basis set restricted to span only SEC channels: comparisons with these two approximations lead to a discussion concerning the role of the electronic correlation during the collision and the underlying mechanisms giving rise to SEC and DEC. In a second stage, the angular-differential cross sections of SEC and DEC processes are presented and compared with available theoretical and experimental results. The main attention is then addressed to the interpretation of oscillatory structures observed in the angular-differential cross sections. To achieve this, simulations are performed using an extend Fraunhofer-type diffraction model. Our investigation suggests that the observed oscillations in the small-angle scattering come from diffractions of direct one-step electron transition processes.

The present Chapter is organized as follows. In section 4.2 we briefly outline the calculation details of the present calculations. In section 4.3, total, state-selective and angular-differential cross sections for single- and double-electron capture are presented. A detailed comparison with available experimental and theoretical data primes the discussion concerning the validity of the existing data and the possible reasons for remaining disagreements. The observed oscillatory structures in the angular-differential cross sections have also been investigated by the simulated Fraunhofer-type diffraction patterns. A brief conclusion will be given in the end of this Chapter.

4.2 Calculation details

To obtain probabilities and cross sections for the SEC and DEC processes occurring in C^{4+}-He collisions in the low- to intermediate-energy range under consideration (i.e., from 0.06 keV/u to 300 keV/u), the two-active-electron semi-classical atomic orbital close-coupling (SCAOCC) method we adopted is presented in the Chapter 2 of this thesis and used for the electronic Hamiltonian $\hat{H}^{el}$ defined as in equation (2.23) with

$$\begin{aligned} V_T(r_i) &= -\frac{2}{r_i} \\ V_P(r_i^p) &= -\frac{4}{r_i^p} - \frac{2}{r_i^p}(1 + \alpha\, r_i^p)e^{-\beta r_i^p}, \end{aligned} \tag{4.3}$$

Table 4.1 – Comparison of energies (in a.u.) of C^{2+} and C^{3+} ions calculated using the model potential [106] with the NIST data [107].

C^{3+}				C^{2+}			
State	E_{GTO}	E_{NIST}	Δ^1	State	E_{GTO}	E_{NIST}	Δ^1
$1s^2 2s\ {}^2S$	-2.3690	-2.3701	0.04%	$1s^2 2s^2\ {}^1S$	-4.1253	-4.1299	0.11%
$1s^2 2p\ {}^2P$	-2.0754	-2.0760	0.02%	$1s^2 2s2p\ {}^1P$	-3.6549	-3.6636	0.24%
$1s^2 3s\ {}^2S$	-0.9909	-0.9902	0.07%	$1s^2 2p^2\ {}^1D$	-3.4592	-3.4653	0.17%
$1s^2 3p\ {}^2P$	-0.9121	-0.9117	0.04%	$1s^2 2p^2\ {}^1S$	-3.2886	-3.2983	0.30%
$1s^2 3d\ {}^2D$	-0.8883	-0.8898	0.17%	$1s^2 2s3s\ {}^1S$	-3.0019	-3.0037	0.06%
$1s^2 4s\ {}^2S$	-0.5417	-0.5414	0.05%	$1s^2 2s3p\ {}^1P$	-2.9489	-2.9502	0.04%
$1s^2 4p\ {}^2P$	-0.5079	-0.5097	0.34%	$1s^2 2s3d\ {}^1D$	-2.8594	-2.8702	0.38%
$1s^2 4d\ {}^2D$	-0.4981	-0.5005	0.47%	$1s^2 2p3s\ {}^1P$	-2.7164	-2.7174	0.04%
				$1s^2 2p4s\ {}^1S$	-2.7074	-2.7096	0.08%
				$1s^2 2p3p\ {}^1P$	-2.6728	-2.6732	0.02%
				$1s^2 2s4p\ {}^1P$	-2.6569	-2.6610	0.15%

[1] $\Delta = |(E_{GTO} - E_{NIST})/E_{NIST}|$.

where V_T corresponds to He^{2+} and V_P corresponds to C^{4+} ion, in the frozen core electron approximation. The latter is taken from Gargaud *et al.* [106] with the variational parameters $\alpha = 8.360572$ and $\beta = 7.72625$ optimized in order to reproduce the experimental energy of the C^{3+} levels. In our calculations, the two active electrons are initially bounded to He, interacting with He^{2+}, and a set of 57 Gaussian-type orbitals (GTOs), denoted as $B1_C$ (13 for $l = 0$, 8×3 for $l = 1$ and 4×5 for $l = 2$) are used on C^{4+} center (28 GTOs, i.e. 10 for $l = 0$ and 6×3 for $l = 1$, on He^{2+}, denoted as $B1_{He}$). This allows the inclusion of 1002 singlet states in total : 146 TT (He), 412 TP (He^+,C^{3+}) and 444 PP (C^{2+}) states. The basis sets, $B1_C$ and $B1_{He}$, are presented in the Appendix B.2. In Table 4.1, we give the energies of the important C^{2+} and C^{3+} states. They are compared with the corresponding experimental data from the NIST tables [107]. The overall agreement between our calculated energies and NIST data is generally very good and at worst equal to about 0.5% for the considered states.

In the same manner as in reference [24], the convergence of the results presented in the following has been checked by computing the cross sections at four distinctive impact energies, 0.25, 4, 49, and 300 keV/u with a series of different GTO basis sets:

- $B2_C$ & $B2_{He}$, a set of 35 Gaussian-type orbitals (GTOs) (10 for $l = 0$, 5×3 for $l = 1$ and 2×5 for $l = 2$) are used on C^{4+} center (19 GTOs, i.e. 7 for $l = 0$ and 4×3 for $l = 1$, on He^{2+}), which allows the inclusion of 517 singlet states in total : 90 TT (He), 232 TP (He^+,C^{3+}) and 195 PP (C^{2+}) states.

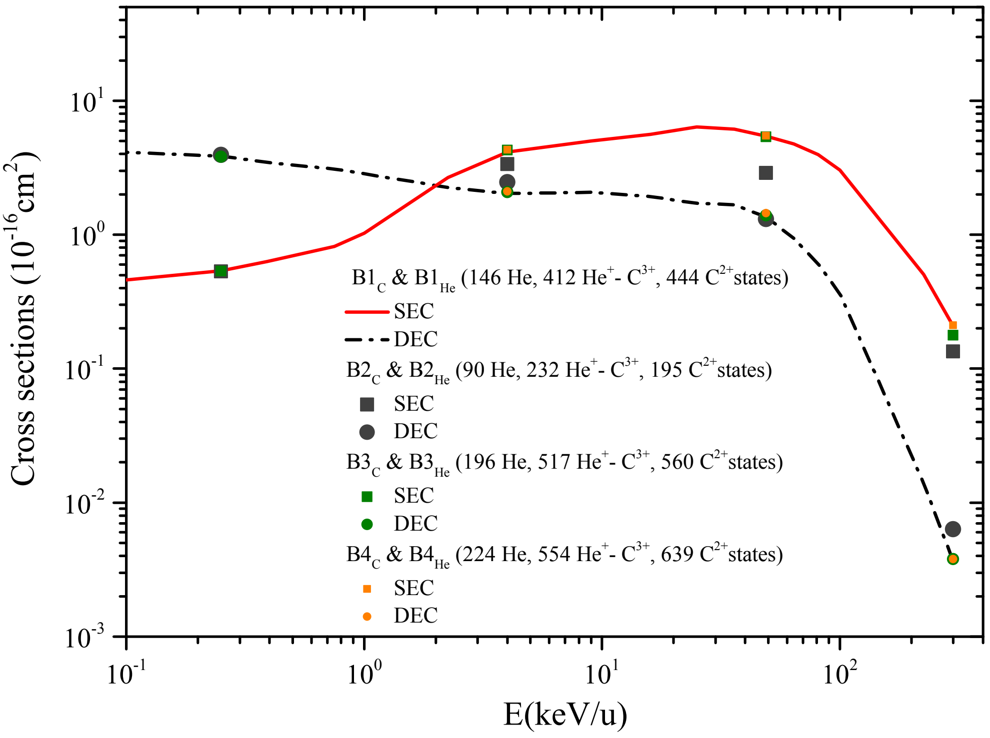

Figure 4.1 – The convergence tests with different basis sets.

- $B3_C$ & $B3_{He}$, a set of 75 Gaussian-type orbitals (GTOs) (15 for $l = 0$, 10×3 for $l = 1$ and 6×5 for $l = 2$) are used on C^{4+} center (36 GTOs, i.e. 12 for $l = 0$ and 8×3 for $l = 1$, on He^{2+}), which allows the inclusion of 1273 singlet states in total : 196 TT (He), 517 TP (He^+,C^{3+}) and 560 PP (C^{2+}) states.
- $B4_C$ & $B4_{He}$, a set of 86 Gaussian-type orbitals (GTOs) (15 for $l = 0$, 12×3 for $l = 1$ and 7×5 for $l = 2$) are used on C^{4+} center (41 GTOs, i.e. 14 for $l = 0$ and 9×3 for $l = 1$, on He^{2+}), which allows the inclusion of 1417 singlet states in total : 224 TT (He), 554 TP (He^+,C^{3+}) and 639 PP (C^{2+}) states.

The detail of these basis sets are presented in the Appendix B.2. As it can be seen, two of them ($B3_C$ & $B3_{He}$ and $B4_C$ & $B4_{He}$) are larger than the one described just above. The SEC and DEC cross sections calculated using these basis sets are presented in Figure 4.1. Comparing the results from these different basis sets, the convergence of both SEC and DEC cross sections was evaluated to be better than 1% in the low impact energy region, to be about 5% for intermediate energies, reaching a maximum of 10% at the highest impact energy (E = 300 keV/u), for which, however, the values of the cross sections are lower than 10^{-17} cm^2.

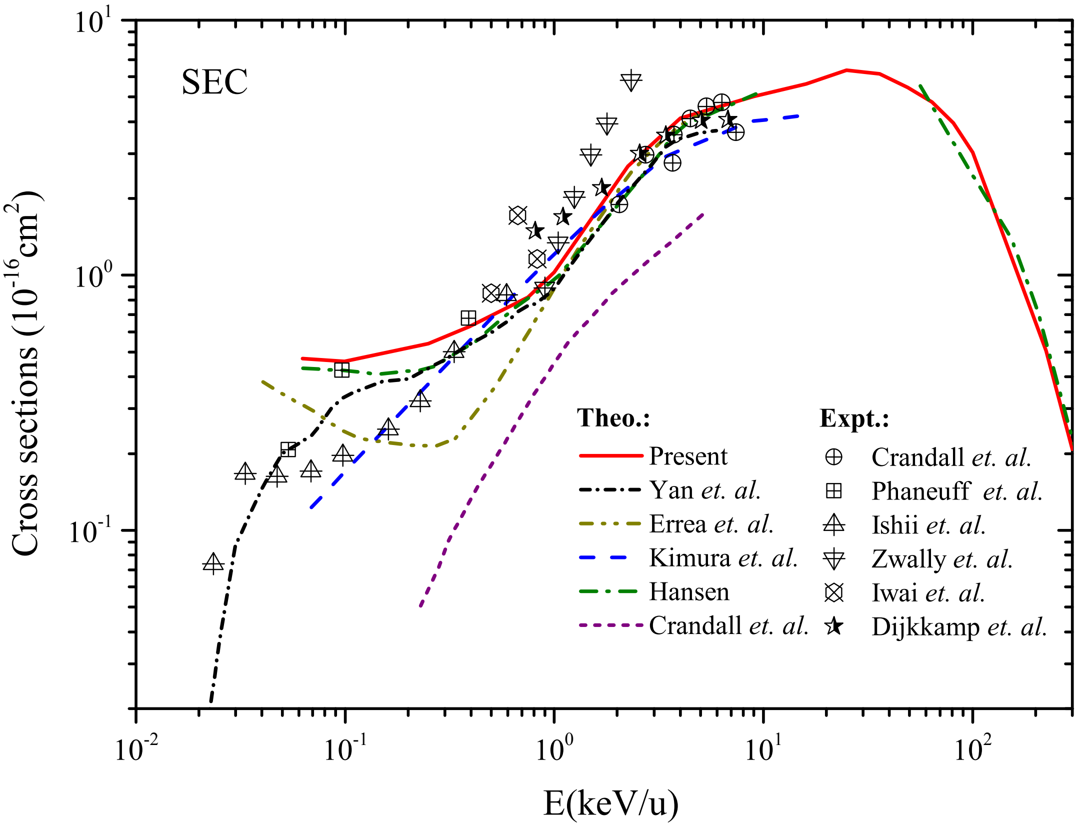

Figure 4.2 – Single-electron-capture (SEC) cross sections as function of impact energy. The theoretical results are from the present calculation (red solid line), Yan *et al.* [94] (black short dash-dot line), Hansen [103] (green dash-dot line), Kimura and Olson [104] (blue dash line), Errea *et al.* [105] (dark yellow dash-dot-dot line), Crandall *et al.* [100] (purple short dash line). The experimental results are from Crandall *et al.* [100] (crossed circles), Phaneuf and Crandall [97] (crossed squares), and Ishii *et al.* [98] (crossed up-triangles), Zwally *et al.* [95] (crossed down-triangles), Iwai *et al.* [101] (crossed diamonds) and Dijkkamp *et al.* [99] (stars).

4.3 Results and discussion

4.3.1 Single electron capture cross sections

Total cross sections

In Figure 4.2, our calculated total SEC cross sections for C^{4+} + He collisions are presented in the energy region 0.06 – 300 keV/u. Previous experimental [95, 97–101] and theoretical [94, 100, 103–105] results are also displayed in the figure for comparison. The cross sections show a maximum around 30 keV/u, following the velocity matching criterion, which predict by simple consideration a maximum for capture when the impact velocity is about equal to the orbital velocity of the active electron in the initial state. As impact energies decrease, the cross sections present a rapid decay; a shoulder, which may be the signature of a molecular-type mechanism, seems to appear around 0.1 keV/u but the general agreement between theoretical and experimental data is rather poor in this energy region so a firm confirmation concerning such structure cannot be made. It can be observed that our results merge very reasonably into the measurements of Crandall *et al.* [100], Phaneuf and Crandall [97], Ishii *et al.* [98], Iwai *et al.* [101] and Dijkkamp *et al.* [99] in the respective overlapping energy regions. However they are slightly higher than the experimental data of Ishii *et al.* for energies below 0.3 keV/u and lower with Zwally's data above 1 keV/u. Comparing with available theoretical results, an excellent agreement is observed between the present results and the AOCC results of Hansen [103] and, for energies above 0.3 keV/u, the QMOCC results of Yan *et al.* [94] and those reported in Kimura and Olson [104]. For $E < 1$ keV/u the SCMOCC results of Errea *et al.* [105] tend to drop faster than our results and present a minimum at about 0.3 keV/u. However the latter results do not match the experimental data of Ishii *et al.* and Phaneuf *et al.* in shape and magnitude. For the lowest energies considered in the Figure 4.2 our results and Hansen's AOCC results lie above the experimental results of Phaneuf and Crandall, Ishii *et al.* and MO-based calculations, [94,104,105]. Since they stem from equivalent atomic orbital based approaches one could speculate that in this energy region (i) the basis sets used in both works may not be large enough to model the active molecular mechanisms responsible for SEC and (ii) the straight-line trajectory approximation starts to fail. We cannot firmly conclude on that issue since large discrepancies exist among the available data for the lowest energy considered in the present work. Note finally that the MOCC results reported in Crandall *et al.* [100] underestimate the SEC cross sections in the whole energy region.

Shell- and state-selective SEC cross sections

In order to provide detailed information about the SEC processes, we now investigate n-resolved and nl-resolved SEC cross sections. Figure 4.3 shows our calculated n-resolved SEC cross sections, in comparison with the very few available data [94, 99, 105]. The analysis is focused on the main capture channels, i.e. $C^{3+}(1s^2n\ell^1\ {}^2L)$ with $n = 2$ and 3. The dominance of the $n = 2$ and $n = 3$ channels follows a complex behavior: our results show that electron capture to $n = 2$ shell dominates the SEC process in a narrow energy region, from 0.8 to 16 keV/u. For this channel, our results are in excellent agreement with the SCMOCC results [105] down to 0.25 keV/u while results reported in [94] lie somewhat higher for $E < 1$ keV/u. Note that below 0.25 keV/u, our results show a plateau-like structure which is not confirmed by other results and may illustrate the limitation of our method at low energy (0.06 keV/u). For $n = 3$ electron capture, our results agree slightly better with the measurements of Dijkkamp *et al.* [99] than the other theoretical results. Our results are in good agreement with the results of Yan *et al.*, but larger than the results of Errea *et al.* below 0.8 keV/u energy. This may be due to the absence of $C^{3+}(1s^23d^1)$ channels in this latter calculation, explaining the low values of the total SEC cross sections reported in [105] for this energy region (see Figure 4.2).

Figure 4.4 shows our calculated $n\ell$-resolved SEC cross sections together with the data presented in [94, 99, 105] and from the one-electron SCAOCC approach of Zhao *et al.* [108]. From Figure 4.4(a) it is clear that capture to C^{3+}(n=2) is

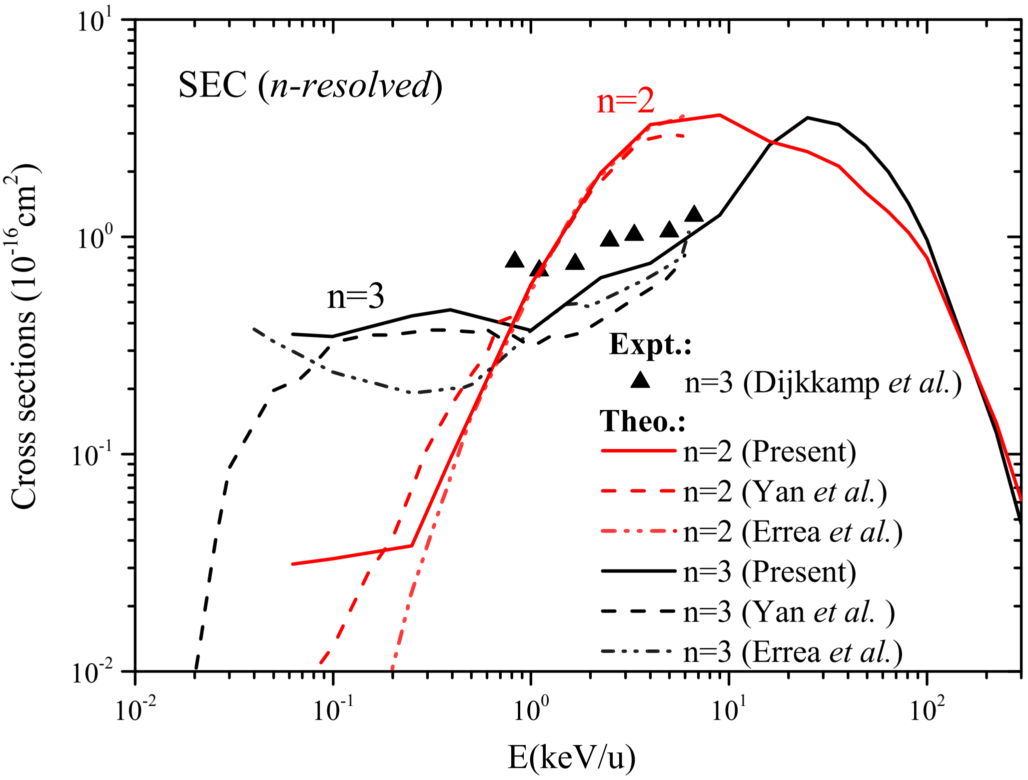

Figure 4.3 – Comparison between the SEC cross sections for electron capture to the n = 2 and 3 shells of the C^{3+} ion with different theoretical and experimental results. The theoretical results are from the present calculation (solid lines), Yan *et al.* [94] (dash lines), Errea *et al.* [105] (dash-dot-dot lines). The experimental results are from Dijkkamp *et al.* [99] (triangle).

induced by a clear dipolar mechanism, with transfer to 2p dominating by at most an order of magnitude the one to 2s in the whole energy domain considered. For electron capture to $C^{3+}(2p)$, see Figure 4.4(a), our results show a nearly perfect agreement with the only experimental data, that of Dijkkamp *et al.* [99] and the theoretical results [94, 105], except again for energies $E < 0.25$ keV/u. The cross sections for capture to $C^{3+}(2s)$ show a similar behavior, though the agreement with previous theoretical results are less satisfactory; no experimental investigation exists to confirm one or the other series of predictions. The cross sections of Yan *et al.* are slightly smaller than our results for the highest energies which may be due again to the neglect of the electron translation factors in their calculations. The cross sections shown in Figure 4.4(b) correspond for electron capture to $C^{3+}(3\ell)$. Our results show that electron capture to $C^{3+}(3d)$ is dominant above 20 keV/u. Below this energy electron capture to $C^{3+}(2p)$ takes over until about 0.8 keV/u for which $C^{3+}(3p)$ starts to dominate. As it can be seen in Figure 4.4(b), the different results are more scattered though the successive dominance of $3d$ and $3p$ channels agree with the experimental results [99] which are somewhat higher in magnitude than ours, as the data reported in [108]. In fact, in this energy region, our calculated

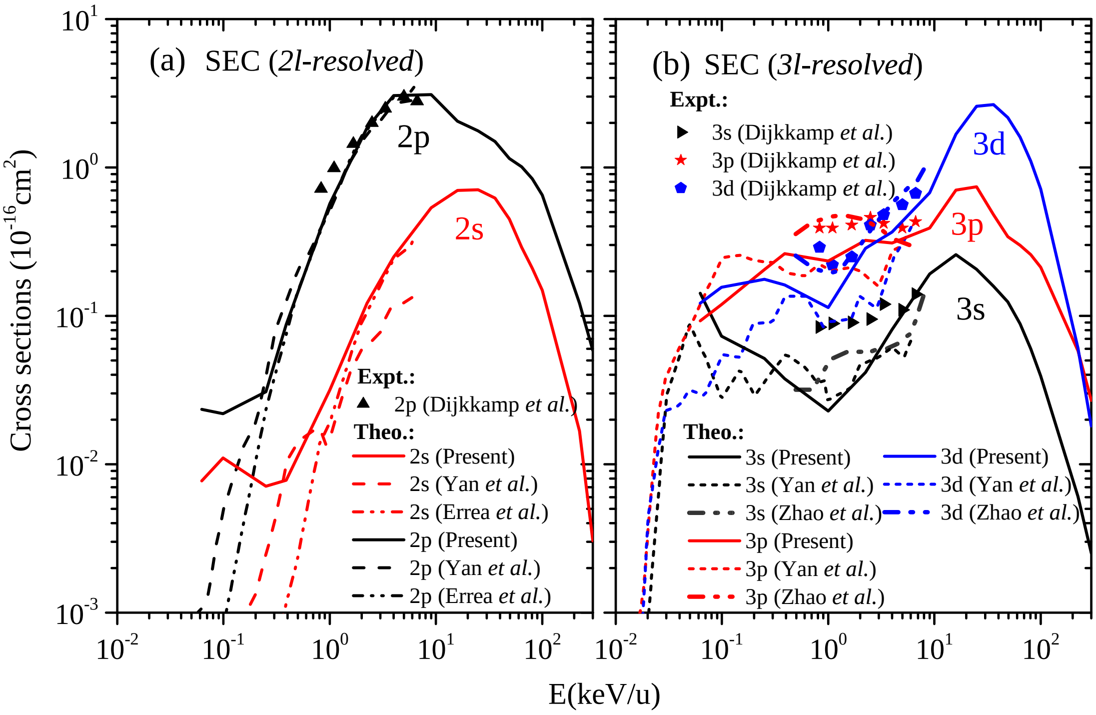

Figure 4.4 – Comparison between the $n\ell$-selective SEC cross sections as function of impact energy : (a) for $n = 2$ and (b) for $n = 3$. The data used for comparison are the same as in the previous figures, except for those reported in Zhao *et al.* [108].

total SEC cross sections shown in Figure 4.2 are also smaller than [99], but in good agreement with the experimental results of Crandall *et al.* [100], Ishii *et al.* [98] and Iwai *et al.* [101]. For all of the results of the investigations available the $3s$ channel is the weakest one; for decreasing energies the experimental data decrease more slowly than the theoretical predictions which present reasonable agreement up to 1 keV/u and with the sudden increase shown in our results. Again, 0.25 keV/u energy may constitute the limit for which the method and the basis set used in the calculations are valid to model some of the weak processes which develop only at low internuclear distances (impact parameters) where refined molecular mechanisms and trajectory effects may take place.

To gain further physical insights into the understanding of SEC processes, a combined analysis of the transition probabilities of SEC as function of impact parameter and the molecular energy curves of the CHe^{4+} molecule is presented in the following. Figure 4.5 shows reduced transition probabilities for SEC to $C^{3+}(1s^2nl$, $n = 2$ or 3; $l = 0$, 1, or 2) as a function of impact parameter b for impact energies 0.25, 4, 25, and 81 keV/u. We have also calculated the molecular energy curves of the CHe^{4+} molecule by diagonalising the molecular (CHe^{4+}) Hamiltonian with our basis set. Our calculated molecular energy curves are presented and compared with the ones of MO-based calculations from Errea *et al.* [105] in Figure 4.6: very good agreements can be found for the lower important states, which indicates that

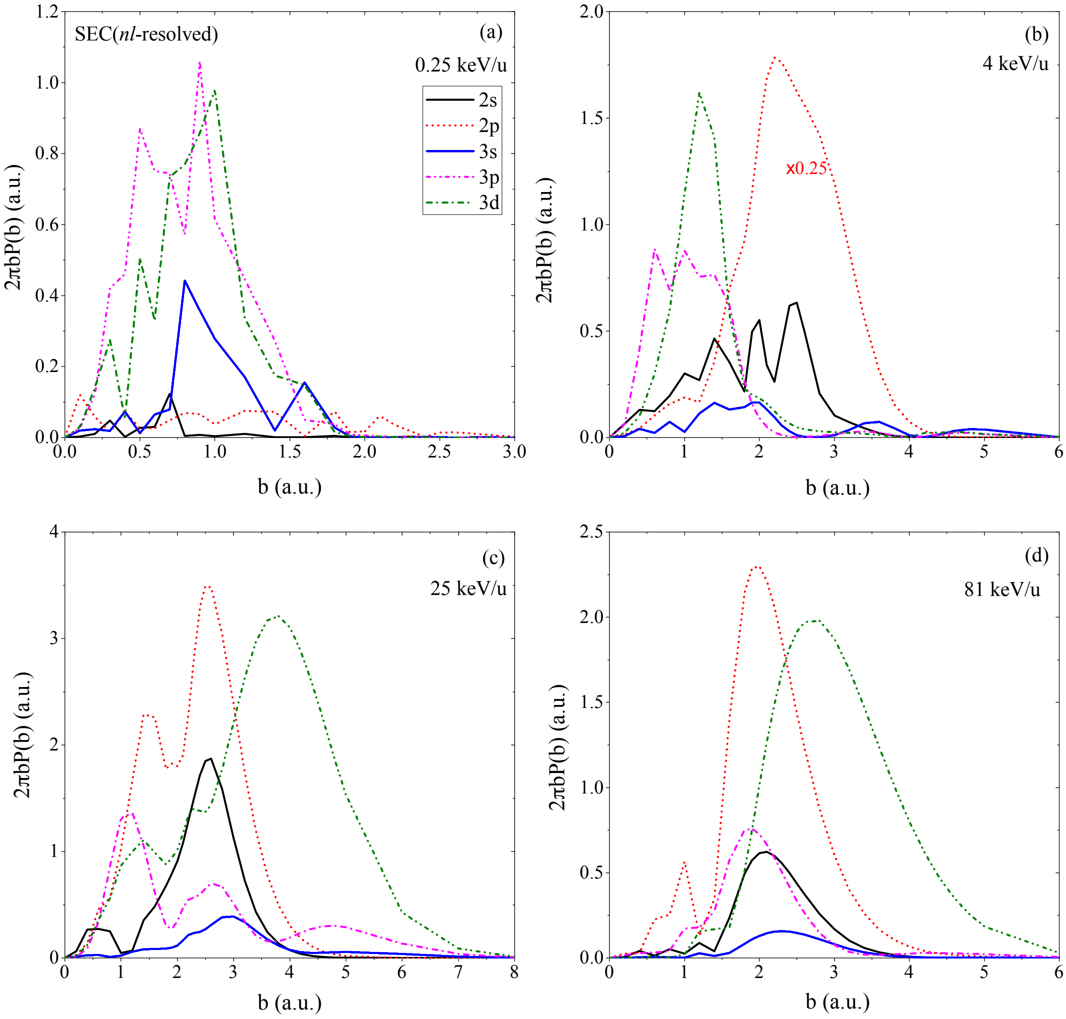

Figure 4.5 – Reduced transition probabilities for SEC to $C^{3+}(1s^2nl$, $n = 2$ or 3; $l = 0$, 1, or 2) as a function of impact parameter b for impact energies 0.25, 4, 25, and 81 keV/u.

the present basis set and calculations can reveal molecular mechanisms as the MO-based calculations do. As it can be observed in Figure 4.4, the $n\ell$-selective SEC cross sections shows the successive dominance of the $3p$ ($3d$), $2p$ and $3d$ capture channels for increasing energies, which stems from three different mechanisms that can be illustrated with transition probabilities for SEC to $C^{3+}(1s^2nl$, $n = 2$ or 3; $l = 0$, 1, or 2) presented in Figure 4.5 and the molecular energy curves of the CHe^{4+} systems shown in Figure 4.6. For lower energies, the SEC to $3p$ dominates the others. As it can be seen in Figure 4.5, the transition probabilities shows a oscillatory structure, and extends only to impact parameter $b < 2$ a.u., which corresponds to a series of crossings shown in the molecular energy curves of the CHe^{4+} molecule for internuclear distances smaller than 2 a.u. (see Figure 4.6). This indicates that the dominant $3p$ capture proceeds through the complex series of crossings occurring at small internuclear distances. On the other hand, for high energies it is a direct -

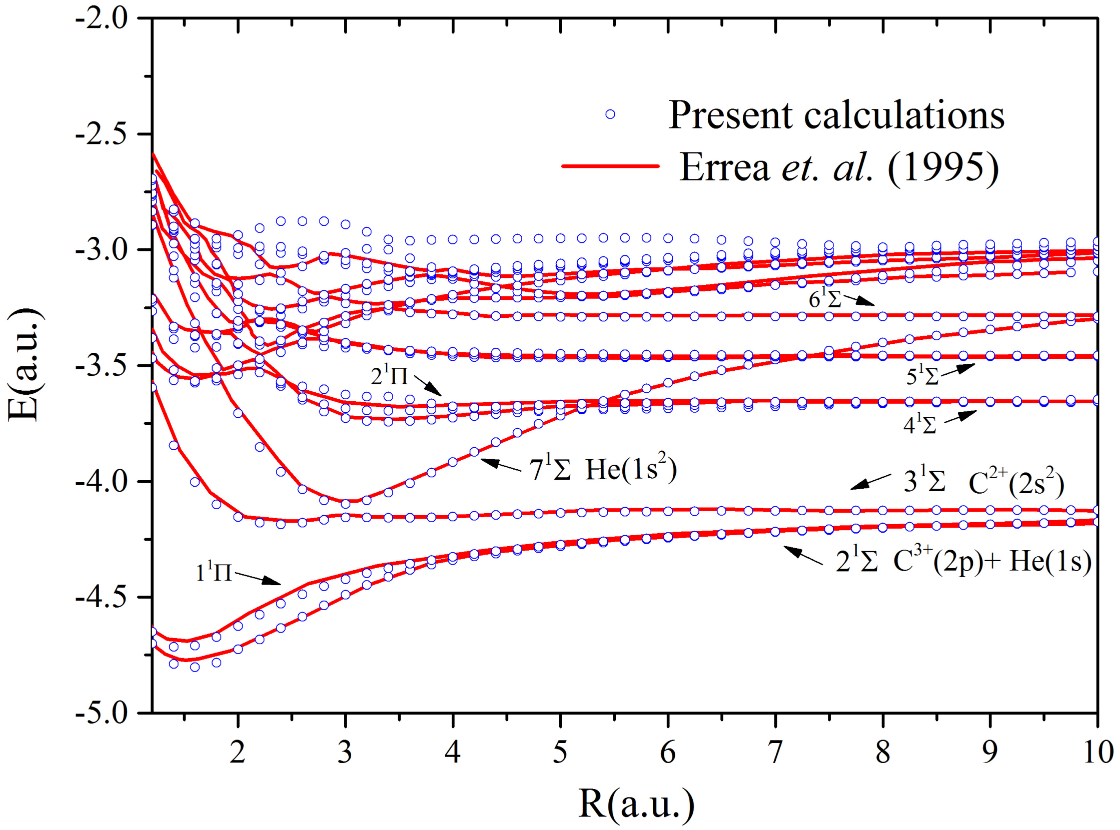

Figure 4.6 – The molecular energy curves for the CHe^{4+} system as a fuction of internuclear distance R: Comparison between present calculations (blue open circle) and the calculations of Errea *et al.* [105] (red solid line).

atomic - mechanism, the transition probabilities fall off only for $b > 7$ a.u., which explains the dominant quasi resonant $C^{3+}(3d)$+$He^{+}(1s)$ channels. In between (around 9 keV/u), as it can be seen in Figure 4.5, the transition probabilities for 9 keV/u extend up to $b = 8$ a.u., and show sharp peaks around $3.0 - 4.0$ a.u. This suggests it is an interplay between a direct mechanism and a molecular one through the avoided crossings around $3.0 - 4.0$ a.u. (see Figure 4.6 and [105]) which may explain the dominance of the $2p$ capture channels. Moreover, the $2p$ and $3p$ cross sections show shoulder-like structures in the energy region above 10 keV/u, which also mark the respective decrease and increase of the contributions of the low-b molecular and larger-b direct mechanisms.

4.3.2 Double electron capture cross sections

Total cross sections

In Figure 4.7 the present total DEC cross sections are presented together with the corresponding data stemming from the same work as the ones used for SEC, i.e. [97,98,100] experimental and [94,100,103–105] theoretical investigations. Compared to SEC, the DEC cross sections show a very different behavior as a function of impact energy: a weak dependence from 0.1 to 10 keV/u and a rapid decrease for high

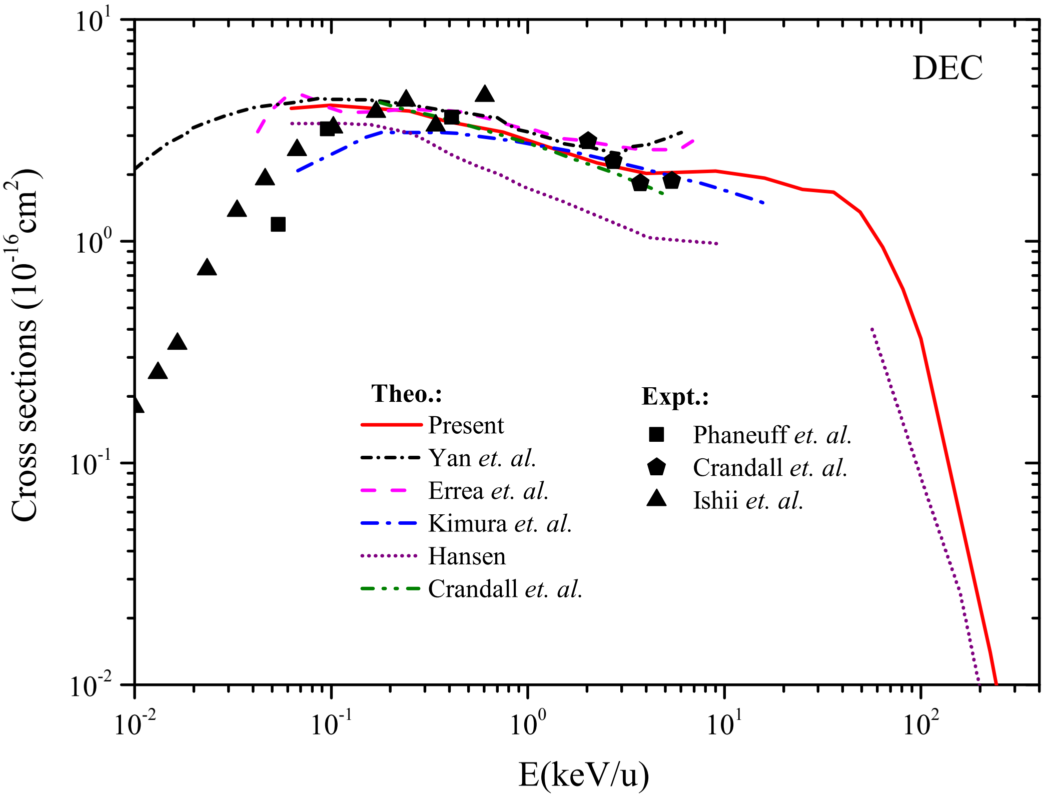

Figure 4.7 – Comparison between the present DEC cross sections with different experimental and theoretical results as a function of impact energy. The theoretical results are from the present calculation (red solid line), Yan *et al.* [94] (black short dash-dot line), Errea *et al.* [105] (magenta dash line), Kimura and Olson [104] (blue dash-dot line), Crandall *et al.* [100] (green dash-dot-dot line), Hansen [103] (purple dot line). The experimental results are from Phaneuf and Crandall [97] (solid squares), Crandall *et al.* [100] (solid pentagons), and Ishii *et al.* [98] (solid triangles).

and low energies, thus in agreement with the data of Phaneuf and Crandall [97] and Ishii *et al.* [98]. In the intermediate energy region the present results agree well with the experiments except for $E < 0.1$ keV/u, where our results do not follow the decrease mentioned before. However, comparing with available theoretical calculations, our present results are in excellent agreement with the results of Yan *et al.*, Errea *et al.*, and Crandall *et al.* for $E < 3$ keV/u; note that, in agreement with our data, the QMOCC results of Yan *et al.* and the SCMOCC results of Errea *et al.* do not show the clear decrease observed in [98] for $E < 0.1$ keV/u. This discrepancy may be due to angular scattering effects in the signal collection of the measurement, which tend to underestimate the absolute cross section for very low collision energies [94]. For $E > 3$ keV/u, our results are slightly lower than the QMOCC [94] and SCMOCC [105] results but agree quite well with the experimental results of Crandall *et al.* [100]. It should be noted that an atomic orbital method is expected to be more appropriate for high impact energies. Moreover, electron translation factors (ETFs) have not been included in [94] though one expect that it can induce larger effects in this region. For the entire energy domain considered the data from Hansen [103], are smaller than most of the theoretical and experimental results. Though stemming from an AOCC approach including ETFs this failure may be due to the minimal basis set used in these early calculations. Note that for the high energy considered Hansen's DEC cross sections are also smaller while SEC ones compare fairly well with ours, see Figure 4.2.

State-selective DEC cross sections

State-selective DEC cross sections are presented in Figure 4.8, together with the only available theoretical results, those of Yan *et al.* [94] and Errea *et al.* [105]. It can be observed that electron capture to C^{2+}($2s^2\ ^1S$) state is dominant in the energy region below 20 keV/u while capture to C^{2+}($2p^2$) states takes over for higher energies. It should be noted that the cross section for this latter electronic configuration is totally dominated (> 90 %) by the contribution of the lowest energy term, i.e. ^1D. For electron capture to $2s^2$ state, our results agree very well with the QMOCC results of Yan *et al.* and the SCMOCC results of Errea *et al.* in the whole overlapping energy region. The agreement with [94, 105] is less satisfactory for the two other electronic configurations, especially for $2s2p$ for which our results are systematically lower than the two previous series of data which agree quite well with each other. For $E > 3$ keV/u the calculations of Yan *et al.* and Errea *et al.* overestimate the total

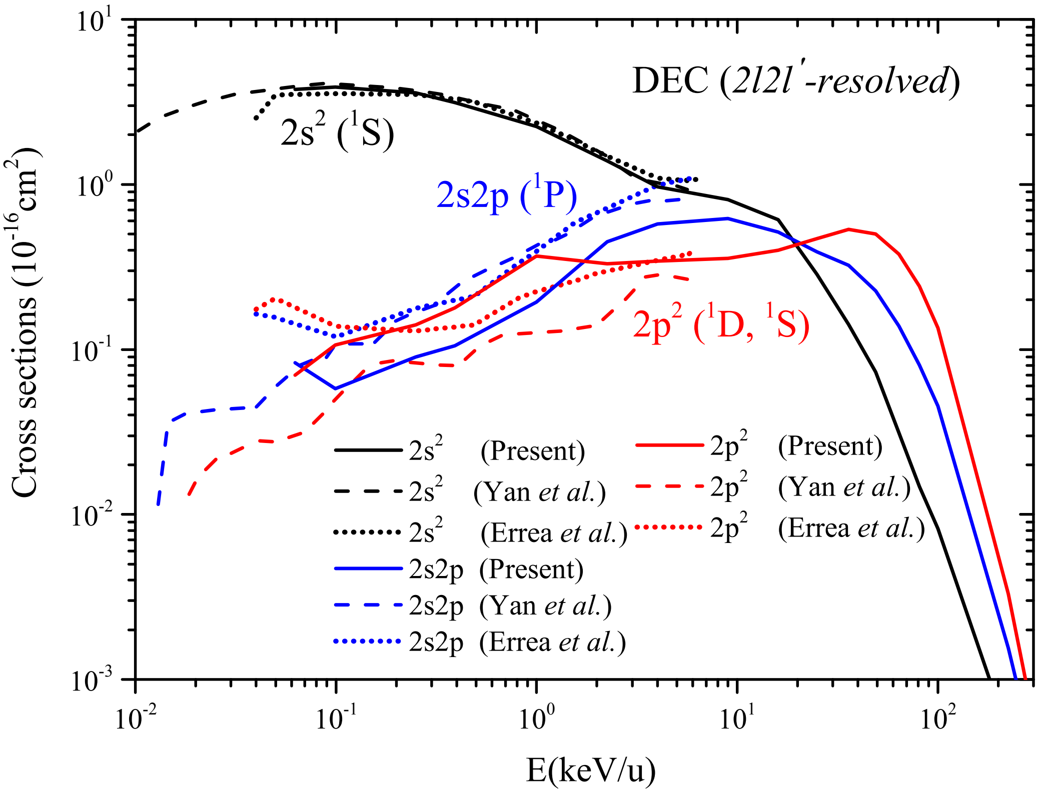

Figure 4.8 – State-selective DEC cross sections as function of impact energy: the present calculations are shown by the solid lines, the results of Yan *et al.* [94] by the dash lines and those of Errea *et al.* [105] by the dot lines.

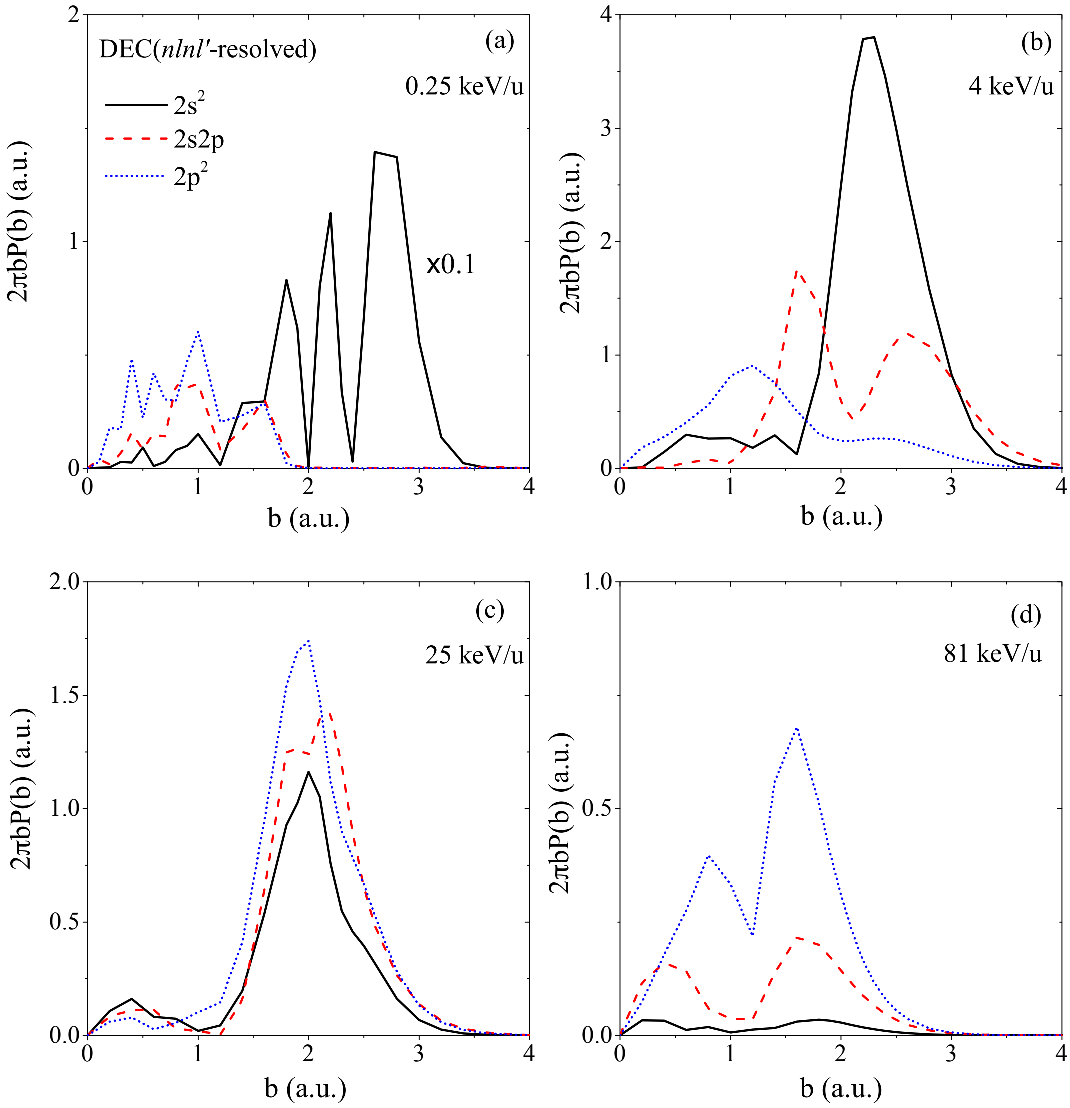

Figure 4.9 – Reduced transition probabilities for DEC to $C^{2+}(1s^2nlnl'$, $n = 2$; $l = 0$ or 1; $l' = 0$ or 1) as a function of impact parameter b for impact energies 0.25, 4, 25, and 81 keV/u.

DEC cross sections of Crandall *et al.* [100] (see Figure 4.7), while our results are in good agreement with these experimental results. It is worth noting, however, that for $E = 2$ keV/u our calculations predict an interchange between the contributions of $2s2p$ and $2p^2$ to DEC. This is not observed in the two other calculations where $2s2p$ dominates. This difference may be due to the fact that our large basis set includes the DEC $2sn\ell$ and $2pn\ell$ ($n \geq 4$) channels which may change the dynamics of the collision.

Furthermore, in order to gain more insights into the mechanisms responsible of the DEC channels, we show in Figure 4.9 the related reduced transition probabilities as a function of the impact parameters for the impact energies 0.25, 4, 25, and 81 keV/u. Compared to the SEC processes, the transition probabilities of DEC processes are confined to near head-on collision trajectories ($b < 4$), where the transitions are more likely to take place through a molecular mechanism. For the lower energies, the transition probabilities for the DEC to $C^{2+}(2s^2)$ are dominated in the impact parameter region $2-4$ a.u., which suggests that transitions leading to $C^{2+}(2s^2)$ take place at the avoided crossing at $R \sim 3$ a.u. (see Figure 4.6) through a simultaneous exchange of both electrons. The latter is also supported by the MO-based calculations of Errea *et al.* [105] (and references therein) where it was shown that the radial coupling between $7^1\Sigma$ (He($1s^2$)) and $3^1\Sigma$ ($C^{2+}(2s^2)$) are significantly strong at $R \sim 3$ a.u., which may explain the fact that DEC cross sections dominate up to nearly 2 orders of magnitude over the SEC ones for $E \leq 2$ keV/u. Unlike the DEC to $C^{2+}(2s^2)$, the transition probabilities for DEC to $C^{2+}(2s2p)$ and $C^{2+}(2p^2)$ extend only to the impact parameter $b < 2$ as shown in Figure 4.9(a), but also present sharp peaks which corresponds to a complex series of avoided crossings in the molecular energy curves of the CHe^{4+} molecule for small internuclear distances (see Figure 4.6). For higher energies, the probabilities have a relatively smooth shape, and show the successive dominance of $2s^2$, 2s2p, and $2p^2$ capture channels as the impact energies increase (see also Figure 4.8). This indicates a complex coupled-channel scheme.

4.3.3 Mechanisms for SEC and DEC processes

We turn now to the study of the role of the electronic correlation during the collision and the underlying mechanisms giving rise to SEC and DEC. In order to have a sharper probe to the dynamics of the collision, additional model calculations have been performed: cross sections stemming from two-active-electron calculations with only SEC channels included in the basis set and single-active-electron calculations (using the model potential reported in [45] for He) are shown in Figure 4.10. They are compared with the results from our full two-active-electron calculations and from limited-basis (including only SEC channels) calculations of Hansen [103]. The SEC results from single-active-electron calculations are shown to be much larger than the results from our full calculations up to $E < 25$ keV/u impact energy beyond which both models converge. This tends to prove that electronic correlations play an important role in C^{4+} + He collisions in low impact energy region. Moreover using one-electron results total DEC cross sections were also calculated within the independent event model (IEV) and independent particle model (IPM) approximations [109]. In the low impact energy region the results (not shown) from IEV and IPM were found to be much smaller than our full calculations and other theoretical predictions [94,100,103–105] as well as experimental measurements [95,97,99–101]. This further demonstrates the inadequacy of one-electron models to describe the main electronic processes in C^{4+} + He collisions and the importance of the inter-electronic interaction. Comparing the results from our full calculations with the two-electron close-coupling calculations restricted to SEC channels, the good agreement observed in the whole energy region indicates that the SEC processes develop independently of the main DEC process. This finding is opposite to Hansen's con-

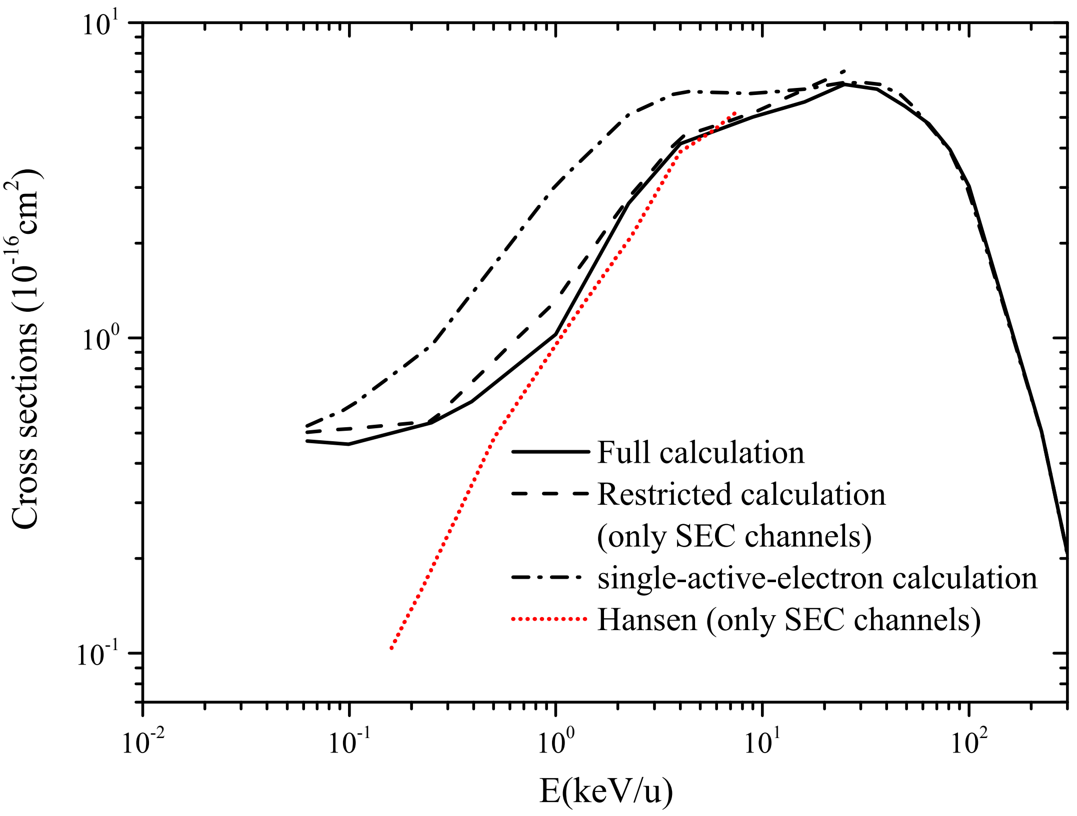

Figure 4.10 – SEC cross sections as function of impact energy. Present full calculations: red solid line; two-active-electron calculations with restricted basis set: blue dash line; single-active-electron calculations: black dash-dot line. The results from Hansen [103] are shown with pink dotted line.

clusion stating that SEC is mediated via DEC channels [103] and drawn in view of the fast decay of the SEC cross sections from his restricted (no DEC channels included) calculations. This behavior does not agree with our calculations stemming from two-active-electron calculations with only SEC channels (dashed line in Figure 4.10) below $E \approx 1$ keV/u and is certainly due to the very limited basis set used in [103]. To reinforce this conclusion we present in Figure 4.11 the transition probabilities to the main SEC channels ($C^{3+}(1s^2 2p^1)$) at $E = 0.75$ keV/u collision energy. As it is shown in Figure 4.6 (see also text and Figure 1 in Errea *et al.* [105]) that at low energies this channel is populated through avoided crossings around $3-4$ a.u. internuclear distances: this region implies the $7^1\Sigma$, $2^1\Sigma$ and $3^1\Sigma$ molecular states correlated asymptotically to the initial (He($1s^2$)), SEC $C^{3+}(1s^2 2p^1)$ and DEC $C^{2+}(1s^2 2s^2)$ atomic states. Our results in Figure 4.11 show that the probabilities calculated with or without DEC channels (i.e. including or not $3^1\Sigma$) agree with each other in shape and extension, except for only slight differences. This indicates that the reaction takes place directly from $7^1\Sigma$ (He($1s^2$)) to $2^1\Sigma$ (C^{3+}(2p)) (in other words, through the radial coupling between these two states, see [105,110]), without having much interaction with the 3 $^1\Sigma$ state, as discussed in [105]. This supports the conclusion concerning the weak dependence of SEC dynamics upon DEC processes

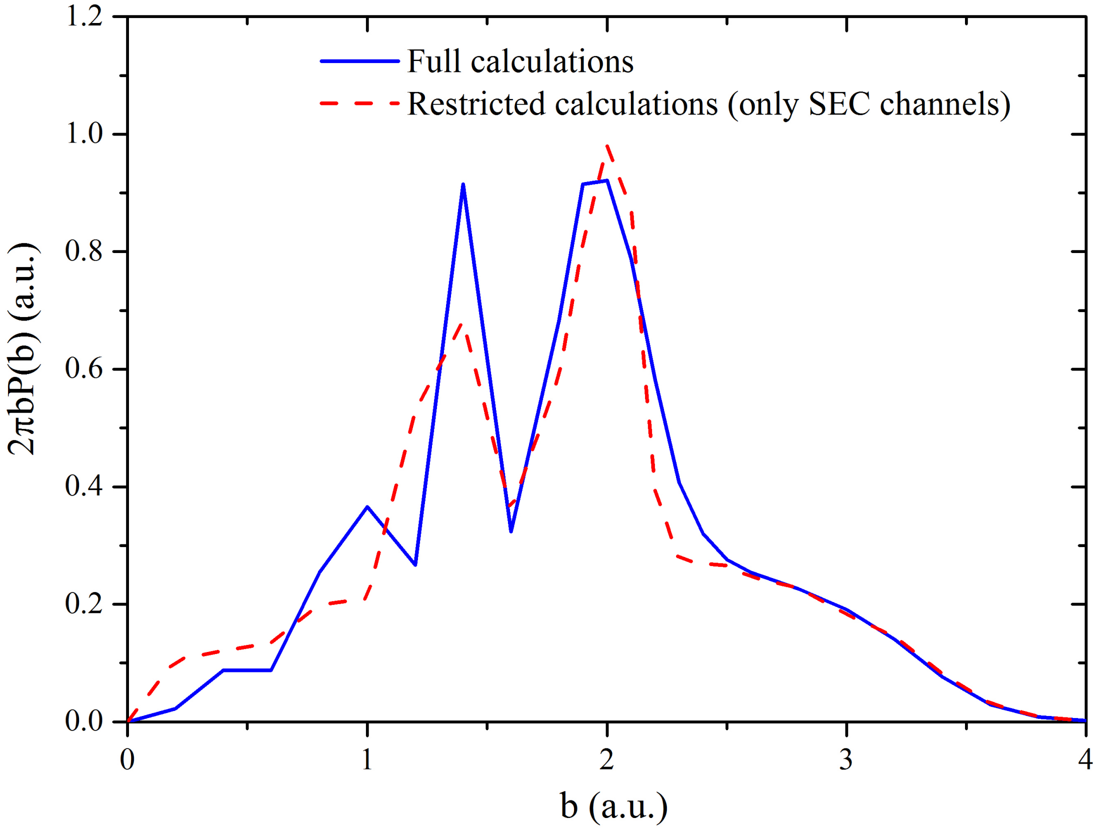

Figure 4.11 – Transition probabilities for SEC as function of impact parameter b, for $E = 0.75$ keV/u. The results are from our full calculations (blue solid line) and two-active-electron calculations restricted to SEC channels (red dash line).

in the energy domain considered. This is rather in qualitative agreement with previous investigations [105,110,111] that have shown that the DEC processes take place through simultaneous exchange of both electrons in the low impact energy region.

On the contrary, in the high energy region, Hansen's comparison [103] between SCAOCC calculations and independent-electron Bohr-Lindhard type model [112] suggested that the DEC process is dominated by independent electron transfer processes. In Figure 4.12, these results [103] are compared with our DEC cross sections stemming from full two-electron calculations as well as IEV and IPM approaches (using the one-electron model already described). One can observe a surprising agreement between the results of the present full calculations and those stemming from the simple, Bohr-Lindhard model. However, though showing similar decays, the results from IEV and IPM are quite different from our close-coupling results. This indicates that electronic correlations are still important in this energy domain, i.e. that the DEC process cannot be described successfully by independent particle processes. In the high impact energy region, the direct two-electron transfer mechanism - from initial state to final state - do dominate also the dynamics of DEC processes. The agreement with the Bohr-Lindhard typed independent-electron predictions reported in [103] may then be simply fortuitous and only restricted to a limited energy domain.

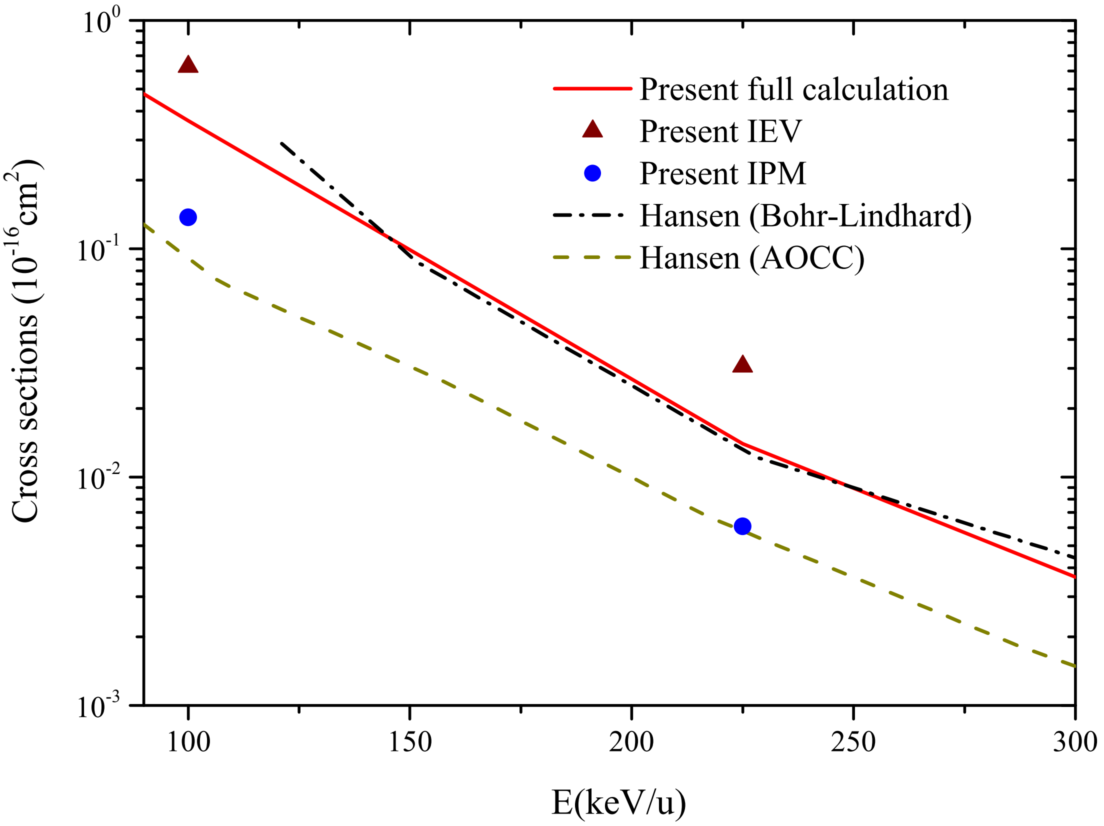

Figure 4.12 – The DEC cross sections from present full calculations (red solid line), present IPM and IEV calculations (solid circles, solid triangles respectively), SCAOCC calculations (green dashed line) and Bohr-Lindhard model calculations (black dash-dot line) of Hansen [103].

4.3.4 Angular-differential cross sections

We now investigate the angular-differential cross sections in the double electron capture (DEC) process,

$$C^{4+}(1s^2) + He(1s^2) \rightarrow C^{2+}(1s^2 2s^2) + He^{2+} \tag{4.4}$$

and the single electron capture (SEC) process,

$$C^{4+}(1s^2) + He(1s^2) \rightarrow C^{3+}(1s^2 2s) + He^{+}(1s), \tag{4.5}$$

which provide a greater benchmark for our calculations.

Double electron capture

Figure 4.13 shows our calculated angular-differential cross sections for the DEC process presented in equation (4.4) for impact energy 0.8 keV/u. The only existing theoretical [105] and experimental [96] results for the considered impact energy are also displayed in the figure. Comparing with the only existing theoretical results, an

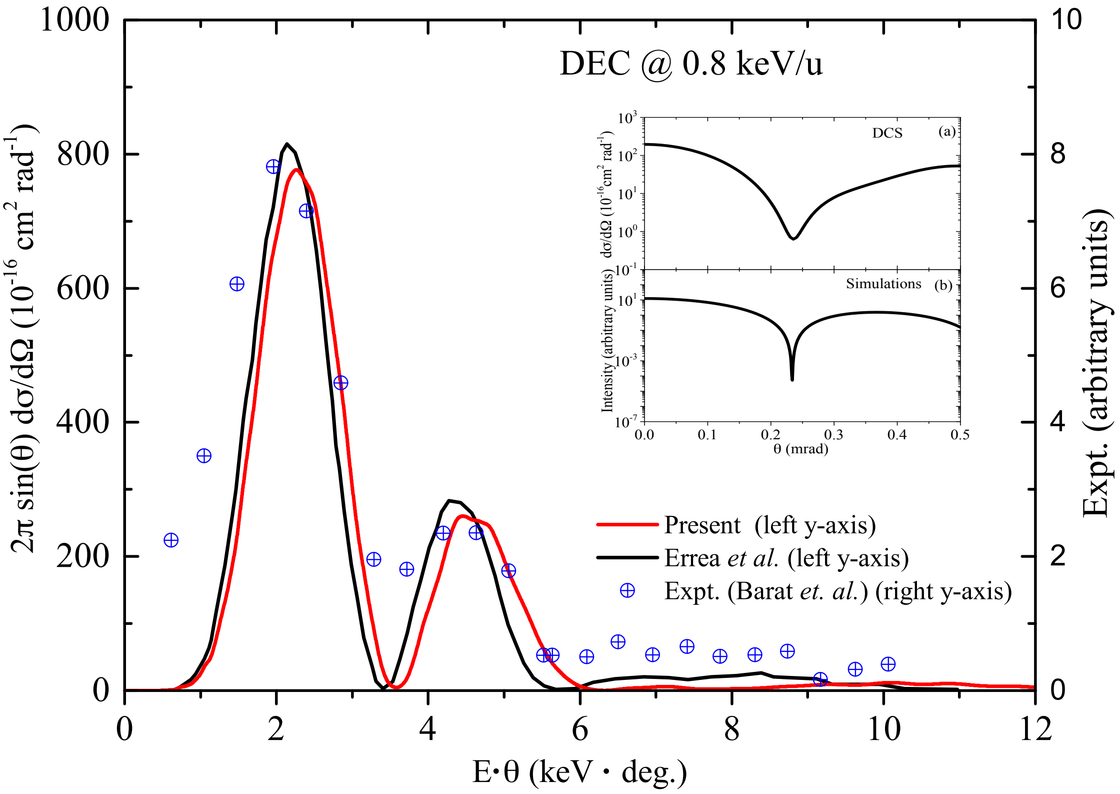

Figure 4.13 – The angular-differential cross sections for the DEC process in equation (4.4) as a function of scattering angle at impact energy 0.8 keV/u. Red solid line: present calculations; black solid line: theoretical results of [105]; blue crossed circles: experimental results from [96]. In the inset: (a) The angular-differential cross sections for the DEC process in equation (4.4) as a function of scattering angle (the small-angle scattering part) at impact energy 0.8 keV/u. (b) The angular intensity distribution of the simulated Fraunhofer-type diffraction patterns for impact energy 0.8 keV/u.

excellent agreement, with only small shift toward smaller angles for Errea's results, is observed between the present results and the semiclassical molecular-orbital close-coupling (SCMOCC) results of Errea *et al.* [105]. In fact, at low impact energies, electronic processes are more likely occurring via the formation of the transient molecule formed by the projectile and target, so that the molecular-orbital (MO)-based approaches are more applicable. In spite of this fact, the agreement between our present calculations and the SCMOCC calculations of Errea *et al.* [105] indicates that, within our SCAOCC approach, the present basis set and calculations can reveal molecular mechanisms as MO-based calculations do. Comparing with the experimental results [96], our present results agree quite well with the experimental ones, except that our calculations, as well as the SCMOCC calculations of Errea *et al.* [105], show rather more clear oscillations. This discrepancy may be related to the experimental resolution, a better agreement could be achieved by the convolution of theoretical calculations with the experimental resolution. Furthermore, one can observe in Figure 4.13 that the cross sections exhibit an oscillatory structure with

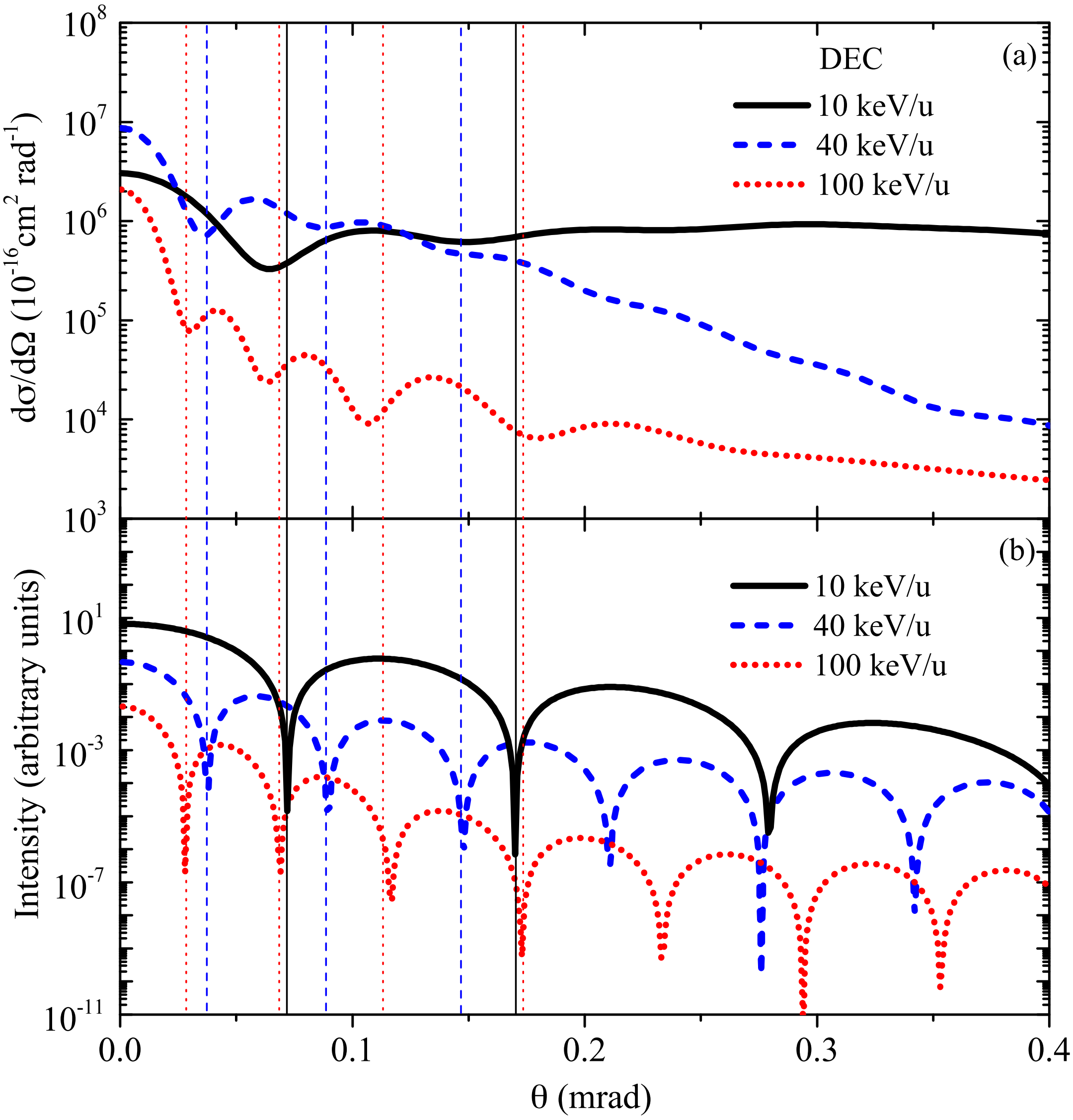

Figure 4.14 – (a) The angular-differential cross sections for the process in equation (4.4) as a function of scattering angle at impact energies 10, 40, and 100 keV/u. (b) The angular intensity distribution of the simulated Fraunhofer-type diffraction patterns for impact energies 10, 40, and 100 keV/u. The vertical lines are the auxiliary lines used for comparison.

two maxima centred around $E \cdot \theta \approx 2$ and 4.5 keV·deg.. Such structures, observed in the angular-differential cross sections for low impact energies, have been interpreted as being due to the well-known Stueckelberg oscillations [96, 102, 113, 114].

We now further investigate the angular-differential cross sections for the DEC process shown in equation (4.4) for higher impact energies. In Figure 4.14(a) our calculated angular-differential cross sections for impact energies 10, 40, 100 keV/u are presented. To our knowledge, no theoretical and experimental results are available for impact energies higher than 0.8 keV/u. In this energy region the SCAOCC method is expected to be more appropriate than MO-based approaches. We thus think that the validity of our calculations for low impact energies, as mentioned above, can ensure the accuracy of these for higher impact energies. As it can be observed in Figure 4.14(a), in the small angles (≤ 0.25 mrad), the cross sections for all the considered impact energies display oscillatory structures whose period decreases with increasing impact energies. To get insight into the mechanisms, the analysis of the impact-parameter-dependent transition probabilities can be useful. In Figure 4.15, we show the transition probabilities of the DEC process presented in equation (5.4) as a function of impact parameter for energies 10, 40, and 100 keV/u. For $b < 1.5$ a.u., the transition probabilities present oscillatory structures with several minima and maxima, which are characteristic of processes occurring through a complex series of avoided crossings. On the contrary, only one giant peak can be observed for $b > 1.5$ a.u., which corresponds to the direct one-step electron transition mechanism, i.e., simultaneous exchange of two electrons, taking place directly from $7^1\Sigma$ (He($1s^2$) to $3^1\Sigma$ $C^{2+}(1s^2 2s^2)$ molecular states through the avoided crossing at $b \approx 3$ a.u. as we discussed in section 4.3.2 (see also [80, 105, 110]). In general, small-angle scattering implies a large impact parameter, and vice-versa. However, the oscillatory structures observed in the cross sections are confined to the small angles (≤ 0.25 mrad, see Figure 4.14(a)), while the transition probabilities in large impact parameters are quite smooth with only one giant peak. To our knowledge, in the intermediate energy region, the oscillatory structure in angular-differential cross sections have been observed in the past [81, 115–121], and being interpreted by Fraunhofer-type diffraction: the angular-differential cross sections present alternately minima and maxima like the diffraction pattern in optics, with alternately dark and bright fringes. In the case of a circular aperture of radius ρ and of a radiation of wavelength λ, the first dark and bright fringes in the diffraction are located at $0.61\lambda/\rho$ and $0.819\lambda/\rho$ respectively, see [122]. However, most of the previous investigations were based on the analogy of the Fraunhofer-type diffraction by a circular aperture with a rough estimate radius from the effective impact parameter range, where electron transitions could take place. Moreover, the distribution of the impact-parameter-dependent transition probabilities is not uniform as the aperture of the diffraction by a circular aperture in optics. In fact, when the diffracting aperture has circular symmetry, the angular intensity distribution of the Fraunhofer-type diffraction can be expressed in the celebrated formula [123],

$$I(\theta) \propto \left| \int_0^\infty d\rho \, \rho A(\rho) \, \boldsymbol{J}_0(k\rho\theta) \right|^2, \tag{4.6}$$

where $\boldsymbol{J}_0$ is the the Bessel functions and $k = 2\pi/\lambda$. $A(\rho)$ is the diffracting aperture function and ρ is the corresponding radius.

In this context, we have simulated diffraction patterns for the DEC process by using equation (4.6), and the aperture function is given by,

$$A(\rho) = \lim_{t\to\infty} |a_f(b,t)| = \sqrt{P(b)}, \tag{4.7}$$

where $\rho = b$, and b is the impact parameter. $a_f(b,t)$ is the collision amplitude and $P(b)$ is the corresponding transition probability. In the present simulations, transition probabilities for $b > 1.5$, 1.7, and 1.3 a.u. are used for impact energies 10,

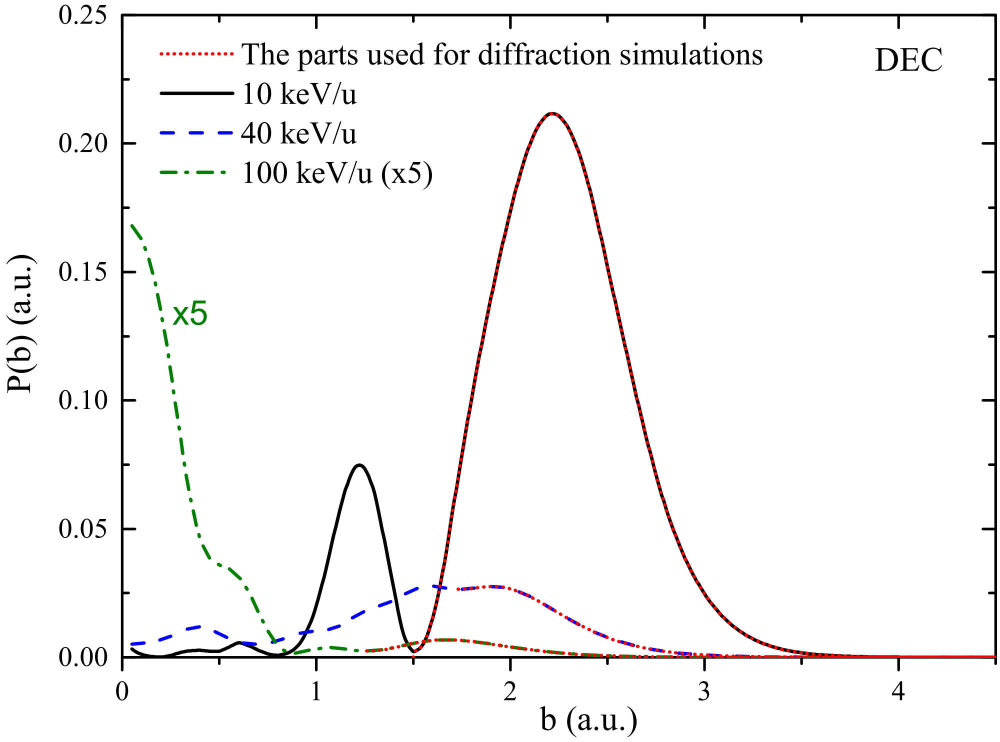

Figure 4.15 – Transition probabilities as functions of impact parameter b for the process presented in equation (4.4) at impact energies 10, 40, and 100 keV/u. The red dot lines denote the parts used in the diffraction simulations.

40, and 100 keV/u, respectively (shown in Figure 4.15 as red dot lines). The latters are selected using two criteria: (i) the small-angle scattering implies a large impact parameter b; (ii) electron transitions occurring at small impact parameters take place through a complex series of avoided crossings, where the interplay between each other may break up the diffraction.

In Figure 4.14(b), the angular intensity distribution of the simulated Fraunhofer-type diffraction patterns are presented for impact energies 10, 40, and 100 keV/u, respectively. The vertical lines shown in Figure 4.14 are the auxiliary lines used for comparison. As it can be seen, the positions of minima in the small-angle angular-differential cross sections and simulated diffraction patterns are in very good agreements for all the considered impact energies. Furthermore, the period of the oscillations in the simulated diffraction patterns also decreases with increasing impact energies, which is a general feature of the diffraction since the wavelength decreases with increasing impact energies according to the *de Broglie* relation. Therefore, we may conclude that the observed oscillations in the small-angle scattering DEC angular-differential cross sections come from Fraunhofer-type diffractions of direct one-step electron transition processes. Note finally that for the angular-differential cross sections at impact energies 0.8 keV/u, one can also observe oscillations in the small-angle scattering, which are also being due to Fraunhofer-type diffractions (see the inset of Figure 4.13).

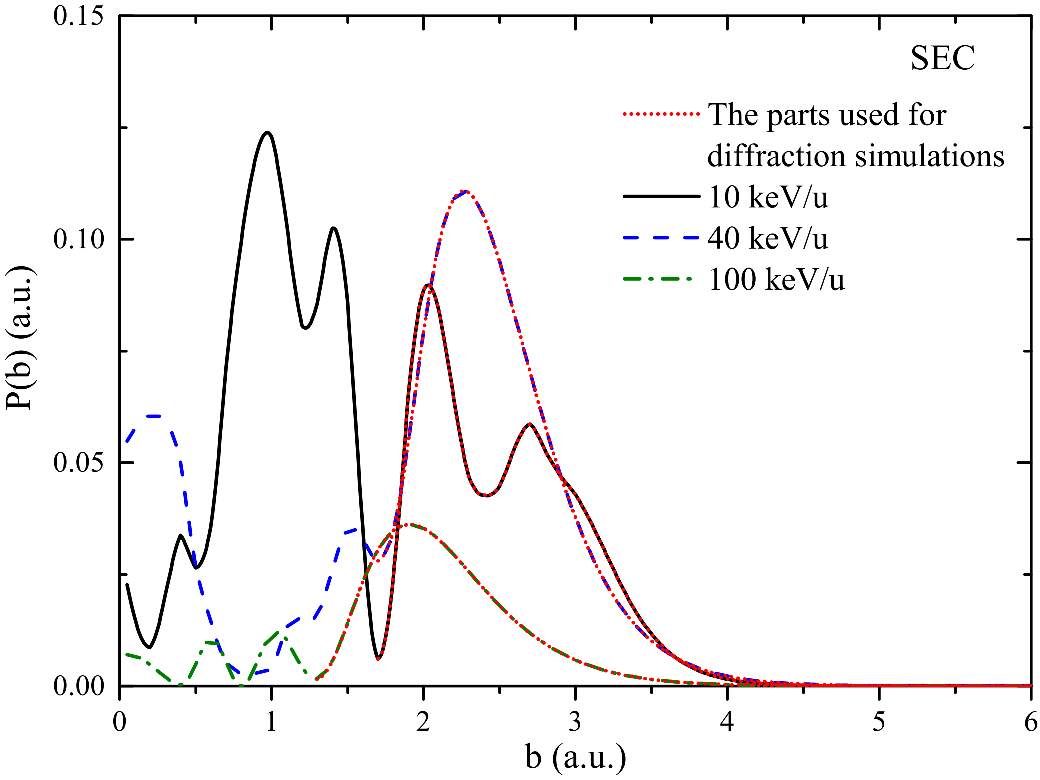

Figure 4.16 – Transition probabilities as functions of impact parameter b for the process presented in equation (4.5) at impact energies 10, 40, and 100 keV/u. The red dot lines denote the parts used in the diffraction simulations.

Single electron capture

We turn now to the investigation of the SEC process shown in equation (4.5). The analysis of transition probabilities is performed first. In Figure 4.16, we display the transition probabilities as a functions impact parameter for impact energies 10, 40, and 100 keV/u, respectively. As it can be observed, the transition probabilities for small impact parameters (around $b < 2$ a.u.) present sharp peaks, which is the character of transitions through the avoided crossings and corresponding to the molecular mechanism. For large impact parameters, the transition probabilities display a relatively smooth shape, implying a direct atomic mechanism. The general discussions above suggests that for the SEC process in the intermediate energy region, it is an interplay between the small-b molecular and large-b direct atomic mechanism, as it was discussed in section 4.3.1 (see also [80]).

Figure 4.17(a) displays our calculated SEC angular-differential cross sections for impact energies 10, 40, and 100 keV/u. The cross sections for all the considered impact energies display oscillatory structures, which are similar with these observed in the DEC process. To interpret the oscillatory structures, in the same manner as we did for DEC process, simulations are performed for the SEC process by using equation (4.6) with transition probabilities in large impact parameters (shown in Figure 4.16 as red dot lines). Note that the transition probabilities in large impact

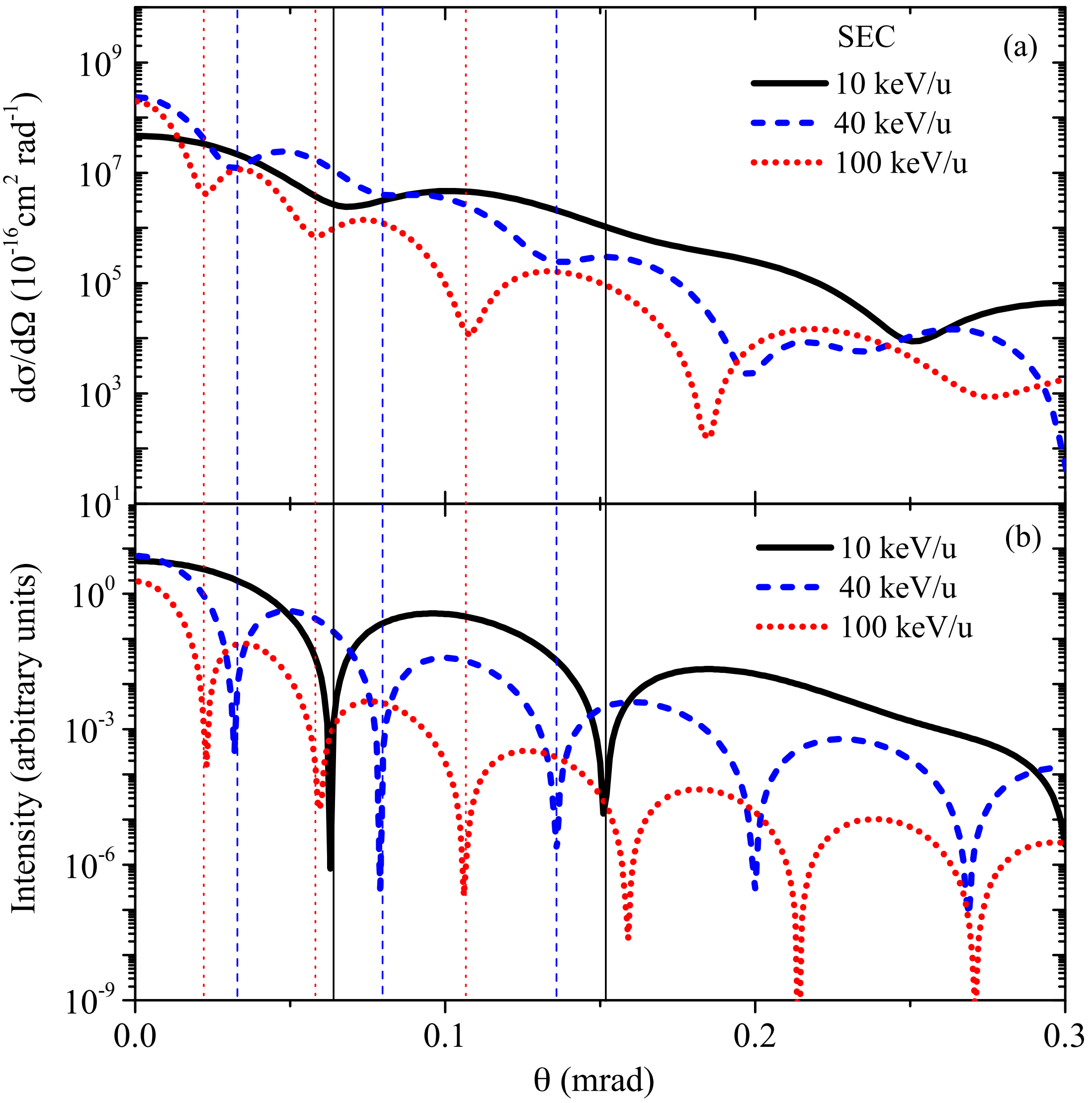

Figure 4.17 – (a) The angular-differential cross sections for the process in equation (4.5) as a function of scattering angle at impact energies 10, 40, and 100 keV/u. (b) The angular intensity distribution of the simulated Fraunhofer-type diffraction patterns for impact energies 10, 40, and 100 keV/u. The vertical lines are the auxiliary lines used for comparison.

parameters are responsible for direct atomic mechanism. The angular intensity distribution of the simulated Fraunhofer-type diffraction patterns are presented in Figure 4.17(b) for the same impact energies 10, 40, and 100 keV/u, respectively. The vertical lines shown in Figure 4.17 are the auxiliary lines used for comparison. As one can observed, the positions of minima in the small-angle angular-differential cross sections agree quite well with these of simulated diffraction patterns for all the considered impact energies. This suggests that the observed oscillations in the small-angle scattering SEC angular-differential cross sections stem from Fraunhofer-type diffractions of direct atomic transition mechanism. For larger angle (> 0.18

mrad), the positions of minima in angular-differential cross sections do not agree with these of the simulated Fraunhofer-type diffraction patterns. This disagreement may be due to the fact that the $P(b)$ used in the simulations are cut off abruptly, for which the transition probabilities responsible for large-b direct atomic mechanism are taken into account approximately. However, the cross sections for larger-angle ($>$ 0.18 mrad) are at least two orders of magnitude smaller than these for small angles.

4.4 Conclusion

In this work, single and double-electron capture processes occurring in the course of C^{4+} + He collisions have been investigated by using the two-active-electron SCAOCC method. First, total and state-selective SEC and DEC cross sections have been calculated in a wide energy region $0.06 - 300$ keV/u using an unique and very large basis set to reach a controlled reasonable convergence. Our present calculations agree well with available measurements and calculations for both total and state-selective SEC and DEC cross sections in the respective overlapping energy regions. It extends the predictions to high energies, especially for $E > 3$ keV/u, where our present calculations are in better agreement with the experimental data of [100] than the molecular basis set calculations [94, 105]. Furthermore, through restricted close-coupling calculations, it is found that electronic correlations play an important role for this collision system for which the IPM and IEV approximations are found to be in poor agreement with our full calculations as well as various experimental and theoretical results. We have also demonstrated that contrary to what was concluded in previous investigations the SEC process is independent of the DEC process in the low impact energy region, where the electron capture process to He($1s^2$)$\rightarrow$ C^{3+}(2p) is dominated by a direct mechanism. At high energies where results are scarce we have shown that a one-step mechanism dominates the DEC dynamics in disagreement with a previous investigation in which an independent transfer mechanism was invoked. For that energy domain experimental investigations will be useful to draw definite conclusions and confirm our data.

In a second stage, we have further reported the investigation on the angular-differential cross sections for impact energies 0.8, 10, 40, and 100 keV/u. Our present calculations agree well with the available experimental and theoretical results, and bring in new cross sections for impact energies higher than 0.8 keV/u, where no previous experimental or theoretical results are available. Furthermore, through the simulated Fraunhofer-type diffraction patterns, we have shown that the observed oscillations in the small-angle angular-differential cross sections for both SEC and DEC stem from Fraunhofer-type diffractions of direct one-step electron transition processes.

Chapter 5

State-selective electron transfer in He^++He collisions

5.1 Introduction

Compared to the two previous collision systems considered in this thesis, another type of ion-atom collision is the one where at least one active electron is bound to each on the two partners and in which electronic processes can be activated on both sides. A prototypical example from this class of problem is the He^+ + He system which consists of a target with two electrons and a single electron on the projectile. Over the last several decades up to very recently, He^+ + He collisions have received a great deal of interest from experimentalists [117, 124–134], due to the fact that helium is particularly well suited for experimental purposes. Most of the early works focused on the total and state-to-state cross sections, from which the selectivity of the processes with respect to impact energies can be well described. However, these quantities do not allow the analysis of the spatial selectivity. This is taken into account by angular differential analysis which provides a much sharper probe of process mechanisms and reveals collision dynamics. In recent works, the ground-state transfer angular-differential cross sections in $^3He^+$ + ^4He collisions have been measured by Schöffler *et al.* [134] at 60, 150, 300 and 600 keV/u impact energies using the cold-target recoil-ion-momentum spectroscopy (COLTRIMS) technique. The authors have also shown the corresponding theoretical cross sections using the four-body distorted-wave theory. A rather poor agreement was found between the calculations and their experimental measurements. On the other hand, Guo *et al.* [117] performed a combined experimental and theoretical investigation on state-selective and angular-differential cross sections in $^4He^+$ + ^4He collisions. The cross sections were obtained experimentally using the COLTRIMS technique at 7.5 and 25 keV/u impact energies. The experimental data were compared with the theoretical results based on the Classical Trajectory Monte Carlo (CTMC) method. It was found that the CTMC calculations failed to reproduce the experimental angular-differential cross sections.

From the theoretical point of views, despite the substantial number of theoretical efforts that have been pursued to understand and model the He^+ + He collision system [135–143], this latter still remains a challenge for theoreticians. In particular, in the intermediate impact energy region, perturbative approaches or model calculations using a model potential with only one- (or two-) active-electron may be inadequate due to the strong coupling between various channels as well as the effects of static and dynamical electronic correlations. Consequently, non-perturbative full three-electron semi-classical or quantum approaches can bring further insights into the understanding of this system.

In this context, Sural *et al.* [139] have developed in 1969 a three-electron coupled-channel method to study electron transfer and excitation processes of He$^+$ + He collisions for the impact energies 0.15−10 keV/u. The authors considered only six channels which allowed for a single excitation and transfer into the first excited states. Direct projectile excitation was however excluded. Later, approximate three-electron coupled-channel calculations were performed for the impact energies 2.5−150 keV/u by Hildenbrand *et al.* [140], where 128 channels were considered in their calculations. However, the couplings between s and p wave-functions were not taken into account in their calculations due to the limited power of the computers at that time. It should be also mentioned that those studies were only focused on the total state-selective cross sections. To date, there is no converged non-perturbative calculations available for this three-electron system covering the wide intermediate impact energy range.

In the present work, we study theoretically the electronic processes occurring in He$^+$ + He collisions, where the concerning processes can be broadly categorized into those that involve (i) one-electron transfer, i.e. transfer to ground state (GT) and transfer to excited state (ET),

$$\begin{aligned} He^+(1s) + He(1s^2) &\rightarrow He(1s^2) + He^+(1s) \quad (GT) \\ &\rightarrow He(1snl) + He^+(1s) \quad (ET); \end{aligned} \tag{5.1}$$

(ii) one-electron excitation, i.e., target (TE) and projectile (PE) excitation,

$$\begin{aligned} He^+(1s) + He(1s^2) &\rightarrow He^+(1s) + He^*(1snl) \quad (TE) \\ &\rightarrow He^{*+}(nl) + He(1s^2) \quad (PE); \end{aligned} \tag{5.2}$$

(iii) two-electron transitions, ie. TTE, simultaneous GT and TE,

$$He^+(1s) + He(1s^2) \rightarrow He(1s^2) + He^+(nl) \quad (TTE). \tag{5.3}$$

We use a three-electron semiclassical atomic-orbital close-coupling (SCAOCC) method, where the calculations were performed using a previous, not optimized code but written for handling up to three active electrons developed in the group [45, 81]. Total and state-selective cross sections are first presented for energies ranging from 1 to 225 keV/u and compared with available theoretical and experimental results. Our computed cross sections agree well with the most recent experimental measurements. Possible reasons for the disagreement with previous calculations are discussed. Furthermore, our calculations show a prominent oscillatory energy dependence structure in the integral TE and ET to He singlet excited states cross sections as well as PE and TTE cross sections, which we assign to the strong competitions between the TE and ET processes, so as the PE and TTE processes. In a further stage, the angular-differential cross sections for the electron transfer processes shown in equation (5.1) and (5.3), which provide more physical insights into the collision dynamics, are presented and compared with the most recent experimental results. It is found that the angular-differential cross sections for most electron transfer processes considered in this work exhibit distinct oscillatory structures which are also discussed and interpreted.

The present Chapter is organised as follows. In section 5.2 we briefly outline main features of our three-electron SCAOCC approach. section 5.3 is devoted to the detailed analysis of the total, state-selective and angular-differential cross sections and direct comparisons with available experimental and theoretical results, followed by the conclusions.

5.2 Calculation details

In Chapter 2 we present our method for true or quasi two-electron collisional systems. For three-electron systems the general equations written in Chapter 2 stay valid but the complexity of the modelling increased dramatically: (i) in a model where one-electron states are described by N GTOs, two-electron states require N^2 products of the same GTOs (with matrices composed of N^4 elements) and three-electron states N^3 products (and N^6 sized matrices); (ii) while for two electrons, the spin functions (singlet and triplet) are factorized out, it is not the case for three electron system, where the total spin of the system does not change but the spin state on both centers can be changed during collisions. For the system considered in this Chapter, though the initial channel is He$^+$ (1s ^{2}S) + He(1s^2 ^{1}S) [total spin = 1/2], one can populate singlet and triplet states on target (after excitation) and on projectile (after capture). These new features make the programming more complex and calculations much more demanding in computer resources, memory, and CPU time.

In the present calculations, a set of 19 Gaussian-type orbitals (GTOs), denoted as B1$_{HeHe}$ (10 for l=0, 3×3 for l =1), are used on both projectile and target centers; this allows the inclusion of 1260 states (states of two electrons on target and one electron on projectile, and vice-versa). Note that this basis has been selected using two criteria: (i) large enough to describe accurately the important target and projectile states and (ii) still computationally tractable. Convergence tests have been performed by comparing the present results using basis B1$_{HeHe}$ with those from a smaller basis set, B2$_{HeHe}$ (12 GTOs on each center, i.e., 6 for l=0 and 2×3 for l = 1) which allows the inclusion of 582 states in total. The detail of basis sets B1$_{HeHe}$ and B2$_{HeHe}$ are presented in Appendix B.1. The convergence[1] was evaluated (i) to be better than 1% for the total single electron transfer (SET) and GT cross sections; (ii) to be about 10% for the ET, TE and PE cross sections, reaching a maximum of 20% for the TTE cross sections, for energies where, however, the values of the cross

---

[1] The relative difference between the results from the two basis. One can therefore expect better convergence if the tests would have been carried out with a larger basis set, not possible to be carried in the present time due to our computer resources.

sections are lower than 5×10^{-18} cm^2 (see Figure 5.8).

5.3 Results and discussion

5.3.1 Total and state-selective cross sections

Single electron transfer

In Figure 5.1, our calculated total single electron transfer (SET) cross sections are presented and compared with experimental data [124, 127, 130, 132, 133] and theoretical calculations [117, 136, 142], as well as the recommended data from Ref. [144]. From Figure 5.1, one can observe a nearly perfect agreement with the different series of experimental data in the whole energy domain. A excellent agreement is also found with the four-body Coulomb-Born distorted-wave approximation (CBDW-4B) calculations [136] for impact energies above 40 keV/u. The cross sections from

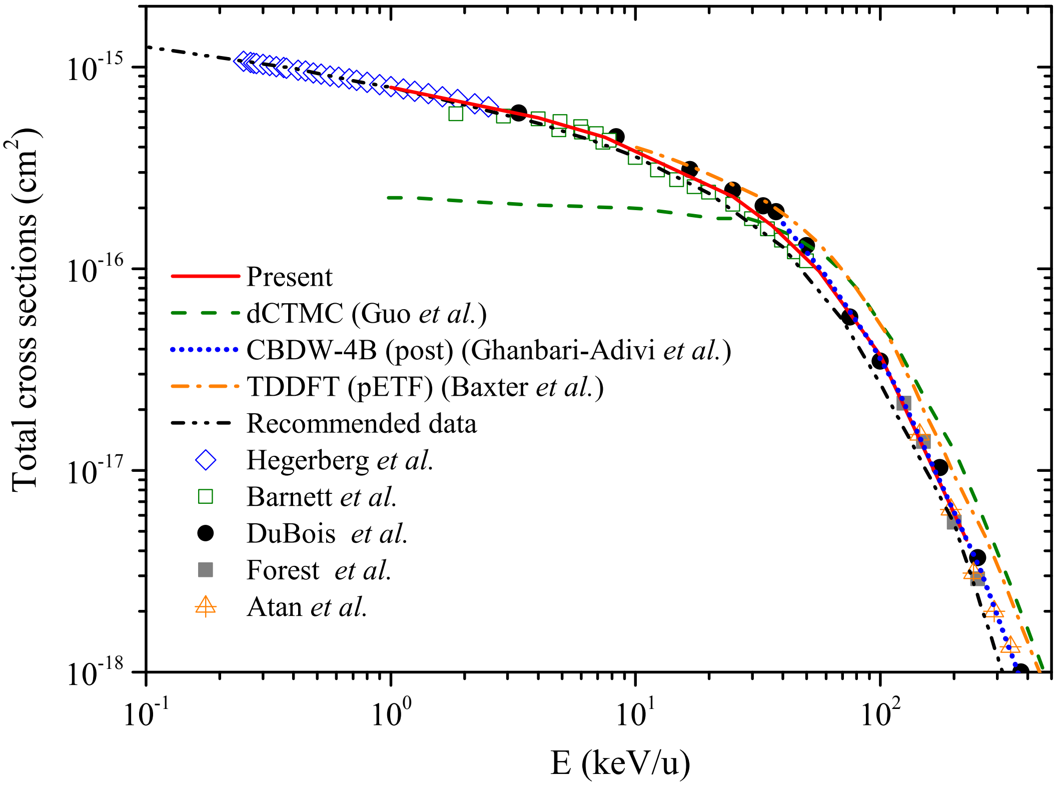

Figure 5.1 – Total SET cross sections as a function of impact energy. The theoretical results are from the present calculations (red solid line), Guo *et al.* [117] (green dash line), Ghanbari-Adivi *et al.* [136] (blue dot line), and Baxter *et al.* [142] (orange dash-dot line). The experimental results are from Hegerberg *et al.* [127] (blue open diamonds), Barnett *et al.* [124] (green open squares), DuBois *et al.* [130] (black solid circles), Forest *et al.* [132] (grey solid squres), and Atan *et al.* [133] (orange crossed triangles). The recommended data from [144] (black dash-dot-dot line) are also presented.

the time-dependent-density-functional-theory (TDDFT) calculations of Baxter *et al.* [142] are higher than our results. In particular, for E > 50keV/u, the TDDFT calculations overestimate the cross sections compared to the experimental data; this failure may be related to the fact that the authors employed an independent electron model (IEM) approximation in their calculations [142]. This indicates that the correlation effects which have been taken into account in the present calculations as well as in the CBDW-4B calculations [136] are most important for impact energies 50−225 keV/u (the highest impact energy we considered). It can also be observed from Figure 5.1, that the CTMC calculations of Guo *et al.* [117] lie below our results and the CBDW-4B calculations [136], as well as the experimental measurements for the impact energies lower than 30 keV/u, while slightly above for the impact energies above 50 keV/u. This could be due to the fact that the interelectronic interactions were taken into account by an approximate way and the lack of the tunneling effect in their CTMC method [117]. Note, finally, that the data from Ref. [144] are also in good agreement with measurements of [124, 127] for E <3 keV, but are slightly lower than [130, 132, 133] for higher impact energies.

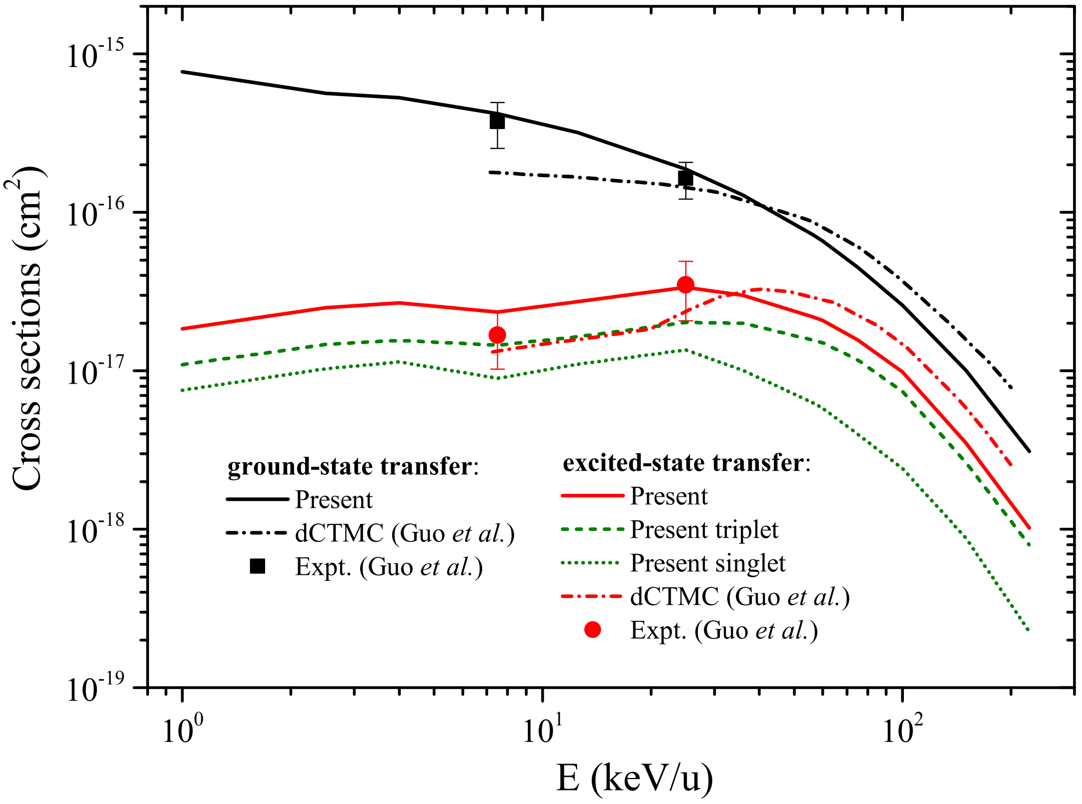

Figure 5.2 – The GT and ET cross sections as functions of impact energy for He$^+$+He collisions: solid line denotes the present calculations; the present calculated cross sections for ET to singlet and triplet states of He are denoted as red dot and dash line, respectively; dash-dot line: theoretical calculations of [117]; solid symbols: experimental measurements of [117].

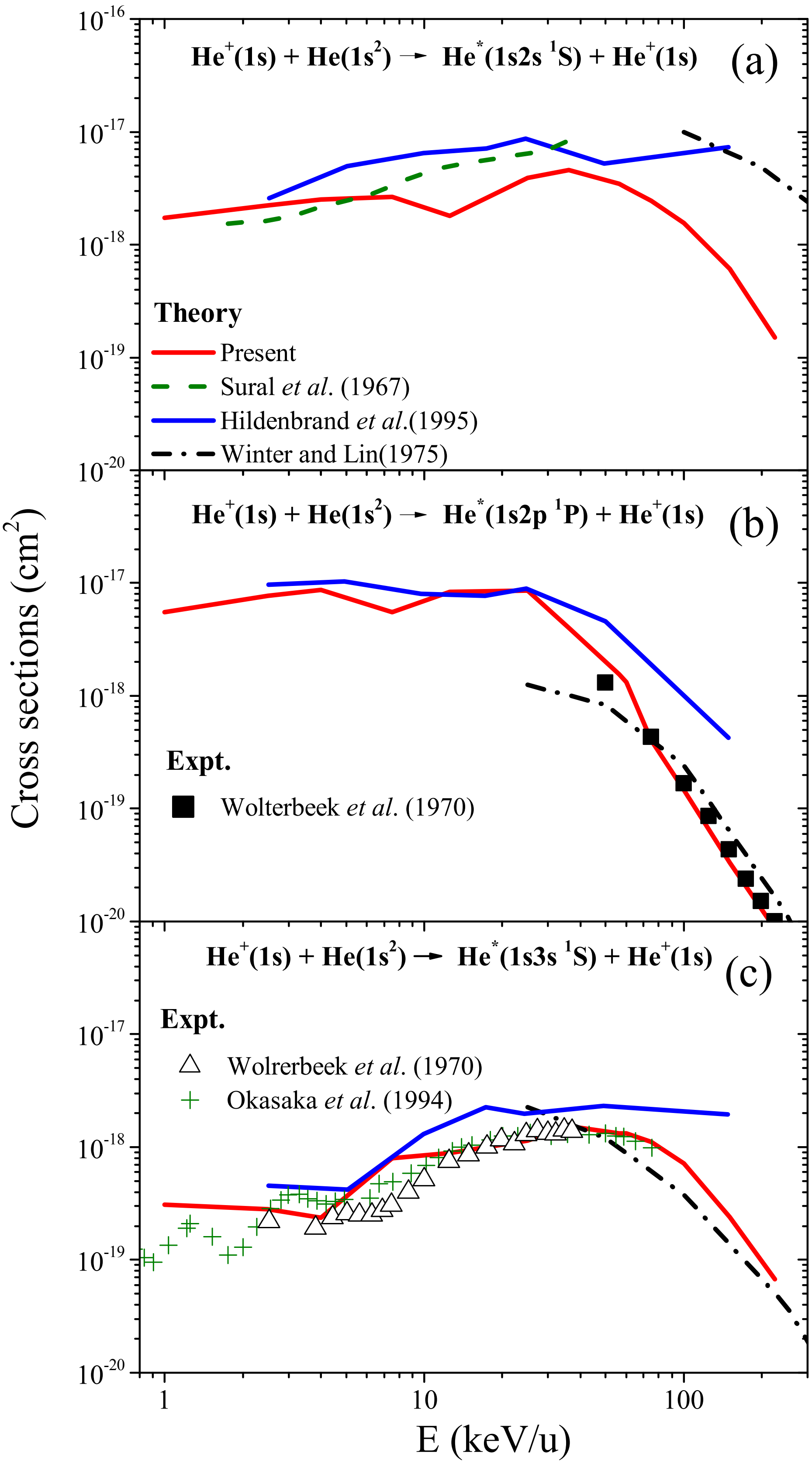

Figure 5.3 – The cross sections as functions of impact energy for ET to He(1s2s ^{1}S, 1s2p ^{1}P and 1s3s ^{1}S) excited states.

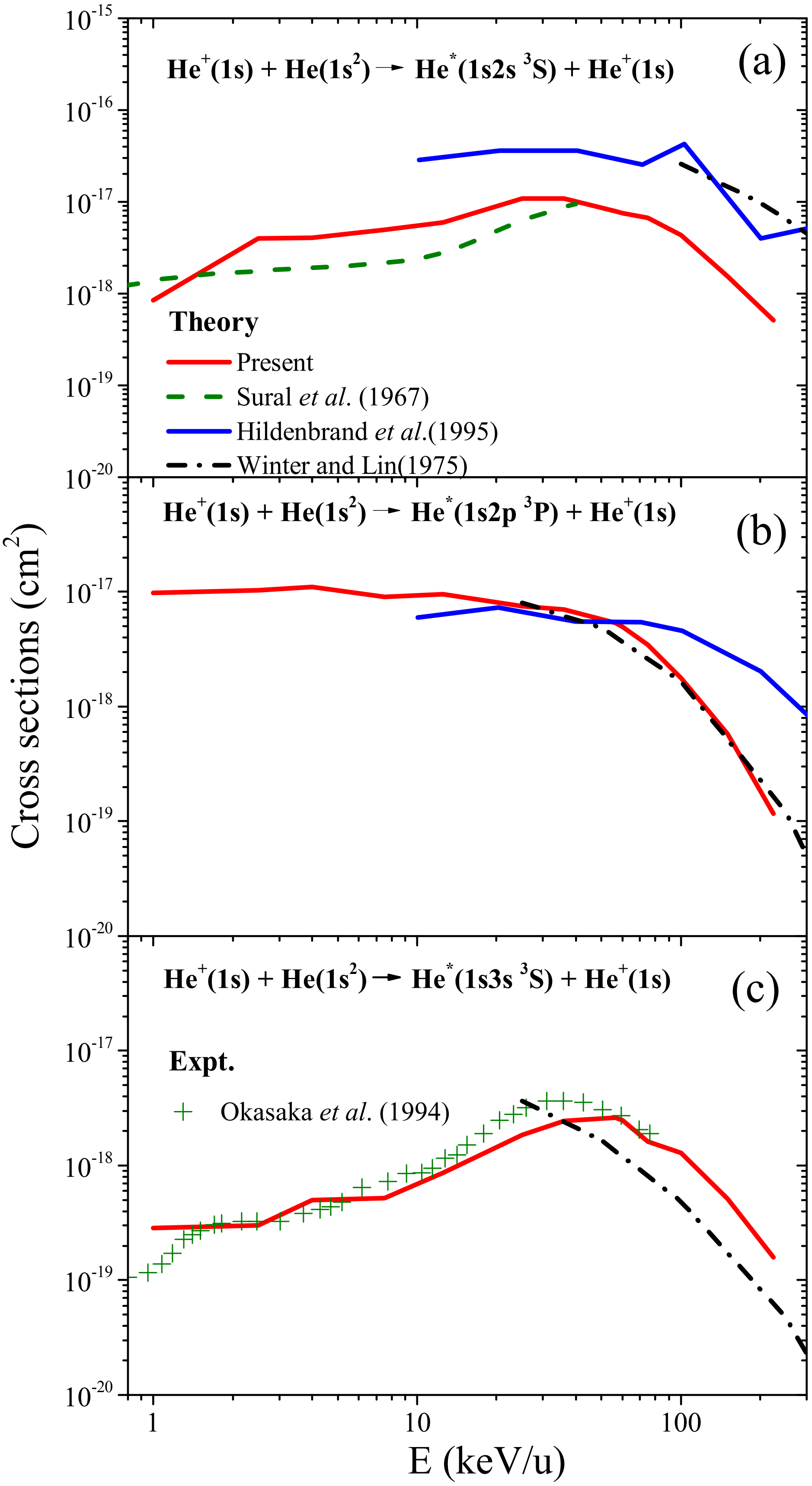

Figure 5.4 – The cross sections as functions of impact energy for ET to He(1s2s ^{3}S, 1s2p ^{3}P and 1s3s ^{3}S) excited states.

The total state-selective GT and ET cross sections as functions of the impact energy are shown in Figure 5.2, together with experimental and theoretical results of Guo *et al.* [117] for comparison. Our results show that the GT process in Figure 5.2 are the dominant channel in the entire energy range with an increase for decreasing impact energies, which is a general feature for the resonant charge-transfer process in a symmetric ion-atom collision system. In contrast to the GT process, the cross sections of ET show a maximum around 25 keV/u with a somewhat flat behavior below 30 keV/u and a monotonous decrease at higher energies. It can also be observed from Figure 5.2 that the electron transfer to He excited triplet states are the dominant contributions of the ET cross sections. For E $>$ 70 keV/u, the ratio of ET to triplet and singlet states is about 3, which is in accordance with straightforward spin statistics. This indicates that it is a direct atomic mechanism which gives rise to the process in this energy range while for E $<$ 70 keV/u one can advocate a complex dynamics, coupling a molecular type mechanism and the direct one. Comparing with experimental results of Guo *et al.* [117], very good agreements can be observed for both GT and ET cross sections.

In order to provide detailed informations about the ET processes, we now investigate $nl-$resolved ET cross sections. Figure 5.3 and 5.4 show our calculated $nl-$resolved dominant ET cross sections. The theoretical results of Sural *et al.* [139], Winter *et al.* [137] and Hildenbrand *et al.* [140] as well as the experimental results reported in [131,145,146] are also shown. However, to our knowledge, no experimental results are available for electron transfer to lower He (1s2s ^{1}S and ^{3}S, 1s2p ^{3}P) excited states. Comparing with available experimental results for electron transfer to higher He (1s2p ^{1}P, 1s3s ^{1}S and ^{3}S) excited states, our results are in excellent agreement with the experimental results [131,145,146] in the overlapping energy regions. Comparing with theoretical results [137,139,140], it can be seen for all these ET processes we considered, large discrepancies exist among all these theoretical results. However, a surprising very good agreement with first-Born calculations [137] is found for the ET to He (1s2p ^{1}P and ^{3}P) at E $>$ 50 keV/u. Note that Winter *et al.* [137] used the first-Born approximation and replaced the interaction potential partly by an effective potential, where the three-electron wavefunction is built up as a product of one- and two-particle functions and not totally antisymmetrized so that target and projectile electrons can be distinguished. From a theoretical point of view, the convergence of our calculations has been checked for these processes presented in equation (5.1) – (5.3) under consideration, as mentioned before. Furthermore, the validity of our results is also supported by the good agreements with experiments concerning electron transfer to higher He (1s2p ^{1}P, 1s3s ^{1}S and ^{3}S) excited states (see Figure 5.3(b), 5.3(c) and 5.4(c)). The validity of our calculated cross sections for ET to lower He (1s2s ^{1}S and ^{3}S, 1s2p ^{3}P) excited states in Figure 5.3 and 5.4 is supported by these agreements, since the lower excited states are obviously better described than the higher excited states with our GTO basis set. Further experimental investigations will be useful to draw definite conclusions.

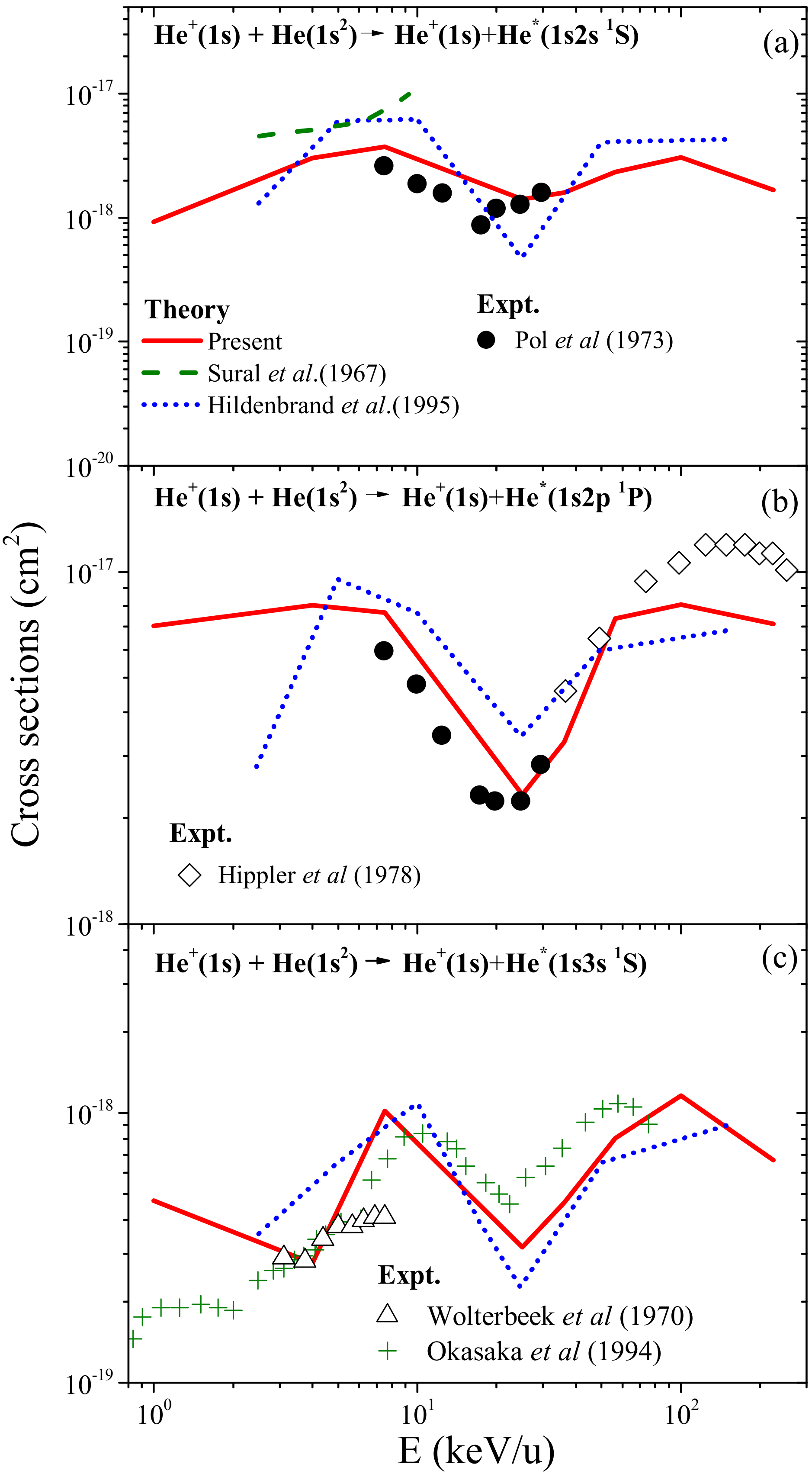

Figure 5.5 – The cross sections as functions of impact energy for TE to He(1s2s ^{1}S, 1s2p ^{1}P and 1s3s ^{1}S) excited states.

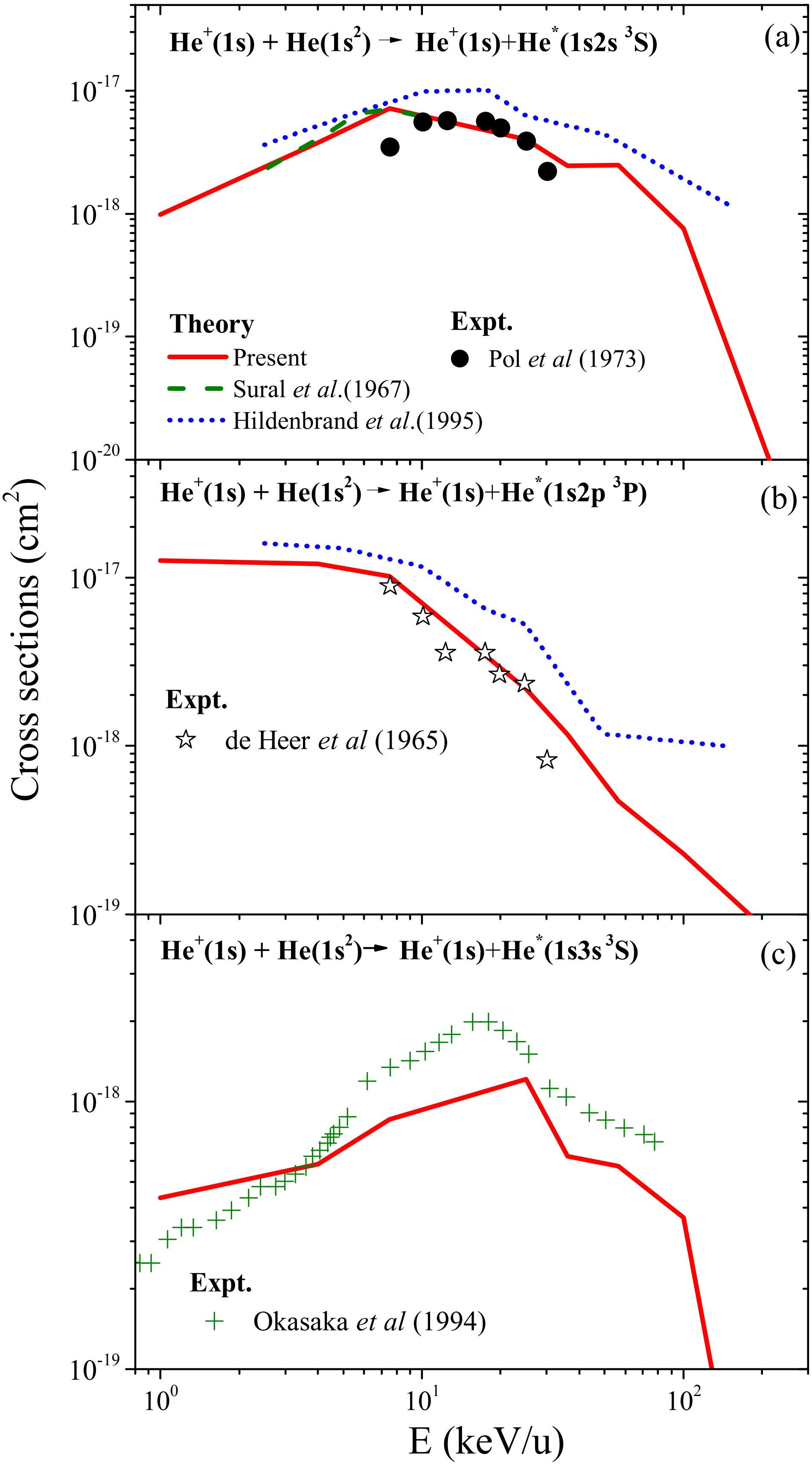

Figure 5.6 – The cross sections as functions of impact energy for TE to He(1s2s ^{3}S, 1s2p ^{3}P and 1s3s ^{3}S) excited states.

Excitation

We first investigate the excitation of target He atom impacted by single charged He^+ projectile. Figure 5.5$(a)-(c)$ shows the cross sections for TE to singlet He(1s2s ^{1}S, 1s2p ^{1}P and 1s3s ^{1}S) excited states, respectively. Previous experimental [126, 131, 145, 146] and theoretical [139, 140] results are also displayed in the figure for comparison. As it can be observed in Figure 5.5, our results show the best overall agreement with experimental results [126, 131, 145, 146], compared to the other two theoretical calculations. This may be due to the fact that only 6 and 128 channels were used in these treatments, while 1260 channels have been included in our calculations, for which the convergence has also been checked, as mentioned before. However, for TE to He (1s3s ^{1}S) at E< 2 keV/u presented in Figure 5.5(c), our results lie above the experimental data of [131]. Since only one series of measurements exists in this energy region, and the values of the cross sections are quite small, lower than 5×10^{-18} cm^2, we cannot firmly conclude on that issue. Furthermore, all the cross sections we considered for TE to He singlet excited states present oscillatory impact energy dependence structures, which we assign to the interplay with ET to He singlet excited states processes. The two inelastic cross sections are in the same magnitude but exhibit oscillations in antiphase (See Figure 5.3). Note that this structure was interpreted by Okasaka *et al.* [131] as an interference effect between even and odd states of the He_2^+ molecule.

In Figure 5.6$(a)-(c)$, the cross sections for TE to triplet He(1s2s ^{3}S, 1s2p ^{3}P and 1s3s ^{3}S) excited states are presented, respectively, together with theoretical [139, 140] and experimetal [126, 131, 147] results for comparison. Note that since the Hamiltonian does not contain spin-dependent interactions, triplet states can only be excited by an exchange of electrons bewteen target and projectile. Compared to TE to singlet He excited states shown in Figure 5.5$(a)-(c)$, it is found that (i) the cross sections for TE to triplet He excited states are about same values at low energy and sometimes higher than these for TE to singlet He excited states, though it requires an exchange of electrons with projectile; (ii) a fast decrease appearing at lower energies for TE to triplet He excited states; (iii) no oscillatory structures in the cross sections for TE to triplet He excited states. For TE to triplet He(1s2s ^{3}S and 1s2p ^{3}P), our results are in very good agreements with experimetal results [126, 131, 147] in the overlapping energy region. However, the theoretical calculations of Hildenbrand *et al.* [140] overestimate the experimental data [126, 147] by a factor of 2, which may be due to again the less channels included in their calculations. For TE to higher triplet He(1s3s ^{3}S) excited state shown in Figure 5.6(c), our results are in less satisfactory agreements with the only one series of data [131], which is the same as the cross sections for TE to He (1s3s ^{1}S) at E< 2 keV/u. Further theoretical and experimental investigations will be useful to draw definite conclusions.

We next investigate the excitation of single charged He^+ projectile occurring in the He^+ + He collisions: in Figure 5.7, is shown only the cross sections for PE process to He^+ $(n = 2)$ excited states in order to compare with the only existing experimental [126] and theoretical [140] results. To our knowledge, no theoretical or experimental investigations are available for other PE processes. As it can be seen from Figure 5.7, our results are in good agreements with the experimental results of Pol *et al.* [126], while the calculations of Hildenbrand *et al.* [140] overestimate

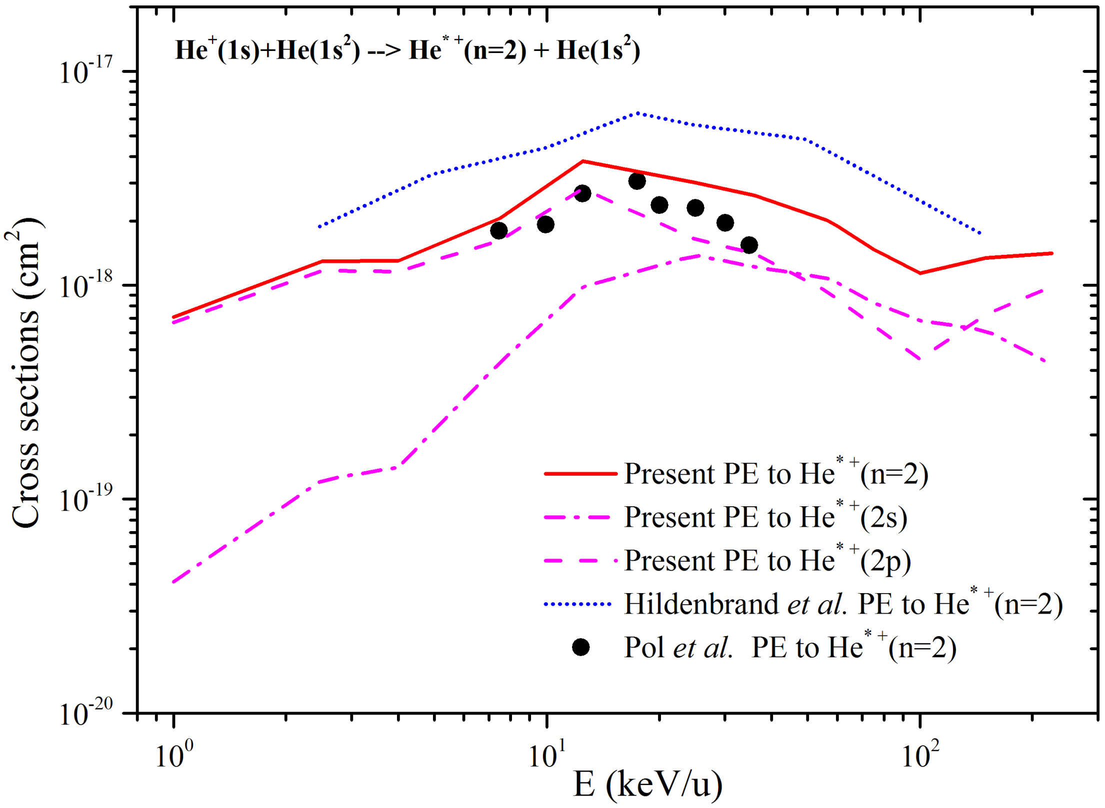

Figure 5.7 – The cross sections as functions of impact energy for PE to He$^+$ ($n = 2$) excited states.

again the experimental data [126] by a factor of 2. It can also be observed that the cross sections for PE to He$^+$(2p) excited states are dominant for the impact energies smaller than 50 keV/u. For E > 50 keV/u the cross sections for PE to He$^+$(2s) excited states become comparable with that for PE to He$^+$(2p) excited states. In addition, the cross sections for PE to He$^+$(2p) excited states present a oscillatory energy dependence structure, which we assign to a strong competition with the TTE processes and will be discussed later.

Electron transfer and target excitation

We now turn to investigate the electronic processes that involve two-electron transitions, i.e., electron transfer and target excitation (TTE) processes. Figure 5.8(a) shows our calculated TTE cross sections as a function of impact energy, together with experimental and theoretical results of Guo *et al.* [117], for comparison. Our results are slightly larger and smaller than the experimental data [117] at respectively E=7.5 keV/u and E=25 keV/u. It should be noted that these cross sections are small and our calculations are less converged (20%) than for the other processes. However, the tendency of our results are in accordance with the data of [117]. In contrast, the CTMC calculations reported in [117] are much larger than their experimental data at 7.5 keV/u, and show a very weak dependence upon impact energy in the range considered. In absence of other independent results, it is difficult to

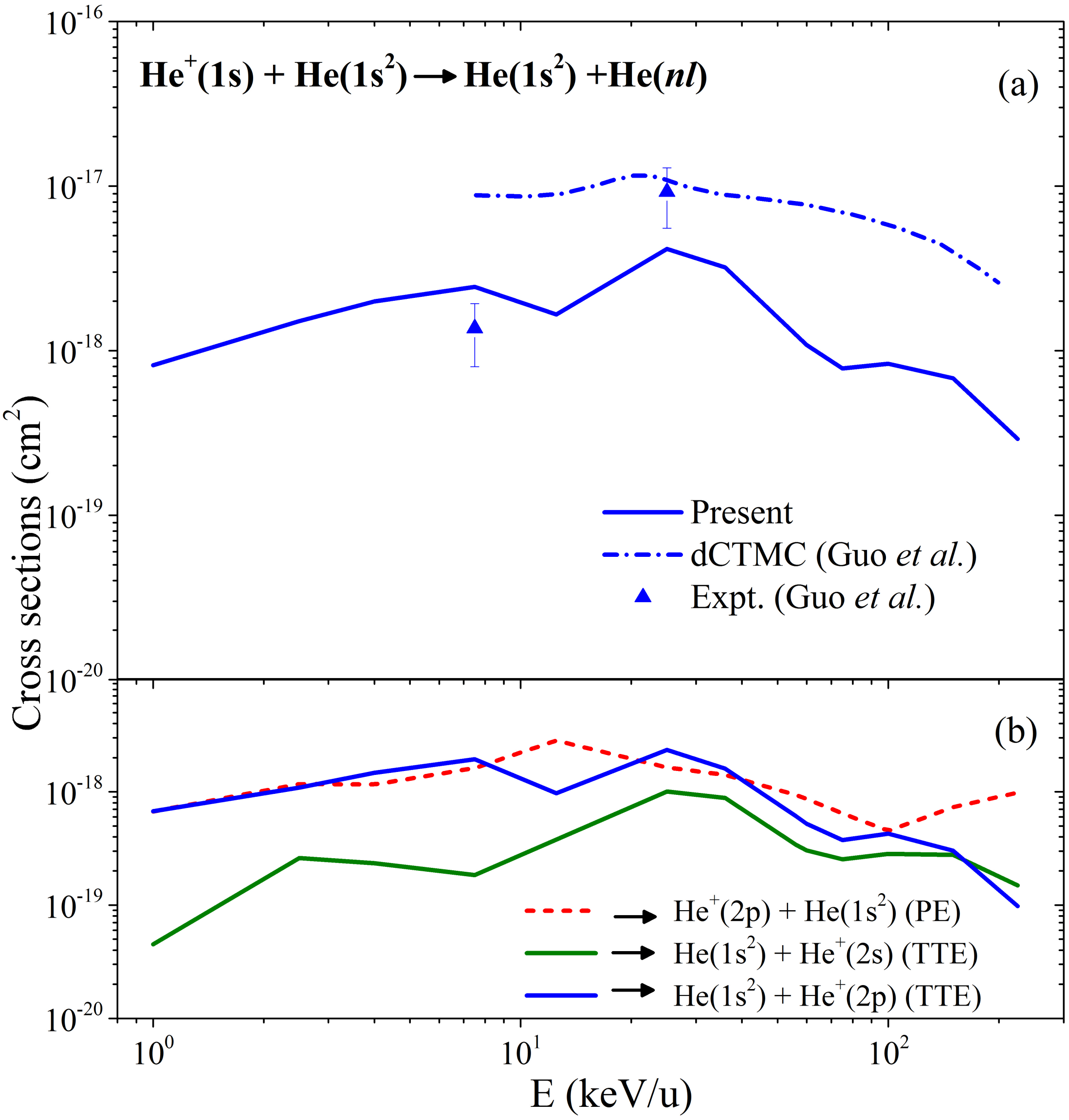

Figure 5.8 – TTE cross sections as a function of impact energy for He$^+$+He collisions. (a) solid line denotes the present calculations; dash-dot line: theoretical calculations of [117]; solid symbols: experimental measurements of [117]. (b) Our calculated cross sections for the dominant TTE and PE processes as functions of impact energy.

draw definite conclusions on that disagreement. However, for the different processes considered, our results show the best overall agreement with experimental results.

Furthermore, it can be seen in Figure 5.8(a) that our calculated TTE cross sections show a clear oscillatory dependence structure as a function of impact energy. In order to get insight into the oscillatory structure, we present in Figure 5.8(b) the cross sections for the dominant channels of two symmetric processes, TTE and PE (see equation (5.2) and (5.3)). It can be observed that the TTE and PE cross sections seem to be out of phase over the energy range 3−225 keV/u, demonstrating the existence of the strong competition between TTE and PE resonant processes. However, there exist only two experimental data for the TE process [117], and further experimental measurements will be useful to confirm our theoretical predicted oscillatory structure.

5.3.2 Angular-differential cross sections

We now investigate the electron transfer angular-differential cross sections concerning the processes presented in equation (5.1) and (5.3), which provide a greater benchmark for our calculations. In Figure 5.9, our calculated GT angular-differential cross sections at 7.5 and 25 keV/u are presented, together with the measurements reported in [117]. In order to compare with the experimental data, we tried to model the experimental conditions by convoluting our raw data by a Gaussian function which corresponding to the experimental resolution. We used the full width at half maximum (FWHM) equal to the experimental resolution: FWHM = 0.18 and 0.1 mrad [117, 148] are used for impact energies 7.5 and 25 keV/u, respectively. Our convoluted cross sections are also presented in Figure 5.9 where, our calculated GT angular-differential cross sections for both 7.5 and 25 keV/u are slightly larger than the experimental measurements. This is due to the fact that the absolute values of the experimental data were determined by normalization with the SET cross sections from Ref. [144], which are slightly smaller than our calculated total SET cross sections for E $>$ 3 keV/u. Except for that scaling factor, an nearly perfect agreement can be seen in Figure 5.9(b) between the present convoluted results and the experimental measurements at impact energy 25 keV/u. For impact energy 7.5 keV/u, our calculated GT angular-differential cross sections with convolution are also in good agreement with experimental measurements of [117], except for a small shift of the positions of maximum and minimum. This may be due to that the FWHM ($\sim$ 0.18 mrad) of the Gaussian function used in our convolution was evaluated too large since the experimental cross sections lie between our convoluted and non-convoluted cross sections. Note that we have also calculated the GT angular-differential cross sections of ^{3}He$^+$ + ^{4}He collisions for 60 and 150 keV/u impact energies to compare with experimental results of Schöffler *et al.* [134], which are presented in Figure 5.10 and 5.11. The four-body distorted-wave theory (CDW-4B) calculations of Schöffler *et al.* [134] and three-body distorted-wave theory (CDW-3B) calculations of Ghanbari-Adivi *et al.* [143] are also presented for comparison. For impact energy 60 keV/u, our results agree quite well with experimental results of [134], while the distorted-wave theory calculations of [134, 143] are in rather poor agreement with the experimental results of [134]. The latter discrepancies may due to the fact that the reduction from a five-body to the four-body or three-body problem is crude and corresponding results should be used only for rough estimation. For impact energy 150 keV/u, our results are also in good agreements with experimental results of [134], but slightly larger at large angles, where the distorted-wave theory calculations of [134, 143] also lie above the experimental data. We cannot firmly conclude on that issue, since large discrepancies exist among the available data.

We now investigate the angular-differential cross sections for other electron trans-

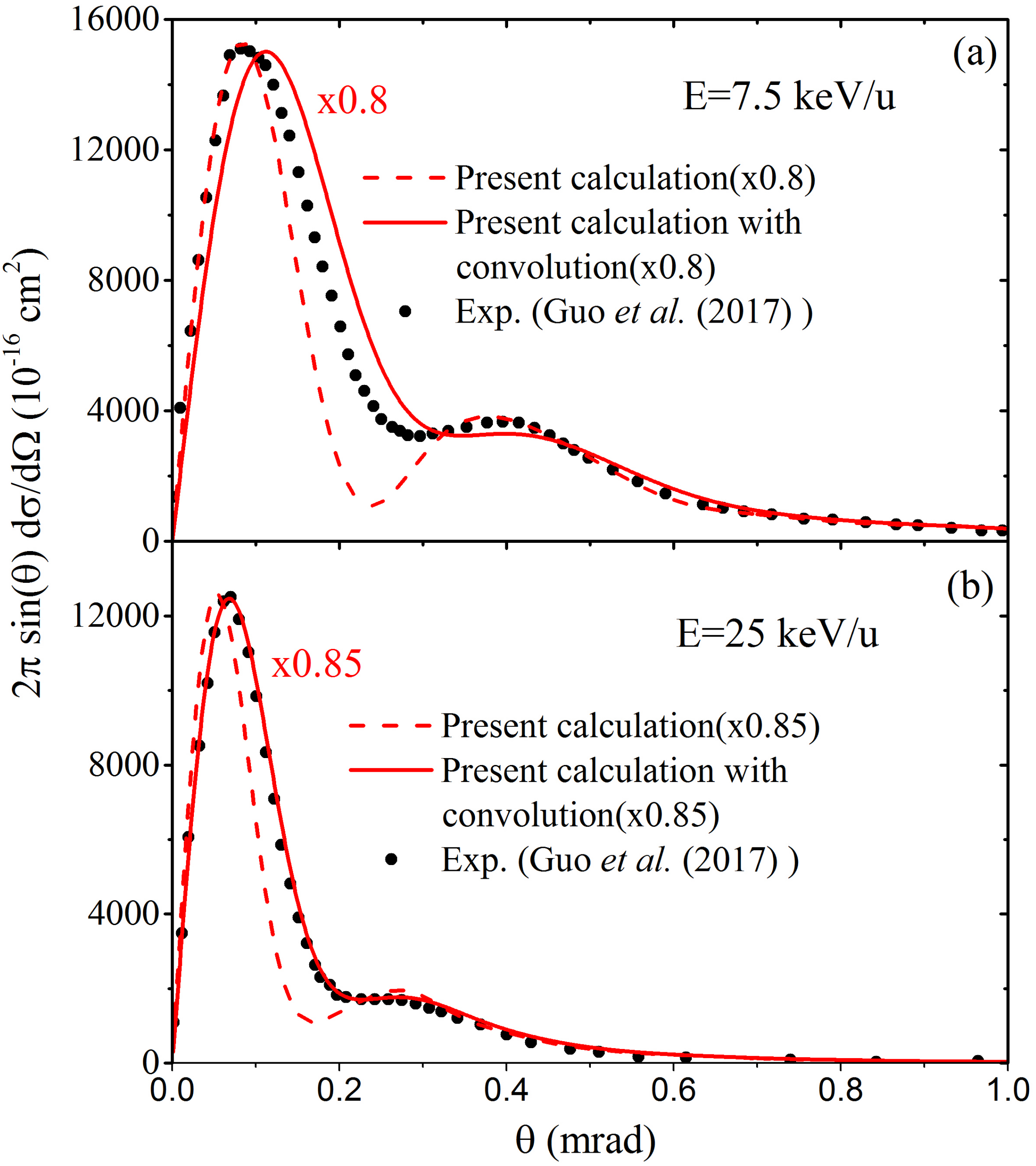

Figure 5.9 – The GT angular-differential cross sections as a function of scattering angle at impact energies 7.5 and 25 keV/u. Red solid line: present calculations; red dash line: present convoluted results; black solid circles: experimental results from [117].

fer processes occurring in the ^{4}He$^+$ + ^{4}He collisions and larger collision energies. Figure 5.12 shows our cross sections for the processes GT, ET to He(1s2s ^{1}S and ^{3}S) excited states and TE to He$^+$(2s) excited state for impact energies 7.5, 25, 60, and 150 keV/u. One can observe in Figure 5.12 that the cross sections for all these processes display a similar oscillatory structure, with a first pronounced minimum followed by shallow ones in some cases. This behaviour has been observed in the past [115–121], the oscillatory structures being interpreted by Fraunhofer-type

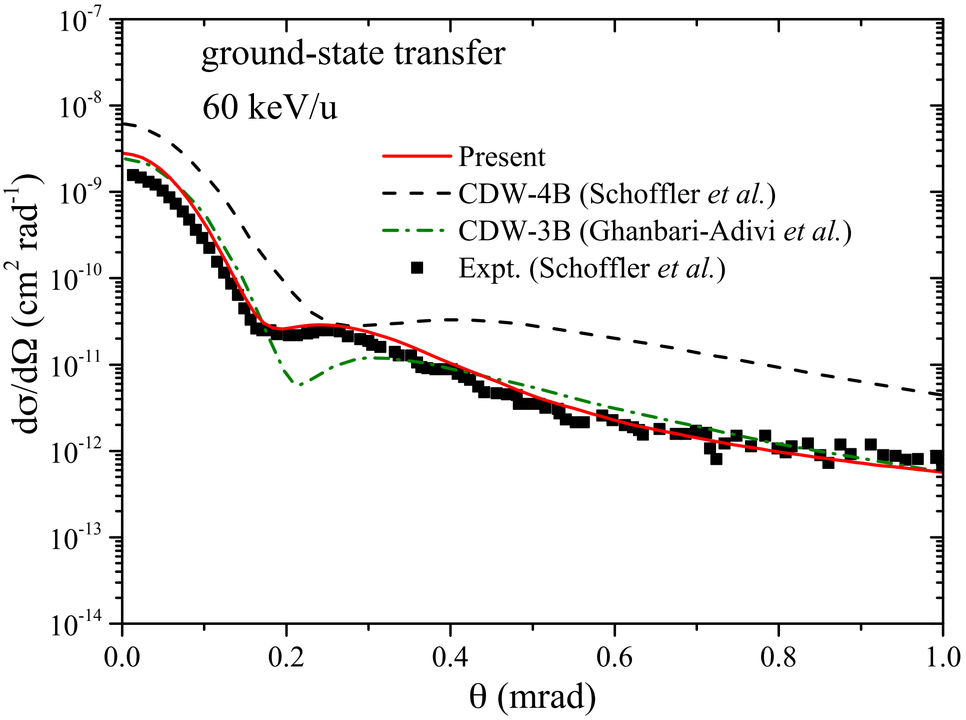

Figure 5.10 – The GT angular-differential cross sections as a function of scattering angle at impact energy 60 keV/u. Red solid line: present calculations; black dash line: theoretical results of Schöffler *et al.* [134]; green dash-dot line: theoretical results of Ghanbari-Adivi *et al.* [143]; black solid squre: experimental results of Schöffler *et al.* [134].

diffraction: the angular-differential cross sections present a minimum and then a maximum like the diffraction pattern in optics, with the first dark and bright fringes located at $0.61\lambda/\rho$ and $0.819\lambda/\rho$ respectively, in the case of a circular aperture of radius ρ and of a radiation of wavelength λ, see [122].

In the following, we check the validity of this interpretation for all processes and energies considered in this work. First, let us apply it on the GT angular-differential cross sections presented in Figure 5.12(a). The positions of the first minimum θ_{min}, marked as dash-line arrows, are determined directly from the calculated cross sections. From these minima, an effective "aperture" radius ρ_{FD} $(=0.61\lambda/\theta_{min})$ is obtained so that the position of first expected Fraunhofer bright fringe θ_{bright} $(=0.819\lambda/\rho_{FD})$ are evaluated. In Table 5.1, the values of our calculated effective "aperture" radius and the positions of first bright fringe are shown, the latter are also marked in Figure 5.12(a) as solid-line arrows. It can be seen in Table 5.1 and in Figure 5.12(a) that, for the four energies under consideration, the positions of the first maximum in our cross sections agree well with the predicted positions stemming from the Fraunhofer-type diffraction model. To compare our calculated effective "aperture" radius with the corresponding effective impact parameter range, the probabilities of the GT process as a function of impact parameter are shown in Figure 5.13(a) for impact energies 7.5, 25, 60, and 150 keV/u. Our calculated ef-

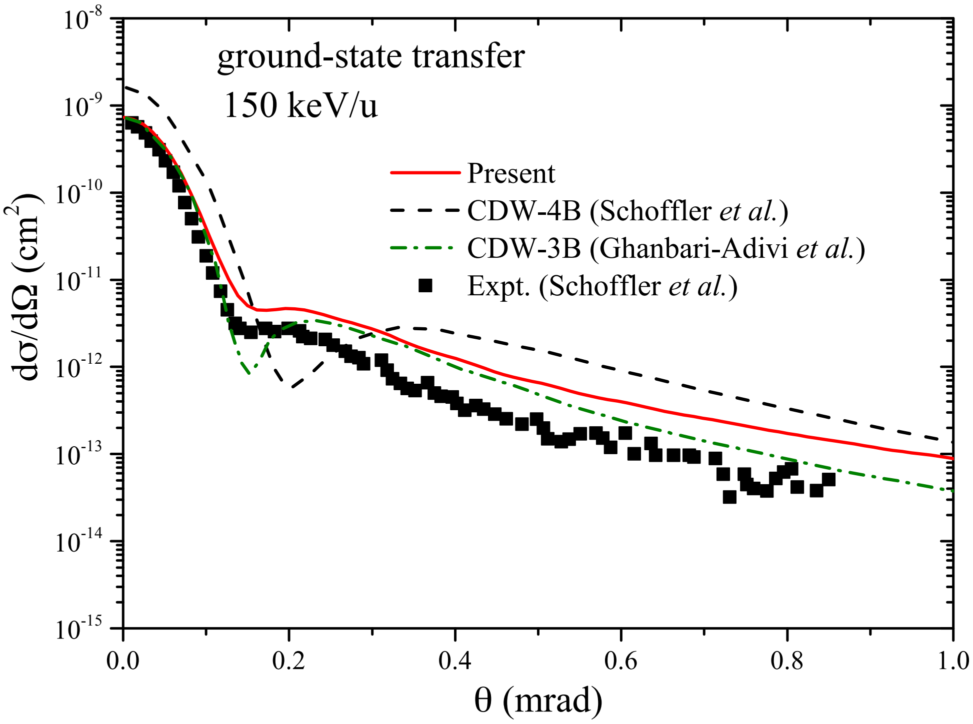

Figure 5.11 – Same as Figure 5.10, but for 150 keV/u.

fective "aperture" radii for the corresponding impact energies are marked as arrows in this figure. It is found that the probabilities of all these impact energies are negligibly small beyond the corresponding positions of the arrow. The effective impact parameter range are therefore in good agreement with the effective "aperture" radius. This tends to demonstrate that the oscillatory structure appearing in the GT angular-differential cross sections originates mainly from Fraunhofer-type diffraction.

We now apply the same analysis on the processes of ET to He(1s2s ^{1}S and ^{3}S) excited states and TE to He$^+$(2s) excited state. The results are presented in Figure 5.12(b)-(d) and in Table 5.1. The overall satisfactory agreement between the positions of the arrow and the first maximum in our calculated angular-differential cross sections suggests that the oscillatory structure observed for the ET and TE processes also originates from Fraunhofer-type diffraction. Note that we have also compared our calculated effective "aperture" radius with the corresponding effective impact parameter range for these processes and a satisfactory agreement was found (see Figure 5.13(b)-(d)).

However, for the TE angular-differential cross sections at 60 keV/u impact energy, one can observe an extra minimum at angle $\theta \approx 0.09$ mrad before the minimum marked as dash-line arrow in Figure 5.12(d). This small angle minimum gives the "aperture" radius to be 3.8 a.u., while the corresponding probability is already negligibly small beyond b $\approx$ 1.5 a.u.. This means that the first minimum and maximum are not stemming from Frauhofer-type diffraction. In contrast, from the second minimum at angle $\theta \approx 0.23$ mrad marked as dash-line arrow in Figure 5.12(d), the

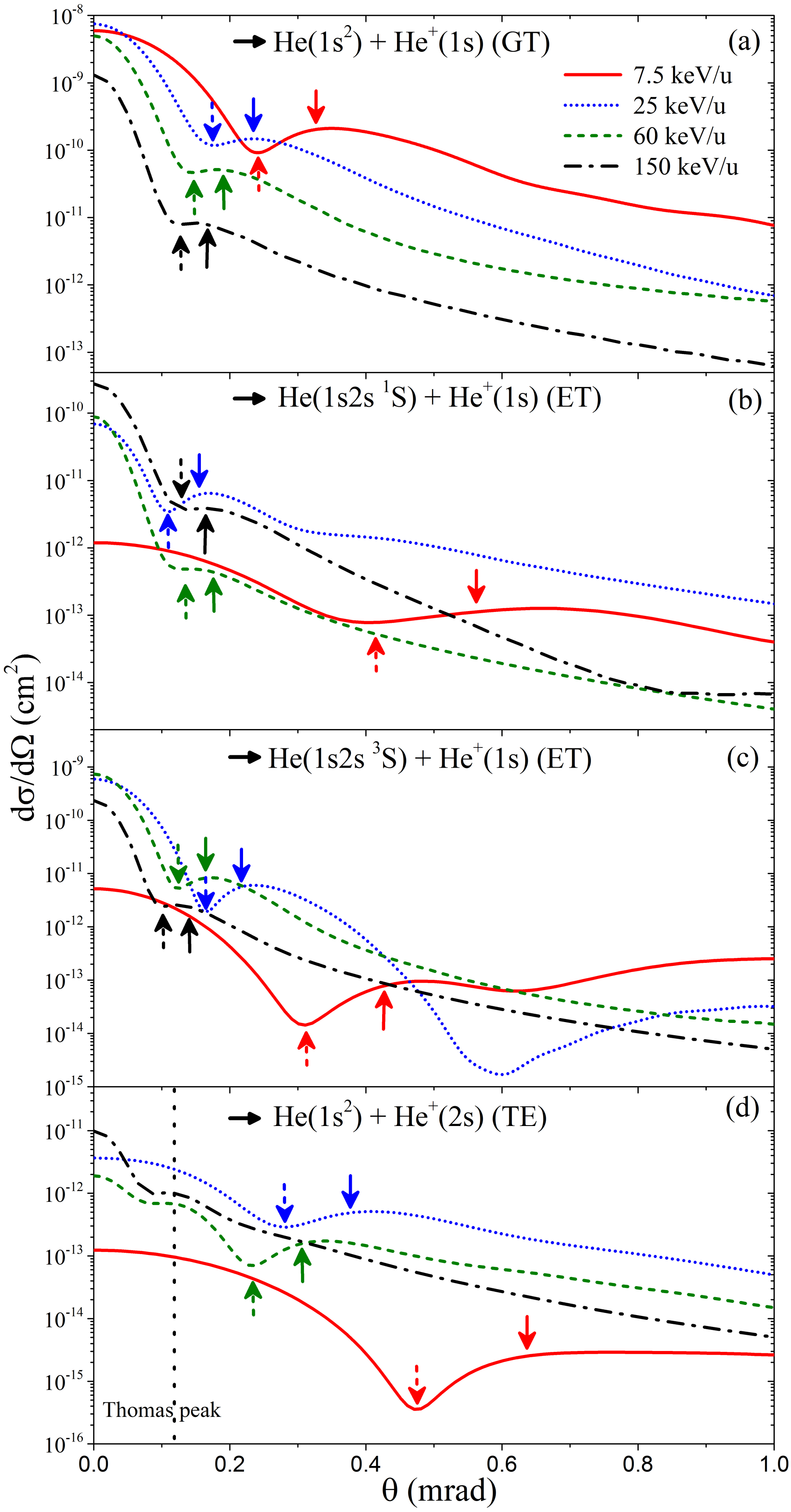

Figure 5.12 – The angular-differential cross sections of GT, ET to He(1s2s ^{1}S and ^{3}S) excited states and TE to He$^+$(2s)+He(1s^2) as functions of scattering angle for impact energies 7.5, 25, 60 and 150 keV/u. The dash-line arrows show the positions of the first minimum in our angular-differential cross sections; the solid-line arrows show the positions of first bright fringe calculated by the Fraunhofer-type diffraction model; the vertical dot-line in (d) shows the position of Thomas peak.

Table 5.1 – The position of the first minimum and maximum in the angular-differential cross sections as well as the effective “aperture” radius ρ_{FD} and the position of the first bright fringe calculated by the Fraunhofer-type diffraction model.

Process	Impact energy (keV/u)	1st minimum (mrad)	ρ_{FD}(a.u.)	1st maximum (mrad)	1st bright fringe (mrad)
GT	7.5	0.24	4.0	0.33	0.32
	25	0.17	3.1	0.23	0.23
	60	0.14	2.4	0.18	0.19
	150	0.13	1.7	0.15	0.17
ET to He(1s2s ^{1}S)	7.5	0.41	2.3	0.65	0.56
	25	0.11	4.8	0.17	0.15
	60	0.13	2.6	0.17	0.18
	150	0.12	1.8	0.15	0.16
ET to He(1s2s ^{3}S)	7.5	0.31	3.1	0.48	0.42
	25	0.16	3.3	0.23	0.21
	60	0.12	2.8	0.17	0.16
	150	0.10	2.1	0.13	0.14
TE to He$^+$(2s)	7.5	0.47	2.0	0.66	0.64
	25	0.28	1.9	0.40	0.37
	60	0.23	1.5	0.33	0.30
	150	0.09	2.4	0.12	0.12

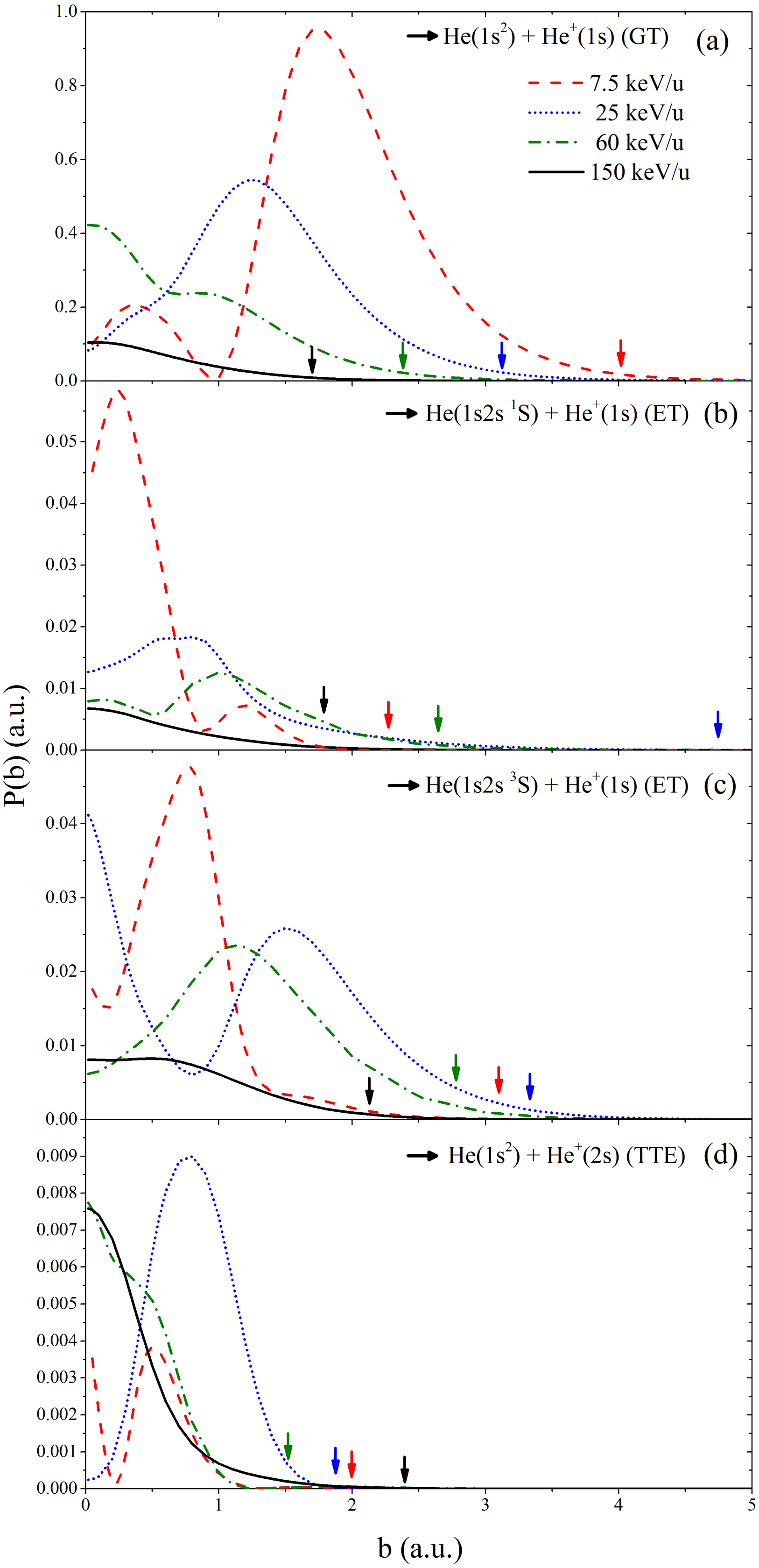

Figure 5.13 – The transition probabilities of the GT, ET and TTE processes as functions of impact parameters and for four different impact energies. The arrows mark the positions of the effective "aperture" radius calculated by the Fraunhofer-type diffraction model, see Table 5.1.

"aperture" radius is determined to be 1.5 a.u., which is in good agreement with corresponding effective probability range; the predicted first bright Fraunhofer fringe is also in agreement with the second maximum in our cross sections (see Table 5.1). In fact, at two highest impact energies, electron transfer is more likely dominated by the Thomas process [8, 149–151], where the Thomas peak is located at $\theta = \sqrt{3}m_e/2M$ (here m_e and M are the mass of electron and projectile, respectively). For the present collision system, $\theta_{Thomas} = 0.119$ mrad, which is also denoted as a vertical dot-line in Figure 5.12(d). An excellent agreement can be found between the vertical dot-line and the first maximum in angular-differential cross sections for impact energy 60 keV/u. This means that the first maximum observed in the TE angular-differential cross sections of impact energy 60 keV/u is the Thomas peak, while the second one originates from Fraunhofer-type diffraction. For E=150 keV/u, the first minimum is observed at angle $\theta \approx 0.09$ mrad, from which the "aperture" radius is determined to be 2.4 a.u. It turns out that the effective impact parameter range for this process at this energy is also around 2.4 a.u. This gives the first bright fringe of Fraunhofer-type diffraction at 0.12 mrad, which agrees well with the position of the first maximum in the angular-differential cross sections (see Table 5.1) and also lies at the Thomas peak position. Therefore, we may conclude that the structure observed for this process at 150 keV/u stems from the overlap between Thomas mechanism and diffraction, while at 60 keV/u the two effects are separated.

Note finally that for some of considered cross sections one can observe a second minimum which does not follow Fraunhofer diffraction prediction: for instance for ET to He(1s2s ^{3}S) excited states (Figure 5.12(c)) at 25 keV/u, a second miminum is located at 0.6 mrad while Fraunhofer theory predicts $\theta = 1.116\lambda/\rho \approx 0.29$ mrad. Furthermore, a second minimum and maximum are not observed in most cases. We attribute this fact to the limit of the Fraunhofer-type model: in particular, (i) the interaction region where electron transfer occurs is not a clean circular aperture and (ii) at larger scattering angles the contribution of hard (small impact parameters) collisions get dominant with important internuclear repulsive interaction, which washes out the diffraction pattern.

5.4 Conclusion

In this Chapter, we have investigated electron transfer processes occurring in the course of He^+ + He collisions by using a three-electron SCAOCC approach. First, total and state-selective cross sections have been calculated in a wide energy region from 1 to 225 keV/u and compared with available experimental and theoretical results: a very good agreement with the most recent and detailed experiments is observed. Comparisons of our results with other theoretical calculations further demonstrate the importance of a non-perturbative approach and of the electronic correlation. Moreover, we have shown that the electron transfer and target excitation (TTE) cross sections exhibit a prominent oscillatory energy dependence structure which was attributed to a strong competition between TTE and projectile-excitation processes, so as the target-excitation (TE) and transfer to excited states (ET) to He singlet excited states cross sections.

Second, we have calculated angular-differential cross sections of ground-state transfer (GT), ET and TTE, where our calculated GT angular-differential cross sections are in excellent agreements with experimental data of [117, 134] for all considered impact energies. Furthermore, the oscillatory structures observed in the GT, ET and TTE angular-differential cross sections have been interpreted by Fraunhofer-type diffraction, which seems to be valid for all processes and energies considered in this work. The Thomas peak has also been observed in the TTE angular-differential cross sections for higher impact energies 60 and 150 keV/u. In the latter case, the Thomas peak overlaps with the Fraunhofer-type maximum.

Conclusions and perspectives

In this thesis, we have presented a semiclassical non perturbative approach for modelling electronic processes occurring in ion-atom collisional systems. The approach is semiclassical in that the relative target-projectile motion is described by classical straight-line constant velocity trajectories, while the electronic dynamics is treated quantum mechanically, by solving non perturbatively the time-dependent Schödinger equation. The latter is solved by expanding the total electronic wavefunction into the eigenstates of the isolated collision partners. We have implemented the approach in a new version of two-active-electron computer code, where an optimized strategy for the evaluations of different coupling matrix elements was adopted so that a considerable reduction of computer resources demanding in memory and CPU time can be achieved. To our acknowledge, it is a unique code, together with the previous code developed in our group, where two active electrons in a scattering event can be described with the semiclassical atomic-orbital close-coupling (SCAOCC) approach with such efficiency that one can achieve very reasonable convergence of the results. This is very invaluable for the interpretation of data at the most fundamental level and also to calculate cross sections of relevance for various applications, as plasmas physics or radiobiology, as mentioned in the introduction. This has allowed us to investigate various collision systems, for which several electrons are involved so that multi-electronic processes are likely to occur and/or electronic correlations play a crucial role.

Besides the long and complex development and tests of the code, the last three years have been especially devoted to understanding of the physics of specific heavy particle scattering events. We have undertaken the study of three collision systems with various features: in order of appearance in this thesis, (i) low charge ion-ion collisions with an extreme importance of electronic correlation (H^+ + H^- collisions), (ii) multiply charged projectile-atom collisions (C^{4+} + He) and (iii) He^+ + He collisions with the dynamical treatment of the three electrons. Our guideline was always to target systems for which experimental and theoretical results were available (at least in some energy domain), with still open questions, related, for example, to strong disagreement between the various data. We have tried as much as our computing resources and allowed it to produce results with controlled convergence. These investigations were carried out in a very wide, up to three decades, energy domain with same collision description (i.e. same basis sets), which brought continuity and coherence on the predictions. Our calculated total and state-selective cross sections showed the best overall agreements with available experimental results for the considered electronic processes, compared to previous theoretical investigations. The important ingredients to describe accurately these processes have also been elucidated. Furthermore, we provided convictive and argued interpretations of the results and of the underlying mechanisms giving rise to the processes considered. In particular, for double electron capture (DEC) process in collisions of H^+ + H^-, our *ab initio* results suggest that the oscillatory structures observed in the cross section do not come from interferences between the gerade and ungerade pathways of the ion-pair configuration as previously put forward, but from interferences between DEC and other two-electron inelastic channels, i.e., the transfer-excitation to H(1s) + H(2ℓ) processes. A more complex mechanism involving a two-crossing model is presented in Chapter 3 and supports this interpretation. For C^{4+} + He collisions presented in Chapter 4, on one hand, we have demonstrated that contrary to what was concluded in previous investigations the single electron capture process (SEC) is independent of the DEC process in the low impact energy region, where the electron capture process is dominated by a direct mechanism. On the other hand, we have shown that a one-step mechanism dominates the DEC dynamics for high impact energies, in disagreement with a previous investigation in which an independent transfer mechanism was invoked. For the study of He^+ + He collision system presented in Chapter 5, we have shown and attributed the prominent oscillatory energy dependence structure observed in the electron transfer and target excitation cross sections to a strong competition with projectile-excitation processes, so as the target-excitation and transfer to excited states to He singlet excited states cross sections. Moreover, we have also investigated the electron transfer differential cross sections in Chapter 4 and 5, which provide a greater benchmark for our calculations. The angular-differential cross sections considered in this thesis exhibited oscillatory structures which were interpreted within Fraunhofer-type diffraction models, which seems to be valid for all the considered processes and energies in C^{4+} + He and He^+ + He collision systems. For high impact energies in the latter case, the Thomas mechanism have to be advocated.

In summary, one can state that thanks to previous developments performed in the group and this three years of work, we have reach an ever achieved quality of the description of multi-electron processes occurring in ion-atom collisions. We have indeed shown that we have obtained results which are in unprecedented agreement with experimental data. This does not mean that there is no need of improvements in the future but that the field is now mature to attack the study of complex systems of relevance for applications.

On one hand, for future, short-term investigations, the present developed two and three-active-electron semiclassical atomic orbital close-coupling computer code can be used to investigate a number of collision systems of importance in cold and hot plasmas physics, involving proton and multiply charged projectiles (e.g., tungsten in various stages of ionization.) colliding with helium, lithium and also simple molecular targets (e.g. H_2.). Furthermore, we can also study the collision systems involving more complex diatomic molecules, such as O_2, N_2 and CO, by using model potentials to describe the electron interaction with nucleus core (in the frozen-core approximation). These collision systems have received a great deal of interest, since they are well suited for experimental purposes [152], but with quite simplified theoretical investigations.

On the other hand, for long-term plans, we would like to extend our collision code to multiple active electrons and multi-center targets, i.e. dealing with more complex molecules beyond the diatomic ones. In fact, the present code is ready for this development, since the coding for evaluations of all coupling matrix elements is already done. However, prohibitive computer time will require further optimization and new strategy, notably for the construction of basis sets. This code would find many applications: a perfect candidate is of course the study of collisions between ions and H_2O molecules. Since the latter represents 70% (in mass) of the human body and is one of the most abundant species in the universe, the understanding of the fundamental mechanisms occurring during collisions with an ion is therefore of significant importance in radiobiology and astrophysics [1]. Another objective for future developments, also related to basis set constructions, is the description of the ionization process through the use of more controlled pseudo-states of energy lying above ionization thresholds. For example, the recent developed wave-packet continuum-discretization approach [153] allows one to generate pseudo-states with arbitrary energies and distribution. The implementation of such kind of method spanning in a rigorous way the continuum in our multiple active electrons approach will improve the accuracy of the calculations and extend the range of predictability of our code to higher impact energies and to ionization processes. For the latters, the approach has particular advantages in the calculation and analysis of angle and energy differential cross sections, and will provide benchmark results.

Appendix A

Atomic units

Atomic units (a.u.) form a system of natural units which is especially convenient for atomic physics calculations. In atomic units, the physical constants are redefined as,

$$e = \hbar = m_e = \frac{1}{4\pi\epsilon_0} = 1, \tag{A.1}$$

where e is the elementary charge, $\hbar$ is the reduced Planck constant, m_e is electron mass, and ϵ_0 is the permittivity of the free space. Table A.1 lists various physical quantities, which define atomic units, and the associated numerical values in the international system of units (SI). The important physical constants and some characteristic quantities expressed in atomic units and SI are shown in Table A.2.

Table A.1 – Fundamental atomic units.

Quantity	Physical meaning	Unit	Value in SI units
Mass	Free-electron mass	m_e	9.10938×10^{-31} kg
Charge	Absolute value of electron charge	e	1.60218×10^{-19} C
Angular momentum	Reduced Planck's constant	$\hbar$	1.05457×10^{-34} Js
Length	Bohr radius of H atom	$a_0 = \frac{4\pi\epsilon_0\hbar^2}{m_e e^2}$	5.29177×10^{-11} m
Velocity	Electron speed in the first Bohr orbit	$v_0 = \frac{e^2}{4\pi\epsilon_0\hbar}$	2.18769×10^{6} m/s
Time	Time it takes an electron in the first Bohr orbit to travel one Bohr radius	$\tau_0 = \frac{a_0}{v_0}$	2.41888×10^{-17} s
Energy	Twice the ionization energy of the H atom	$E_0 = \frac{e^2}{4\pi\epsilon_0 a_0}$	4.35974×10^{-18} J

In the present thesis, we mainly study electronic processes occurring in the course

Table A.2 – The important physical constants and some characteristic quantities expressed in atomic units and international system of units (SI).

		Value in atomic units	Value in SI units
Planck constant	h	2π	6.62618×10^{-34} Js
Speed of light	c	137.036	2.99792×10^{8} m/s
Atomic mass unit	u	1836.15	1.67265×10^{-27} kg
Ionization energy of H	ϵ_0(H)	-0.5	-2.17991×10^{-18} J
1 femtosecond	fs	41.3413	10^{-15} s
1 angstrom	$\overset{\circ}{A}$	1.8897	10^{-10} m
1 electron-Volt	eV	0.036749	1.60219×10^{-19} J

of atomic and molecular collisions. In general, the cross sections are preferably expressed as a function of the impact energy E defined as the kinetic energy of the system in the center of mass divided by its reduced mass. The unit associated with E is the keV/u: "kilo-electron-volt per atomic mass unit", it is related to the relative velocity of nuclei in a.u.,

$$E_{keV/u} = 24.98 v_{a.u.}^2. \tag{A.2}$$

The usual unit for cross sections is 10^{-16} cm^2, or 1 $\overset{\circ}{A}^2$,

$$\begin{aligned} 10^{-16} cm^2 &= 3.57\ a.u.\ of\ surface, \\ 1\ a.u.\ of\ surface &= 0.28 \times 10^{-16} cm^2. \end{aligned} \tag{A.3}$$

Appendix B

Basis sets of Gaussian-type orbitals

In the present thesis, we use a linear combination of Cartesian Gaussian-type orbitals (GTOs) to describe the states of isolated collision partners, written as,

$$\chi_k(\vec{r}) = N_k x^{u_k} y^{v_k} z^{w_k} e^{-\alpha_k r^2}; k = 1, 2, ..., N, \tag{B.1}$$

where N_k is a normalization factor, u_k, v_k and w_k are positive integers or zero. For a given angular momentum ℓ, the relationship, $\ell = u_k + v_k + w_k$, has to be satisfied and all combinations of u_k, v_k, w_k allows the description of all Cartesian spherical harmonics for a given ℓ. The exponents α_k in the GTOs have been optimized to obtain a good description of the important states of isolated collision partners for the collision systems under consideration. We present in this appendix the optimized basis sets of GTOs used in the investigations of each collision systems.

B.1 $\mathrm{H}^+ + \mathrm{H}^-$ collisions (Chapter 3)

For $\mathrm{H}^+ + \mathrm{H}^-$ collsions, a set of 45 GTOs (11 for $l = 0$, 8×3 for $l = 1$, and 2×5 for $l = 2$), named $\mathrm{B1}_H$, were used on both projectile and target centers; this allows the inclusion of 1977 states, describing elastic, SEC and DEC channels, as well as ionization, through the pseudostates of energy lying above ionization thresholds. We have shown, in chapter 3, that the important eigenstates of the isolated collision partners, H and H^-, are both described properly with the basis set $\mathrm{B1}_H$. Furthermore, convergence tests have been performed by comparing the results from $\mathrm{B1}_H$ with those from two different basis sets (i) $\mathrm{B2}_H$ includes 32 GTOs, 9 for $l = 0$, 6×3 for $l = 1$, and 1×5 for $l = 2$, which allows the inclusion of 1425 states and (ii) $\mathrm{B3}_H$ includes 55 GTOs, 11 for $l = 0$, 8×3 for $l = 1$, and 4×5 for $l = 2$, which allows the inclusion of 3725 states. In Table B.1, parameters of the GTOs in basis set $\mathrm{B1}_H$, $\mathrm{B2}_H$ and $\mathrm{B3}_H$ are presented.

Table B.1 – Parameters of the GTOs centered on each nucleus used to describe states of H and H^-.

B1$_H$			B2$_H$			B3$_H$		
i	ℓ	α	i	ℓ	α	i	ℓ	α
1	0	82.640000	1	0	82.640000	1	0	82.640000
2	0	12.410000	2	0	17.201505	2	0	12.410000
3	0	2.8240000	3	0	3.5813594	3	0	2.8240000
4	0	0.7977000	4	0	0.7456402	4	0	0.7977000
5	0	0.2581000	5	0	0.1552425	5	0	0.2581000
6	0	0.0898900	6	0	0.0323215	6	0	0.0898900
7	0	0.0251300	7	0	0.0067293	7	0	0.0251300
8	0	0.0078770	8	0	0.0014010	8	0	0.0078770
9	0	0.0029256	9	0	0.0002917	9	0	0.0029256
10	0	0.0008852	10	1	2.2920000	10	0	0.0008852
11	0	0.0002917	11	1	0.4922220	11	0	0.0002917
12	1	2.2920000	12	1	0.1057079	12	1	2.2920000
13	1	0.8380000	13	1	0.0227014	13	1	0.8380000
14	1	0.2920000	14	1	0.0048752	14	1	0.2920000
15	1	0.0848000	15	1	0.0010470	15	1	0.0848000
16	1	0.0275700	16	2	0.0147500	16	1	0.0275700
17	1	0.0094220				17	1	0.0094220
18	1	0.0031910				18	1	0.0031910
19	1	0.0010470				19	1	0.0010470
20	2	0.0147500				20	2	0.0147500
21	2	2.0620000				21	2	2.0620000
						22	2	0.6620000
						23	2	0.1900000

B.2 C^{4+}+He collisions (Chapter 4)

In the study of C^{4+}+He collsions, a set of 57 GTOs (13 for $l = 0$, 8×3 for $l = 1$ and 4×5 for $l = 2$) are used on C^{4+} center, denoted as B1$_C$ (28 GTOs, i.e. 10 for $l = 0$ and 6×3 for $l = 1$, on He^{2+}), which allows the inclusion of 1002 singlet states in total : 146 TT (He), 412 TP (He^+,C^{3+}) and 444 PP (C^{2+}, denoted as B1$_{He}$) states. The convergence of the results has also been tested from a series of different GTO basis sets, namely B2$_C$, B3$_C$, B4$_C$ and B2$_{He}$, B3$_{He}$, B4$_{He}$. The basis sets B1$_C$, B2$_C$, B3$_C$ and B4$_C$ are presented in Table B.2, and B1$_{He}$, B2$_{He}$, B3$_{He}$ and B4$_{He}$ are shown in Table B.3.

B.3 He$^+$+He collisions (Chapter 5)

For the investigation of He$^+$+He collisions, we use a set of 19 GTOs (10 for l=0, 3×3 for l =1), denoted as B1$_{HeHe}$ on both projectile and target centers; this allows the inclusion of 1260 states (states of two electrons on target and one electron on projectile, and vice-versa). A smaller basis set (12 GTOs on each center, i.e., 6 for l=0 and 2×3 for $l = 1$), namely B2$_{HeHe}$, are used for convergence test which allows the inclusion of 582 states in total. In Table B.4, basis sets B1$_{HeHe}$ and B2$_{HeHe}$ are presented.

Table B.2 – Parameters of the GTOs used to describe states of C^{2+} and C^{3+} .

$B1_C$			$B2_C$			$B3_C$			$B4_C$		
i	ℓ	α	i	ℓ	α	i	ℓ	α	i	ℓ	α
1	0	0.0070000	1	0	0.0070000	1	0	0.0070000	1	0	0.0070000
2	0	0.0177659	2	0	0.0242335	2	0	0.0155526	2	0	0.0155526
3	0	0.0450896	3	0	0.0838950	3	0	0.0345547	3	0	0.0345547
4	0	0.1144368	4	0	0.2904392	4	0	0.0767738	4	0	0.0767738
5	0	0.2904392	5	0	1.0054823	5	0	0.1705762	5	0	0.1705762
6	0	0.7371310	6	0	3.4809162	6	0	0.3789865	6	0	0.3789865
7	0	1.8708287	7	0	12.050711	7	0	0.8420321	7	0	0.8420321
8	0	4.7481382	8	0	41.718798	8	0	1.8708280	8	0	1.8708280
9	0	12.050711	9	0	144.42780	9	0	4.1566083	9	0	4.1566083
10	0	30.584541	10	0	499.99999	10	0	9.2351571	10	0	9.2351571
11	0	77.623164	11	1	0.0320000	11	0	20.518682	11	0	20.518682
12	0	197.00655	12	1	0.1536295	12	0	45.588424	12	0	45.588424
13	0	499.99999	13	1	0.7375635	13	0	101.28840	13	0	101.28840
14	1	0.0320000	14	1	3.5409858	14	0	225.04266	14	0	225.04266
15	1	0.0784293	15	1	17.000000	15	0	499.99999	15	0	499.99999
16	1	0.1922236	16	2	0.0554000	16	1	0.0320000	16	1	0.0320000
17	1	0.4711240	17	2	1.1100000	17	1	0.0642629	17	1	0.0566114
18	1	1.1546853				18	1	0.1290541	18	1	0.1001518
19	1	2.8300367				19	1	0.2591689	19	1	0.1771794
20	1	6.9361823				20	1	0.5204679	20	1	0.3134496
21	1	17.000000				21	1	1.0452133	21	1	0.5545263
22	2	0.0554000				22	1	2.0990169	22	1	0.9810173
23	2	0.1504691				23	1	4.2152849	23	1	1.7355259
24	2	0.4086817				24	1	8.4652137	24	1	3.0703336
25	2	1.1100000				25	1	17.000000	25	1	5.4317531
						26	2	0.0554000	26	1	9.6093601
						27	2	0.1008956	27	1	17.000000
						28	2	0.1837532	28	2	0.0554000
						29	2	0.3346552	29	2	0.0913016
						30	2	0.6094812	30	2	0.1504691
						31	2	1.1100000	31	2	0.2479798
									32	2	0.4086817
									33	2	0.6735256
									34	2	1.1100000

Table B.3 – Parameters of the GTOs used to describe states of He$^+$ and He.

B1$_{He}$			B2$_{He}$			B3$_{He}$			B4$_{He}$		
i	ℓ	α	i	ℓ	α	i	ℓ	α	i	ℓ	α
1	0	0.0855000	1	0	0.0855000	1	0	0.0855000	1	0	0.0855000
2	0	0.0247268	2	0	0.0420503	2	0	0.0203851	2	0	0.0178344
3	0	0.0715105	3	0	0.2068104	3	0	0.0486027	3	0	0.0372009
4	0	0.2068101	4	0	1.0171283	4	0	0.1158797	4	0	0.0775974
5	0	0.5981012	5	0	5.0024063	5	0	0.2762834	5	0	0.1618606
6	0	1.7297245	6	0	24.602662	6	0	0.6587219	6	0	0.3376253
7	0	5.0024062	7	0	121.00000	7	0	1.5705412	7	0	0.7042532
8	0	14.467086	8	1	0.0110000	8	0	3.7445234	8	0	1.4690028
9	0	41.839186	9	1	0.0612603	9	0	8.9277856	9	0	3.0641951
10	0	121.00000	10	1	0.3411666	10	0	21.285848	10	0	6.3916092
11	1	0.0110000	11	1	1.9000000	11	0	50.750247	11	0	13.332267
12	1	0.0308221				12	0	121.00000	12	0	27.809795
13	1	0.0863642				13	1	0.0110000	13	0	58.008492
14	1	0.2419961				14	1	0.0229623	14	0	121.00000
15	1	0.6780805				15	1	0.0479334	15	1	0.0110000
16	1	1.9000000				16	1	0.1000603	16	1	0.0209441
						17	1	0.2088741	17	1	0.0398779
						18	1	0.4360212	18	1	0.0759281
						19	1	0.9101869	19	1	0.1445683
						20	1	1.9000000	20	1	0.2752600
									21	1	0.5240990
									22	1	0.9978918
									23	1	1.9000000

Table B.4 – Parameters of the GTOs centered on each nucleus used to describe states of He and He$^+$.

	$\mathrm{B1}_{HeHe}$			$\mathrm{B2}_{HeHe}$	
i	ℓ	α	i	ℓ	α
1	0	0.0099013	1	0	0.0099013
2	0	0.0285723	2	0	0.0650313
3	0	0.0831588	3	0	0.4271237
4	0	0.2280758	4	0	2.8053336
5	0	0.6489438	5	0	18.425331
6	0	1.8464388	6	0	121.01689
7	0	5.2536688	7	1	0.0330000
8	0	14.948253	8	1	0.8000000
9	0	42.532238			
10	0	121.01689			
11	1	0.0330000			
12	1	0.1624807			
13	1	0.8000000			

References

[1] T. E. Cravens, “X-ray Emission from Comets”, *Science* **296**, 1042 (2002).

[2] C. M. Lisse, *et al.*, “Charge Exchange-Induced X-Ray Emission from Comet C/1999 S4 (LINEAR)”, *Science* **292**, 1343 (2001).

[3] R. C. Isler, “An overview of charge-exchange spectroscopy as a plasma diagnostic”, *Plasma Phys. Control. Fusion* **36**, 171 (1994).

[4] M. Reich, *et al.*, “Lithium beam charge exchange diagnostic for edge ion temperature measurements at the ASDEX Upgrade tokamak”, *Plasma Phys. Control. Fusion* **46**, 797 (2004).

[5] S. Fiedler, *et al.*, “Edge plasma diagnostics on W7-AS and ASDEX-Upgrade using fast Li beams”, *J. Nucl. Mater.* **266**, 1279 (1999).

[6] U. Amaldi, G. Kraft, “Radiotherapy with beams of carbon ions”, *Rep. Prog. Phys.* **68**, 1861 (2005).

[7] D. Belkić, “Review of theories on double electron capture in fast ion-atom collisions”, *J. Math. Chem.* **47**, 1420 (2010).

[8] L. H. Thomas, “On the capture of electrons by swiftly moving electrified particles”, *Proc. Roy. Soc. London, Ser. A* **114**, 561 (1927).

[9] D. R. Bates, J. T. Lewis, “Inelastic Heavy Particle Collisions Involving the Crossing of Potential Energy Curves III: Charge Transfer from Negative Ions of Atomic Hydrogen to Protons”, *Proc. Phys. Soc, Sec. A* **68**, 173 (1955).

[10] A. Dalgarno, N. Lynn, “Resonance forces at large separations”, *Proc. Phys. Soc., Sec. A* **69**, 821 (1956).

[11] B. Zygelman, A. Dalgarno, “Direct charge transfer of He^+ in neon”, *Phys. Rev. A* **33**, 3853 (1986).

[12] M. Kimura, N. F. Lane, “The Low-Energy, Heavy-Particle Collisions-A Close-Coupling Treatment”, *Adv. At. Mol. Opt. Phys.* **26**, 79 (1989).

[13] M. Barat, “The Quasi-Molecular Model in Heavy Particle Collisions”, Springer US, Boston, MA (1976).

[14] J. B. Delos, “Theory of electronic transitions in slow atomic collisions”, *Rev. Mod. Phys.* **53**, 287 (1981).

[15] D. S. F. Crothers, M. McCartney, “ION — a program to evaluate cross-sections for ionisation in ion-atom collisions”, *Comput. Phys. Commun.* **72**, 288 (1992).

[16] P. D. Fainstein, V. H. Ponce, R. D. Rivarola, “Single-electron ionisation of helium by anti-proton and proton impact”, *J. Phys. B* **22**, L559 (1989).

[17] R. Abrines, I. C. Percival, *Proc. Phys. Soc.* (Kingston College of Technology, London, 1966).

[18] M. Schulz, *et al.*, “Correlated three-electron continuum states in triple ionization by fast heavy-ion impact”, *Phys. Rev. A* **61**, 022703 (2000).

[19] J. P. Hansen, A. Dubois, S. E. Nielsen, “Orientation and alignment in H^+-H collisions”, *Phys. Rev. A* **44**, 6130 (1991).

[20] J. P. Hansen, A. Dubois, “Procedures for analytical and numerical calculation of Coulombic one- and two-centre integrals”, *Comput. Phys. Commun.* **67**, 456 (1992).

[21] J. Caillat, A. Dubois, J. P. Hansen, “On the discrepancies of the calculated C^{5+}(n = 5) capture cross sections in C^{6+}-H collisions”, *J. Phys. B* **33**, L715 (2000).

[22] J. Wang, J. P. Hansen, A. Dubois, “Neutralization and charge transfer in H^+-H^- and H-H collisions”, *J. Phys. B* **33**, 241 (2000).

[23] N. Sisourat, I. Pilskog, A. Dubois, “Nonperturbative treatment of multielectron processes in ion-molecule scattering: Application to He^{2+}-H_2 collisions”, *Phys. Rev. A* **84**, 052722 (2011).

[24] A. Ibaaz, R. E. Hernandez, A. Dubois, N. Sisourat, “Excitation into high-lying states in Li^{3+} –H collisions”, *J. Phys. B* **49**, 085202 (2016).

[25] B. H. Bransden, M. R. C. McDowell, *Charge Exchange and the Theory of Ion-Atom Collisions* (Clarendon Press. Oxford, 1992).

[26] D. R. Bates, R. McCarroll, “Electron Capture in Slow Collisions”, *Pro. R. Soc. A* **245**, 175 (1958).

[27] C. Joachain, “Quantum collision theory”, *Netherlands: North-Holland* (1975).

[28] R. McCarroll, *“Charge Exchange and Ionization in Ion-Atom Collisions”*, F. A. Gianturco, ed., NATO Adv. Sci. Inst.(ASI) Ser. B (1982).

[29] R. McCarroll, “Resonance Charge Transfer Between H(1s) and H^+ Calculated by Means of an Approximation Based on an Expansion in Atomic Eigenfunctions”, *Proc. R. Soc. London, Ser. A* **264**, 547 (1961).

[30] W. Fritsch, C. D. Lin, “Atomic-Orbital Expansions for Describing Charge Transfer in Slow Ion-Atom Collisions”, *Phys. Scr.* **1983**, 241 (1983).

[31] R. D. Piacentini, A. Salin, “Multistate molecular treatment of atomic collisions in the impact parameter approximation. II - Calculation of differential cross-sections from the transition amplitudes for the straight line case.”, *Comput. Phys. Commun.* **13**, 57 (1977).

[32] R. Y. Cusson, R. K. Smith, J. A. Maruhn, “Time-Dependent Hartree-Fock Calculation of the Reaction $^{16}O^+ + ^{16}O$ in Three Dimensions”, *Phys. Rev. Lett.* **36**, 1166 (1976).

[33] R. Y. Cusson, J. Maruhn, “Dynamics of $^{12}C + ^{12}C$ in a realistic time-dependent, Hartree-Fock model”, *Phys. Lett. B* **62**, 134 (1976).

[34] K. T. R. Davies, V. Maruhn-Rezwani, S. E. Koonin, J. W. Negele, “Test of the Time-Dependent Mean-Field Theory in Kr-Induced Strongly Damped Collisions”, *Phys. Rev. Lett.* **41**, 632 (1978).

[35] S. E. Koonin, *et al.*, "Time-dependent Hartree-Fock calculations for ^{16}O + ^{16}O and ^{40}Ca + ^{40}Ca reactions", *Phys. Rev. C* **15**, 1359 (1977).

[36] C. Bottcher, "Accurate Quantal Studies of Ion-Atom Collisions Using Finite-Element Techniques", *Phys. Rev. Lett.* **48**, 85 (1982).

[37] V. Maruhn-Rezwani, N. Grün, W. Scheid, "Numerical Solution of the Time-Dependent Schrödinger Equation and Application to H^+-H", *Phys. Rev. Lett.* **43**, 512 (1979).

[38] Q. Su, J. H. Eberly, "Model atom for multiphoton physics", *Phys. Rev. A* **44**, 5997 (1991).

[39] A. D. Bandrauk, H. Lu, "Laser-induced electron recollision in H_2 and electron correlation", *Phys. Rev. A* **72**, 023408 (2005).

[40] K. J. Schafer, K. C. Kulander, "Energy analysis of time-dependent wave functions: Application to above-threshold ionization", *Phys. Rev. A* **42**, 5794 (1990).

[41] L. Ponce, R. Taïeb, V. Véniard, A. Maquet, "Dynamics of the ionization mechanism in ion–atom collisions at intermediate velocities", *J. Phys. B* **37**, L297 (2004).

[42] M. S. Pindzola, D. R. Schultz, "Time-dependent lattice methods for ion-atom collisions in Cartesian and cylindrical coordinate systems", *Phys. Rev. A* **77**, 014701 (2008).

[43] T. Minami, M. S. Pindzola, T. G. Lee, D. R. Schultz, "Lattice, time-dependent Schrödinger equation approach for charge transfer in collisions of Be^{4+} with atomic hydrogen", *J. Phys. B* **39**, 2877 (2006).

[44] M. Chassid, M. Horbatsch, "One-dimensional quantum model for ion-atom collisions: analysis of longitudinal ionized electron momenta", *J. Phys. B* **31**, 515 (1998).

[45] G. Labaigt, *et al.*, "Electron capture and ionization processes in high-velocity C_n^+, C-Ar and C_n^+, C-He collisions", *J. Phys. B* **48**, 075201 (2015).

[46] W. Fritsch, C. D. Lin, "The semiclassical close-coupling description of atomic collisions: Recent developments and results", *Phys. Rep.* **202**, 1 (1991).

[47] J. Caillat, A. Dubois, J. P. Hansen, "Semiclassical Close-Coupling Description of Electron Transfer in Multicharged Ion-Atom Collisions", Dordrecht (2000).

[48] J. P. Hansen, A. Dubois, "Excitation in H(1s) - H(1s) collisions", *J. Phys. B* **31**, L861 (1998).

[49] J. B. Wang, J. P. Hansen, A. Dubois, "Spin Anisotropy for Excitation in Collisions between Two One-Electron Atoms", *Phys. Rev. Lett.* **85**, 1638 (2000).

[50] L. Shampine, M. Gordon, "Computer solution of ordinary differential equations: the initial value problem" (Freeman, San Francisco, CA, 1975).

[51] S F Boys, "Electronic wave functions - I. A general method of calculation for the stationary states of any molecular system", *Proc. R. Soc. Lond. A* **200**, 542 (1950).

[52] C. M. Reeves, M. C. Harrison, “Use of Gaussian Functions in the Calculation of Wavefunctions for Small Molecules. II. The Ammonia Molecule”, *J. Chem. Phys.* **39**, 11 (1963).

[53] R. C. Raffenetti, “Even-tempered atomic orbitals. II. Atomic SCF wavefunctions in terms of even-tempered exponential bases”, *J. Chem. Phys.* **59**, 5936 (1973).

[54] I. Cherkes, S. Klaiman, N. Moiseyev, “Spanning the Hilbert space with an even tempered Gaussian basis set”, *Int. J. Quantum Chem* **109**, 2996 (2009).

[55] M. Abramowitz, I. A. Stegun, “Handbook of mathematical functions with formulas, graphs, and mathematical tables”, *Dover Books on Advanced Mathematics* **32**, 239 (1965).

[56] J. Caillat, N. Sisourat, A. Dubois, I. Sundvor, J. P. Hansen, “Orientation effects in He^{2+} - H_2^+ collisions at intermediate collision energies”, *Phys. Rev. A* **73**, 014701 (2006).

[57] J. Caillat, A. Dubois, I. Sundvor, J. P. Hansen, “Classical and semiclassical calculations of electron transfer cross sections in keV -energy ion-molecule collisions”, *Phys. Rev. A* **70**, 032715 (2004).

[58] I. Rabadán, L. Méndez, J. W. Gao, Y. Wu, J. G. Wang, “Ab initio calculation of electron-capture cross sections in $H^+ + BeH$ collisions”, *Phys. Rev. A* **96**, 032714 (2017).

[59] L. F. Errea, J. D. Gorfinkiel, A. Macías, L. Méndez, A. Riera, “Implementation of the sudden approximation eikonal method in ion - diatom collisions”, *J. Phys. B* **30**, 3855 (1997).

[60] D. R. Bates, A. R. Holt, “Impact Parameter and Semi-Classical Treatments of Atomic Collisions”, *Pro. R. Soc. London, Ser. A* **292**, 168 (1966).

[61] L. Wilets, S. J. Wallace, “Eikonal Method in Atomic Collisions. I”, *Phys. Rev.* **169**, 84 (1968).

[62] R. McCarroll, A. Salin, “Impact parameter treatment of atomic collisions”, *J. Phys. B* **1**, 163 (1968).

[63] A. Dubois, S. E. Nielsen, J. P. Hansen, “State selectivity in H -Na (3s/3p) collisions: differential cross sections, alignment and orientation effects for electron capture”, *J. Phys. B* **26**, 705 (1993).

[64] B. H. Bransden, C. J. Joachain, *Physics of Atoms and Molecules* (Prentice Hall (Pearson Prentice Hall (Pearson Education Ltd), 2003).

[65] N. Toshima, “Convergence and completeness of the pseudostate expansion for proton-hydrogen collisions in two-center close-coupling calculations”, *Phys. Rev. A* **59**, 1981 (1999).

[66] J. Caillat, *et al.*, “Correlated multielectron systems in strong laser fields: A multiconfiguration time-dependent Hartree-Fock approach”, *Phys. Rev. A* **71**, 012712 (2005).

[67] B. Peart, M. A. Bennett, K. Dolder, “New measurements of the mutual neutralisation of H^+/H^- and He^+/H^- ions”, *J. Phys. B* **18**, L439 (1985).

[68] A. M. Ermolaev, “Neutralisation and detachment in collisions between protons and negative hydrogen ions in the proton energy range from 0.62 to 80.0 keV lab”, *J. Phys. B* **21**, 81 (1988).

[69] B. Peart, D. A. Hayton, “Merged beam measurements of mutual neutralization of H^+ and H^- ions”, *J. Phys. B* **25**, 5109 (1992).

[70] L. F. Errea, *et al.*, “Molecular treatment of $H^+ + H^-$ collisions at intermediate energies”, *Nucl. Instr. and Meth. in Phys. Res. B* **98**, 335 (1995).

[71] W. Schon, *et al.*, “Mutual neutralisation in $H^+ + H^-$ collisions”, *J. Phys. B* **20**, L759 (1987).

[72] R. Shingal, B. H. Bransden, “Neutralisation in $H^+ + H^-$ and ion pair production in H + H collisions”, *J. Phys. B* **23**, 1203 (1990).

[73] M. Stenrup, Å. Larson, N. Elander, “Mutual neutralization in low-energy $H^+ + H^-$ collisions: A quantum ab initio study”, *Phys. Rev. A* **79**, 012713 (2009).

[74] I. Mančev, N. Milojević, D. Belkić, “Mutual neutralization in $H^+ + H^-$ collisions by electron capture”, *Europhys. Lett.* **103**, 23001 (2013).

[75] A. Jorge, C. Illescas, L. Méndez, B. Pons, “Switching classical trajectory monte carlo method to describe two-active-electron collisions”, *Phys. Rev. A* **94**, 022710 (2016).

[76] F. Brouillard, W. Claeys, G. Poulaert, G. Rahmat, G. Van Wassenhove, “Double charge transfer in $H^+ + H^-$ collisions”, *J. Phys. B* **12**, 1253 (1979).

[77] B. Peart, R. A. Forrest, “Measurements of cross sections for double charge transfer in collisions between H^+ and H^- ions”, *J. Phys. B* **12**, L23 (1979).

[78] H. Bräuning, H. Helm, J. S. Briggs, E. Salzborn, “Double-Electron Transfer in $H^- + H^+$ Collisions”, *Phys. Rev. Lett.* **99**, 173202 (2007).

[79] J. Z. Mezei, M. Stenrup, N. Elander, Å. Larson, “Double charge transfer in low-energy $H^+ + H^-$ collisions”, *Phys. Rev. A* **82**, 014701 (2010).

[80] J. W. Gao, Y. Wu, N. Sisourat, J. G. Wang, A. Dubois, “Single- and double-electron transfer in low- and intermediate-energy C^{4+} + He collisions”, *Phys. Rev. A* **96**, 052703 (2017).

[81] J. W. Gao, Y. Wu, J. G. Wang, N. Sisourat, A. Dubois, “State-selective electron transfer in He^+ + He collisions at intermediate energies”, *Phys. Rev. A* **97**, 052709 (2018).

[82] J. W. Gao, Y. Wu, J. G. Wang, A. Dubois, N. Sisourat, “Double Electron Capture in $H^+ + H^-$ Collisions”, *Phys. Rev. Lett.* **122**, 093402 (2019).

[83] C. Froese Fischer, “The Hartree Fock method for atoms. A numerical approach”, Wiley-Interscience (1977).

[84] S. Szucs, M. Karemera, M. Terao, F. Brouillard, “Experimental study of the mutual neutralisation of H^+ and H^- between 5 and 2000 eV”, *J. Phys. B* **17**, 1613 (1984).

[85] L. Wolniewicz, K. Dressler, “Adiabatic potential curves and nonadiabatic coupling functions for the first five excited $^1\sum_g^+$ states of the hydrogen molecule”, *J. Chem. Phys.* **100**, 444 (1994).

[86] F. Melchert, S. Krudener, K. Huber, E. Salzborn, “Electron detachment in H^+ - H^- collisions”, *J. Phys. B* **32**, L139 (1999).

[87] B. Peart, R. Grey, K. T. Dolder, “Measurements of cross sections for electron detachment from H^- ions by proton impact”, *J. Phys. B* **9**, 3047 (1976).

[88] L. F. Errea, *et al.*, “Molecular treatment of electron detachment in H^++H^- collisions”, *Phys. Rev. A* **54**, 967 (1996).

[89] H. Rosenthal, H. M. Foley, “Phase-Interference Effects in Inelastic He^+ + He Collisions”, *Phys. Rev. Lett.* **23**, 1480 (1969).

[90] H. Rosenthal, “Nonadiabatic Effects in Slow Atomic Collisions. I. He^+ + He”, *Phys. Rev. A* **4**, 1030 (1971).

[91] S. Y. Ovchinnikov, Y. Kamyshkov, T. Zaman, D. R. Schultz, “Ionization, negative ion formation, elastic scattering and spin exchange in H + H collisions at low- to intermediate-energies”, *J. Phys. B* **50**, 085204 (2017).

[92] W. G. Planje, W. B. Westerveld, A. Niehaus, “Oscillations Due to Two-Electron Exchange during He-Ne Collisions”, *Phys. Rev. Lett.* **85**, 2713 (2000).

[93] T. Sharp, “Potential-energy curves for molecular hydrogen and its ions”, *At. Data. Nucl. Data Tables* **2**, 119 (1970).

[94] L. L. Yan, Y. Wu, Y. Z. Qu, J. G. Wang, R. J. Buenker, “Single- and double-electron-capture processes in the collisions of C^{4+} ions with He”, *Phys. Rev. A* **88**, 022706 (2013).

[95] H. J. Zwally, D. W. Koopman, T. D. Wilkerson, “Development and Application of a Spark Source for Multiply Charged Carbon Ions”, *Rev. Sci. Insrum.* **40**, 1492 (1969).

[96] Barat, M and Roncin, P and Guillemot L and Gaboriaud M N and Laurent H, “Single and double electron capture by C^{4+} ions colliding with helium target”, *J. Phys. B* **23**, 2811 (1990).

[97] R. A. Phaneuf, D. H. Crandall (unpublished data, reported in [104]).

[98] K. Ishii, A. Itoh, K. Okuno, “Electron-capture cross sections of multiply charged slow ions of carbon, nitrogen, and oxygen in He”, *Phys. Rev. A* **70**, 042716 (2004).

[99] D. Dijkkamp, D. Ciric, A. de Boer, F. J. De Heer, E. Vlieg, “Subshell-selective electron capture in collisions of C^{4+}, N^{5+}, O^{6+} with H, H_2 and He”, *J. Phys. B* **18**, 4763 (1985).

[100] D. H. Crandall, R. E. Olson, E. J. Shipsey, J. C. Browne, “Single and double change transfer in C^{4+} - He collisions”, *Phys. Rev. Lett.* **36**, 858 (1976).

[101] T. Iwai, *et al.*, “Cross sections for one-electron capture by highly stripped ions of B, C, N, O, F, Ne, and S from He below 1 keV/amu”, *Phys. Rev. A* **26**, 105 (1982).

[102] M. Hoshino, *et al.*, “Experimental and theoretical study of double-electron capture in collisions of slow $C^{4+}(1s^2\ ^1S)$ with $He(1s^2\ ^1S)$”, *Phys. Rev. A* **75**, 012716 (2007).

[103] J. P. Hansen, “Dynamics of single- and double-electron capture in C^{4+} - He collisions”, *J. Phys. B* **25**, L17 (1992).

[104] M. Kimura, R. E. Olson, “Electron capture to (nl) states in collisions of C^{4+} and C^{6+} with He”, *J. Phys. B* **17**, L713 (1984).

[105] L. F. Errea, B. Herrero, L. Méndez, A. Riera, “Molecular calculation of total and differential charge transfer cross sections in C^{4+} + He collisions”, *J. Phys. B* **28**, 693 (1995).

[106] M. Gargaud, J. Hanssen, R. McCarroll, P. Valiron, “Charge exchange with multiply charged ions at low energies: application to the N^{3+}/H and C^{4+}/H systems”, *J. Phys. B* **14**, 2259 (1981).

[107] A. Kramida, Yu. Ralchenko, J. Reader, and NIST ASD Team, NIST Atomic Spectra Database (ver. 5.3), [Online]. Available: `http://physics.nist.gov/asd` [2017, March 1]. National Institute of Standards and Technology, Gaithersburg, MD. (2015).

[108] Yiqing Zhao, *et al.*, “Polarization Degrees for 3p $^2P_{3/2}$ - 3s $^2S_{1/2}$ Transition of $C^{3+}(1s^2 3p)$ Produced in Collisions of C^{4+} with He and H_2”, *J. Phys. Soc. Jpn.* **79**, 064301 (2010).

[109] A. L. Ford, L. A. Wehrman, K. A. Hall, J. F. Reading, “Single and double electron removal from helium by protons”, *J. Phys. B* **30**, 2889 (1997).

[110] L. F. Errea, B. Herrero, L. Méndez, A. Riera, “Active Electrons in the CHe^{4+} Quasimolecule”, *Few Body Syst.* **19**, 31 (1995).

[111] M. Barat, P. Roncin, “Multiple Electron-Capture by Highly Charged Ions at keV Energies”, *J. Phys. B* **25**, 2205 (1992).

[112] N. Bohr, J. Lindhard, *D. Kgl. Danske Vidensk. Selskab, Math Fys. Medd* **28**, 7 (1954).

[113] A. Barany, *et al.*, “Stueckelberg angular scattering oscillations in two-electron capture by C^{4+} from He at low energies”, *J. Phys. B* **19**, L427 (1986).

[114] L. Pichl, *et al.*, “Angular dependence of double electron capture in collisions of C^{4+} with He. Stueckelberg oscillations in the differential cross-section for capture into $C^{2+}(1s^2 2s^2\ ^1S)$”, *Eur. Phys. J. D* **38**, 59 (2006).

[115] M. van der Poel, C. V. Nielsen, M. A. Gearba, N. Andersen, “Fraunhofer Diffraction of Atomic Matter Waves: Electron Transfer Studies with a Laser Cooled Target”, *Phys. Rev. Lett.* **87**, 123201 (2001).

[116] M. van der Poel, *et al.*, “Atomic scattering in the diffraction limit: electron transfer in keV Li^+ - Na(3s, 3p) collisions”, *J. Phys. B* **35**, 4491 (2002).

[117] D. L. Guo, *et al.*, “State-selective electron capture in 30- and 100-keV He^++He collisions”, *Phys. Rev. A* **95**, 012707 (2017).

[118] Q. Wang, X. Ma, X. L. Zhu, S. F. Zhang, “Observation of atomic-size Fraunhofer-type diffraction for single electron capture in He^{2+} + He collision”, *J. Phys. B* **45**, 025202 (2011).

[119] H. Agueny, “Fraunhofer-type diffraction patterns of matter-wave scattering of projectiles: Electron transfer in energetic ion-atom collisions”, *Phys. Rev. A* **92**, 012702 (2015).

[120] M. Gudmundsson, *et al.*, "Angular scattering in fast ion–atom electron transfer collisions: projectile wave diffraction and Thomas mechanisms", *J. Phys. B* **43**, 185209 (2010).

[121] S. E. Nielsen, *et al.*, "Electron transfer from optically prepared states: He^{+} + Na(3 ^{2}P) → He(2 ^{1,3}P) + Na^{+} angular differential scattering", *J. Phys. B* **37**, 2119 (2004).

[122] M. Born, E. Wolf, "Principles of Optics: Electromag- netic Theory of Propagation, Interference and Diffraction of Light, 7th ed.", *Principles of Optics: Electromag- netic Theory of Propagation, Interference and Diffraction of Light, 7th ed. (Cambridge University Press, Cambridge, 2003)* .

[123] G. B. Airy, "On the Diffraction of an Object-glass with Circular Aperture", *Trans. Cambridge Philos. Soc.* **5**, 283 (1835).

[124] C. F. Barnett, P. M. Stier, "Charge Exchange Cross Sections for Helium Ions in Gases", *Phys. Rev.* **109**, 385 (1958).

[125] W. N. Shelton, P. A. Stoycheff, "Measurement of the Total Cross Section for Single-Electron Transfer in Collisions of He^{+} with He in the Energy Range 2-22 keV", *Phys. Rev. A* **3**, 613 (1971).

[126] V. Pol, W. Kauppila, J. T. Park, "Absolute Differential Elastic- and Inelastic-Scattering Cross Sections in 25-140 keV He^{+} + He Collisions", *Phys. Rev. A* **8**, 2990 (1973).

[127] R. Hegerberg, T. Stefansson, M. T. Elford, "Measurement of the symmetric charge-exchange cross section in helium and argon in the impact energy range 1-10 keV", *J. Phys. B* **11**, 133 (1978).

[128] E. A. Hinds, R. Novick, "Precise resonant charge-transfer cross sections for He - He^{+} between 2 and 100 eV", *J. Phys. B* **11**, 2201 (1978).

[129] N. V. de Castro Faria, F. L. Freire, A. G. de Pinho, "Electron loss and capture by fast helium ions in noble gases", *Phys. Rev. A* **37**, 280 (1988).

[130] R. D. DuBois, S. T. Manson, "Electron emission in He^{+} - atom and He^{+} - molecule collisions: A combined experimental and theoretical study", *Phys. Rev. A* **42**, 1222 (1990).

[131] R. Okasaka, *et al.*, "Excitation functions of He(n=3) levels in the intermediate-velocity regime of He^{+} - He collisions", *Phys. Rev. A* **49**, 246 (1994).

[132] J. L. Forest, *et al.*, "Single and double ionization of helium by intermediate-to-high-velocity He^{+} projectiles", *Phys. Rev. A* **52**, 350 (1995).

[133] H. Atan, W. Steckelmacher, M. W. Lucas, "Single electron loss and single electron capture for 0.6-2.2 MeV He^{+} colliding with rare gases", *J. Phys. B* **24**, 2559 (1999).

[134] M. S. Schöffler, *et al.*, "State-selective differential cross sections for single and double electron capture in $\mathrm{He}^{+,2+}$ - He and p - He collisions", *Phys. Rev. A* **79**, 064701 (2009).

[135] M. Barat, *et al.*, "Inelastic processes in He^{+} - He collisions", *J. Phys. B* **5**, 1343 (1972).

[136] E. Ghanbari-Adivi, H. Ghavaminia, “Projectile angular-differential cross sections for single electron transfer in fast He^+ - He collisions”, *Chin. Phys. B* **24**, 033401 (2015).

[137] T. G. Winter, C. C. Lin, “Electron capture into excited states of helium by helium-ion impact on helium”, *Phys. Rev. A* **12**, 434 (1975).

[138] W. Lichten, “Resonant Charge Exchange in Atomic Collisions”, *Phys. Rev.* **131**, 229 (1963).

[139] D. P. Sural, S. C. Mukherjee, N. C. Sil, “Electron Capture and Excitation in He^+ - He Collisions”, *Phys. Rev.* **164**, 156 (1967).

[140] R. Hildenbrand, N. Grun, W. Scheid, “Coupled channel calculations with Cartesian Gaussian basis functions for H + He and He^+ + He reactions”, *J. Phys. B* **28**, 4781 (1999).

[141] I. Mančev, “Four-body continuum-distorted-wave model for charge exchange between hydrogenlike projectiles and atoms”, *Phys. Rev. A* **75**, 052716 (2007).

[142] M. Baxter, T. Kirchner, E. Engel, “Time-dependent spin-density-functional-theory description of He^+-He collisions”, *Phys. Rev. A* **96**, 032708 (2017).

[143] E. Ghanbari-Adivi, H. Ghavaminia, “Single-electron capture from helium atoms by fast singly positive charged helium ions”, *Eur. Phys. J. D* **66**, 350 (2012).

[144] C. F. Barnett, *et al.*, “Atomic data for fusion. Volume 1: Collisions of H, H_2, He and Li atoms and ions with atoms and molecules” (Oak Ridge National Laboratory, 1990).

[145] L. Wolterbeek Muller, F. J. De Heer, “Electron capture into excited states by helium ions incident of noble gases”, *Physica* **48**, 345 (1970).

[146] R. Hippler, K. H. Schartner, H. F. Beyer, “Direct and charge-exchange excitation of the 2^1P level in He^+ - He collisions”, *J. Phys. B* **11**, L337 (1978).

[147] F. D. Heer, L. W. Muller, R. Geballe, “Electron capture into excited states by helium ions incident on helium”, *Physica* **31**, 1745 (1965).

[148] *Private communications with the authors of Ref. [117]* .

[149] E. Horsdal-Pedersen, C. L. Cocke, M. Stockli, “Experimental Observation of the Thomas Peak in High-Velocity Electron Capture by Protons from He”, *Phys. Rev. Lett.* **50**, 1910 (1983).

[150] D. Fischer, *et al.*, “Experimental separation of the Thomas charge-transfer process in high-velocity p-He collisions”, *Phys. Rev. A* **73**, 052713 (2006).

[151] V. Mergel, *et al.*, “Intra-atomic electron-electron scattering in p-He collisions (Thomas process) investigated by cold target recoil ion momentum spectroscopy”, *Phys. Rev. Lett.* **79**, 387 (1997).

[152] S. Figueira da Silva, H. Winter, F. Aumayr, “Single- and double-electron capture cross sections for slow He^{2+} impact on O_2, H_2, and D_2”, *Phys. Rev. A* **75**, 042706 (2007).

[153] I. B. Abdurakhmanov, J. J. Bailey, A. S. Kadyrov, I. Bray, “Wave-packet continuum-discretization approach to ion-atom collisions including rearrangement: Application to differential ionization in proton-hydrogen scattering”, *Phys. Rev. A* **97**, 032707 (2018).